Doctoral Dissertations   Graduate School

8-2007

Investigation of Non-Conventional Bio-Derived Fuels for Hybrid Rocket Motors

Scott Grayson Putnam
University of Tennessee - Knoxville

Follow this and additional works at: https://trace.tennessee.edu/utk_graddiss

Part of the Propulsion and Power Commons

To the Graduate Council:

I am submitting herewith a dissertation written by Scott Grayson Putnam entitled "Investigation of Non-Conventional Bio-Derived Fuels for Hybrid Rocket Motors." I have examined the final electronic copy of this dissertation for form and content and recommend that it be accepted in partial fulfillment of the requirements for the degree of Doctor of Philosophy, with a major in Aerospace Engineering.

James Evans Lyne, Major Professor

We have read this dissertation and recommend its acceptance:

Ke Nguyen, Viatcheslav Naoumov, William S. Johnson, Duane D. Bruns

Accepted for the Council:

<u>Carolyn R. Hodges</u>

Vice Provost and Dean of the Graduate School

(Original signatures are on file with official student records.)

To the Graduate Council:

I am submitting herewith a dissertation written by Scott Grayson Putnam entitled "Investigation of Non-Conventional Bio-Derived Fuels for Hybrid Rocket Motors." I have examined the final electronic copy of this dissertation for form and content and recommend that it be accepted in partial fulfillment of the requirements for the degree of Doctor of Philosophy, with a major in Aerospace Engineering.

James Evans Lyne, Major Professor

We have read this dissertation
and recommend its acceptance:

Ke Nguyen

Viatcheslav Naoumov

William S. Johnson

Duane D. Bruns

Acceptance for the Council:

Carolyn Hodges
Vice Provost and Dean of the Graduate School

(Original signatures are on file with official student records.)

Investigation of Non-Conventional Bio-Derived Fuels for Hybrid Rocket Motors

A Dissertation
Presented for the
Doctor of Philosophy
Degree
The University of Tennessee, Knoxville

Scott Grayson Putnam
August 2007

Acknowledgements

Abstract

Non-conventional bio-derived fuels have been evaluated for use in hybrid rocket motors. Tests were conducted at combustion pressures in the range of 100 – 220 psig and thrust levels of 40 – 170 newtons. Beeswax was tested with oxygen as the oxidizer and showed a regression rate at least three times as high as traditional hybrid propellant combinations such as hydroxyl-terminated polybutadiene (HTPB) and liquid oxygen (LOX). This provides the promise of a high thrust hybrid rocket motor using a simple, single port geometry and overcomes the main weakness of traditional hybrid rocket motor propellants, which are low regression rates. Beeswax was also tested with nitrous oxide as an oxidizer, but further testing is needed to attain high enough combustion chamber pressures to achieve stable combustion. Experimental evaluation of the specific impulse for beeswax and oxygen was moderately successful for lab scale testing, but needs further refinement. Analytical studies were performed to evaluate the theoretical performance of non-conventional hybrid rocket motors. This analysis indicates beeswax, lard, a mixture of paraffin and lard, and combinations of beeswax and aluminum should all perform better than traditional hybrid rocket propellants considered when burned with oxygen. For a combustion chamber pressure of 500.38 psig, beeswax and oxygen yielded a maximum specific impulse of 327 s. The high specific impulse combined with a high regression rate combine to make beeswax and oxygen a potentially high performing hybrid rocket motor propellant for launch vehicles, suborbital rockets, or orbital kick motors.

Table of Contents

List of Tables

List of Figures

List of Symbols

Symbol	Definition
A/D	Analog to Digital
A_e	Nozzle exit cross-sectional area
A_p	Combustion port cross-sectional area
A_t	Nozzle throat cross-sectional area
c*	Characteristic exhaust velocity
°C	degrees Celsuis
cm	Centimeter
d_e	Nozzle exit diameter
d_t	Nozzle throat diameter
g_0	Acceleration due to gravity
(g)	Gas phase
G_{ox}	Oxidizer mass flux rate
G_{TOT}	Total propellant mass flux rate
g/cc	Gram/cubic centimeter
in	Inch(es)
I_{sp}	Specific Impulse
K	Kelvin
kg	Kilogram
kcal	Kilocalories
lbf	Pounds force
M	Molecular mass of combustion products
m	meter
$\dot{m}$	mass flow rate
M_e	Exit plane Mach number
m_f	Final fuel grain mass
m_i	Initial fuel grain mass
mm	millimeter
mol	mole
$\dot{m}_{ox}$	oxidizer mass flow rate
MPa	Megapascals
m_{prop}	Mass of propellant
N	Newtons
O/F	Oxidizer to fuel ratio
P_0, P_c	Combustion chamber pressure
P_e	Nozzle exit plane pressure
psi	Pounds per square inch
psig	Pounds per square inch gage
$\dot{r}$	Regression rate
r_i	Initial combustion port radius
R_u	Universal Gas Constant

s	seconds
T	Thrust
T_0	Combustion chamber temperature
t_b	Burn time
T_e	Nozzle exit plane temperature
t_{gi}	Initial fuel grain thickness
t_{gf}	Final fuel grain thickness
T_i	Thrust at current time step
t_i	Time at current time step
$T_{i+\Delta t}$	Thrust at next time step
$t_{i+\Delta t}$	Time at next time step
V_e	Nozzle exit velocity
α	Equivalence ratio
γ	Ratio of specific heats
λ	Thrust efficiency
μm	Micrometers
θ_{cn}	Nozzle half angle

I. INTRODUCTION AND BACKGROUND

I.I Background on Hybrid Rockets

Hybrid rocket motor technology has been around since the 1930s. A hybrid rocket motor typically uses a solid fuel and a liquid, or gas, oxidizer. There are several reasons hybrid rocket motors are desirable compared to solid rocket motors or liquid rocket engines. Better performance can sometimes be achieved by propellants that are in different states (i.e. liquid/solid or gas/solid). Some solid fuels that can be used in hybrid rocket motors can't be used in solid rocket motors due to incompatibility with other solid fuels and oxidizers. Hybrid rocket motors are safer than solid rocket motors because it is virtually impossible to have a combination of the fuel and oxidizer that can result in an explosion due to the unique combustion process in a hybrid motor. If a crack develops in the solid fuel grain, the combustion process will not allow a dramatic increase in burn surface area as occurs in a solid rocket, which in turn prevents a continuously increasing chamber pressure that would eventually result in an explosion. This is due to the combustion occurring in a diffusion flame, as shown in Figure 1.
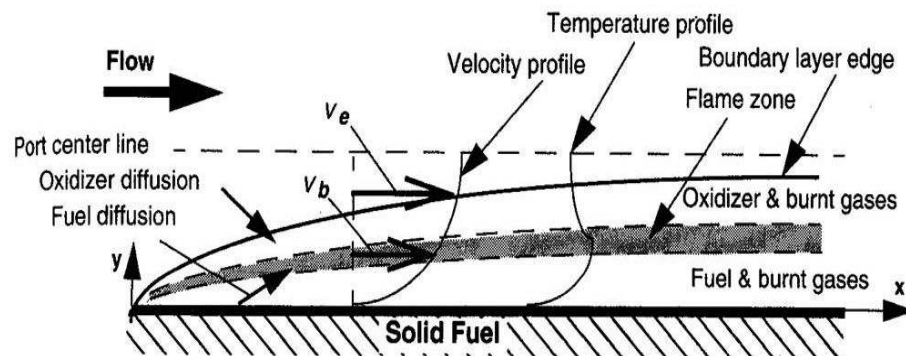
Figure 1: Hybrid Rocket Motor Combustion Process

1

The fuel enters the boundary layer by vaporization at the solid fuel surface, and the oxidizer enters the boundary layer from the free-stream flow by diffusion. When the fuel and oxidizer meet at approximately the stoichiometric ratio, a combustion zone occurs. Due to the diffusion flame occurring in the boundary layer, there is no increase in surface area when a crack forms in the solid fuel grain because there is little to no oxidizer within the crack. Finally, unlike solid rocket motors, a hybrid can be shutdown, restarted, and throttled. In general, traditional choices for propellants in hybrid rockets have one primary weakness. Due to the regression rate being low as compared to solid rocket propellants, a high thrust hybrid motor requires multiple combustion ports to produce thrust levels similar to those of a solid rocket motor using a single combustion port. This is necessary because the thrust produced by the motor is a function of the propellant mass flow rate, which is a function of the fuel regression rate. With a low regression rate, a motor needs more combustion ports to increase the propellant mass flow rate to produce a high thrust level. This results in increased complexity in the solid grain fabrication and poor volumetric efficiency. Unlike liquid rocket engines, the fuel mass flow rate in a hybrid rocket motor depends on the oxidizer mass flow rate through the combustion port. The thrust of the motor also depends on the specific impulse, which is a function of the combustion chamber temperature. Another negative aspect of hybrid rocket motors is their unproven flight heritage compared to liquid and solid rockets (1,2).

I.II Review of Outside Hybrid Rocket Research

Over the years, there has been an extensive amount of work on hybrid rocket motor technology. A significant amount of this work has been on improving the performance of hybrid rockets in order to develop an efficient, high thrust rocket motor

with a simple grain geometry. Hybrid rockets have been considered for uses in launch vehicles, sounding rockets, and satellite propulsion systems. In fact, due to the extremely safe nature of hybrid rockets, they are being used extensively in the amateur rocket community.

One typical goal of hybrid rocket research is to evaluate the regression rate as a function of the oxidizer mass flux rate (1). The oxidizer mass flux rate is defined as the ratio of the oxidizer mass flow rate to the combustion port cross-sectional area as shown in Equation 1

$$G_{ox} = \frac{\dot{m}_{ox}}{A_p} \tag{1}$$

where G_{ox} is the oxidizer mass flux rate, $\dot{m}_{ox}$ is the oxidizer mass flow rate, and A_p is the combustion port cross-sectional area. The regression rate can be expressed as a function of the oxidizer mass flux rate as shown in Equation 2

$$\dot{r} = aG_{ox}{}^n \tag{2}$$

where $\dot{r}$ is the regression rate and a and n are experimentally derived constants.

Research at the University of Surrey has shown that hybrid rockets can be a feasible option for satellite propulsion (3). A satellite requires a propulsion system for orbit maneuvering, orbit maintenance, and stationkeeping maneuvers. It has been demonstrated that a hybrid rocket system using 85% hydrogen peroxide (HTP) as the oxidizer and polyethylene as the solid fuel can serve as a cost-effective solution to satellite propulsion requirements. The hydrogen peroxide was passed through a catalyst to decompose it into steam and oxygen at a temperature of approximately 630 °C before injection into the combustion port. This hybrid rocket motor displayed regression rates

similar to hydroxyl-terminated polybutadiene (HTPB) and liquid oxygen (LOX). Combustion chamber pressures achieved were 250 psi. It was shown that a hybrid rocket motor can be a safe, reliable, and cost-effective alternative to a solid rocket motor for an upper stage to boost a satellite into a higher orbit. Work at Purdue University has also shown that 80-88% hydrogen peroxide and polyethylene can function as an effective hybrid rocket system. The tests at Purdue were conducted over a range of combustion chamber pressures of 100 – 400 psi, but a typical test chamber pressure was 200 psi. As with the tests at Surrey, they used a catalyst pack to decompose the HTP for the ignition. This type of process provides a self-ignition behavior that precludes the need for an ignition system and provides a reliable and repeatable ignition process. Smooth, stable combustion with 90% efficiency has been achieved (4). Amateur rocket enthusiasts have focused on hybrid motors for use in suborbital rockets all over the world due to their inherent safety. The MARS Amateur Rocket Society (MARS) in England has developed hybrid rocket motors for sounding rockets using nitrous oxide as the oxidizer and polyethylene as the fuel (5). Their B4 hybrid motor has been successfully static tested and produced a thrust level of 3,000 newtons (N). They have tested a down rated version of the B4 (1,400 N), and it achieved an altitude of approximately one mile. The B4 hybrid rocket motor is being designed as an upper stage for MARS' Deimos-3 hybrid rocket. The Deimos-3 is being designed as a two stage, hybrid rocket that will be able to put a small payload to an altitude of 62 miles, which is the edge of space. The combination of polyethylene and nitrous oxide exhibits the same low regression rate as HTP and polyethylene, so it is difficult to obtain high thrust levels. MARS has the distinction of launching the first hybrid rocket, amateur or professional, from British soil.

4

Orion Propulsion has produced a hybrid motor for the X-Prize competition that uses asphalt as the solid fuel and nitrous oxide as the oxidizer (6). The hybrid motor was be mounted on a Chevy pickup truck for demonstration purposes, and has a maximum thrust of 3,000 pounds force (lbf) with a maximum combustion chamber pressure of approximately 400 psig. Using this hybrid rocket motor, the truck has been accelerated from 0 to 60 miles per hour in 4.18 s. The hybrid motor has an oxidizer to fuel ratio of 6.0, an average thrust level of 1,725 lbf, an average combustion chamber pressure of 207 psig, and a burn time of 10 seconds. One method attempted to increase the regression rate in hybrid rocket motors has been to introduce aluminum into the solid fuel. At Penn State University, nano-sized particles of aluminum powder with diameters of 70 – 150 μm were mixed into HTPB fuel grains and tested (7). Pure oxygen was used as the oxidizer at combustion chamber pressures up to 1,750 psig. Typical tests were run at oxidizer mass flux rates of 140 – 850 kg/m^{2}s and chamber pressures of 320 – 650 psig. The result of these tests showed the regression rate increased by 50% over the HTPB without aluminum. At Stanford University, research has been conducted on solid fuels in the hope of producing higher regression rates than previous hybrid rocket fuels, such as HTPB and Plexiglas (8). This was based on previous research by the U.S. Air Force into solid cryogenic fuels such as frozen pentane and frozen oxygen. Pentane is an alkane hydrocarbon that is used as a fuel or a lubricant. These tests showed frozen pentane exhibited regression rates three to four times higher than with HTPB. The hypothesis for the increased regression rates was a lower heat of vaporization of the cryogenic solid fuels. Stanford developed a liquid layer hybrid combustion theory in an attempt to explain the higher regression rates using frozen pentane (9,10). It was determined that

the liquefying nature of the fuel was the primary characteristic that contributed to the increased regression rates. This led to the choice of paraffin as the solid fuel, and when combined with gaseous oxygen as the oxidizer, yielded significantly higher regression rates than HTPB in lab tests. In larger scale tests, it has been used in a 10 foot long sounding rocket launched to an altitude of 16,000 feet in Nevada. They have conducted over 250 lab tests to evaluate the regression rate of paraffin and test fired motors with thrust levels up to 2,500 N. The proposed mechanism behind these higher regression rates is the formation of a melting layer at the burning surface (11-14). This melt layer is hydrodynamically unstable, which results in droplets of the fuel being entrained in the combustion zone as well as the normal gasification of the solid fuel. One conclusion from the research was that the surface tension and melt layer viscosity play an important part in determining how well the entrainment of the liquid fuel droplets occurs. For high regression rates, the desired characteristics are low surface tension and low viscosity. Fuels like HTPB, polyethylene, and Plexiglas have high surface tension and viscosity, which explains why they have lower regression rates than paraffin. Paraffin and oxygen yielded regression rates 3 to 4 times higher than HTPB. Further research on paraffin as a high regression rate hybrid fuel has been conducted at the United States Air Force Academy (15). Paraffin was tested with 90% pure hydrogen peroxide as the oxidizer. Small scale lab tests were conducted with the hydrogen peroxide flowing through a catalyst to decompose it into steam and oxygen at a temperature of 800 °C where it auto-ignited the fuel. The tests resulted in regression rates of 2.87 – 5.28 mm/s for oxidizer mass flux rates of 111 – 162 kg/m^2s. These regression rates were higher than with HTPB/LOX and even paraffin and oxygen. For a oxidizer mass flux rate of 130 kg/m^2s,

paraffin with hydrogen peroxide had a regression rate of 3.23 mm/s where paraffin with oxygen yielded a regression rate of only 2.6 mm/s. It is theorized that the increased temperature of the oxygen after the hydrogen peroxide decomposes is the main driver of the increase in the regression rate over using paraffin with gaseous oxygen. This would indicate that other materials with similar physical properties as paraffin could also potentially have equally as high regression rates.

I.III Review of University of Tennessee Hybrid Rocket Research

Work on hybrid rockets at the University of Tennessee, Knoxville (UTK) began in the fall of 1999 (16). A project was funded by Lockheed Martin to develop a hybrid rocket test stand and initial research into hybrid rocket propulsion. A test stand was constructed by a group of undergraduate students working under Dr. Evans Lyne, and tests were run using polymethyl methacrylate (PMMA) as the solid fuel and gaseous oxygen as the oxidizer. It utilized an ignition system using an injection of propane in conjunction with the firing of a spark plug to provide the initial heat of vaporization to the solid fuel. The test stand was used successfully to test fire hybrid rocket motors with combustion chamber pressures ranging between 50-150 psig.

Further work at UTK progressed into working with paraffin and lard as the solid fuels (17). Following on the work at Stanford University, lab-scale tests were conducted to verify the regression rates reported for paraffin and oxygen. These tests were successful in showing the elevated regression rates previously documented. Testing then proceeded with lard to determine its suitability as a hybrid fuel. Compared to paraffin, lard has a relatively low melting temperature, and this caused some problems with its physical stability. During testing, due to the fairly low combustion pressures, spallation

7

of unburned lard through the nozzle occurred. This led to mixing the lard with paraffin in

an attempt to improve the mechanical stability of the solid fuel grain. It was hoped that

the increased melting temperature of a 50%/50% mixture by weight would improve the

mechanical properties of the fuel grain and reduce spallation. Despite this mixture, the

fuel had to be stored in a freezer until the time of firing. Results of the testing showed the

lard/paraffin mixture, when burned with oxygen, showed a significant increase in

regression rate over HTPB/oxygen. Another attempt to improve the mechanical stability

of lard used a sponge soaked in lard as the solid fuel grain. Once the sponge was fully

saturated with lard, it was placed in a freezer to solidify. This seemed to work fairly well

in keeping the lard from leaving the nozzle without having been burned.

I.IV Motivation For Current Research

There are several motivations to pursue a non-toxic propellant combination for

use in hybrid rocket motors. One is to find a propellant combination that has less toxic

exhaust products when compared to some solid and liquid rockets. For example, a

typical Ariane 5 launch releases 270 tons of concentrated hydrochloric acid into the

atmosphere per launch (18). Rockets using unsymmetrical dimethyl hydrazine (UDMH)

release so-called nitrogen radicals, which are potentially damaging to the ozone layer.

Also, some oxidizers (i.e. HNO_3, F_2, ClF_3) are toxic to handle, and therefore require

additional safety precautions during fabrication and loading, which increases the cost of

hybrid motor production. Another consideration is the contamination of groundwater due

to the chemicals used in rocket propellants (19,20). Perchlorate is commonly used in

solid rocket motors in the form of ammonium perchlorate. Perchlorate has been found to

be linked to thyroid problems, especially in children. Many military sites have a

significant amount of perchlorate contamination and the cleanup will come at significant financial expense. Civilian rocket manufacturers have also felt the cost of cleaning up perchlorate contamination (21). Aerojet has spent an estimated $250 million over the past 25 years to reduce the levels of perchlorate contamination to groundwater at its Sacramento facility. Aerojet also had to pay a $25 million settlement due to a jury decision finding them responsible for the deaths of three individuals and the illnesses of four others due to drinking tap water contaminated with perchlorate. The three deaths were the result of lymphoma and the four who survived had a thyroid disease. Studies have also shown that Lockheed Martin is responsible for perchlorate contamination to lettuce grown using water from the Colorado River, which has been contaminated over the years by Lockheed Martin (22). This could affect what the FDA decides as to what level to set for safe exposure to perchlorate. Knowing that tap water and lettuce, along with other vegetables, exposes people to perchlorate could lower the threshold they set. The combination of environmental and safety issues emphasize the need for a propellant that is non-toxic, and has relatively benign combustion products. At the same time, the motor should achieve a high regression rate and a high thrust level utilizing a simple, single combustion port design similar to solid rocket motors.

Beeswax was singled out as a candidate for our solid fuel for several reasons. First, it is very similar to paraffin and could potentially have a comparable regression rate. Second, as a natural substance produced by bees, it is non-toxic and can be easily obtained in mass quantities from commercial companies. Third, it is inexpensive, widely available, and easily formed into fuel grains. A hybrid rocket system using beeswax as the solid fuel would have a lower cost compared to other rocket systems since there

would be no requirement for elaborate safety precautions. When burned with oxygen or nitrous oxide, some of the combustion products are carbon dioxide, water, carbon monoxide, nitrogen oxide, etc. These exhaust products are similar to the emissions from automobiles, which are considerably less toxic than other substances released into the atmosphere from some rockets.

Two oxidizers were considered for this research. Gaseous oxygen was chosen because it is easily obtainable, has a history of good performance as an oxidizer, and is easy to handle. Also, based on the research at Stanford with paraffin and gaseous oxygen, it seemed a reasonable choice for use with beeswax. Nitrous oxide was also considered because it is easy to obtain, safe, has so-called "self-pressurizing" characteristics, and is commonly used in hybrid rockets around the world.

This present research will have both an analytical and an experimental component. There are four major parameters to be determined in the experimental research program. The most important goal is to determine the regression rate of non-conventional, bio-derived propellants and determine functional relationships between this rate and various test conditions. An understanding of the regression rate for a fuel is critical when designing a hybrid rocket motor to produce a desired thrust level. Additional goals will be to measure combustion chamber pressure, thrust levels, and flow rates for the fuel and oxidizer. These measurements will allow the calculation of specific impulse. The main objectives of the analytical work are to obtain theoretical values of specific impulse, thrust, and other performance parameters, compare them to the experimental values, and determine the theoretical performance of a wide variety of propellants over a range of equivalence ratios to help explain the experimental results.

The result of this analytical work will be the formation of a repository of thermodynamic and thermophysical properties for previously not considered fuel/oxidizer combinations that may be used by future designers of hybrid rocket motors.

The analytical approach and methods will be outlined in Chapter 2. The analytical research results will be discussed in Chapter 3. The experimental setup and procedures for the experimental testing will be discussed in Chapter 4. Evaluation of the results of the experimental research effort and a comparison to the some of the analytical results will be presented in Chapter 5. Some conclusions and recommendations for future work will be presented in Chapter 6

II. DESCRIPTION OF ANALYTICAL RESEARCH PROGRAM

The analytical portion of this research was accomplished by taking various oxidizer/fuel combinations and determining the theoretical performance parameters in order to use them in future design of hybrid rocket motors. The goal was to determine the influence of equivalence ratio on combustion temperature, specific impulse (I_{sp}), ratio of specific heats of combustion products (γ), and molecular mass of combustion products. Fuel/oxidizer combinations analyzed were 50%/50% (by mass) lard/paraffin and O_2 (g), 50%/50% lard/paraffin and N_2O (g), beeswax and O_2 (g), beeswax and N_2O (g), lard and O_2 (g), lard and N_2O (g), beeswax + Al and O_2 (g), and beeswax + Al and N_2O (g). Additives to the solid fuel were examined, such as powdered aluminum, to increase the density of the fuel and the specific impulse. For the beeswax/Al combinations, various percentages of aluminum were examined.

The analysis was accomplished using the Air Force Chemical Equilibrium Specific Impulse Code, also referred to as the Isp code (23). It has an input file utility written by Curtis Selph which aids in setting up the inputs to the program. This code accomplishes the thermodynamic calculations required to determine a theoretical value for the specific impulse (I_{sp}) for a fuel/oxidizer combination. It takes as inputs the propellants, the proportions of the propellants, and the combustion chamber pressure. It can be specified either to set an area ratio for the nozzle or to set a specific nozzle exit pressure in which case the code will compute the required nozzle area ratio. When calculating the conditions in the combustion chamber, the code accounts for all possible chemical species during the combustion and accounts for dissociation. An example of the mole fractions of different chemical species present in the combustion process of

12

beeswax and gaseous oxygen is shown in Table 1. These were computed at a combustion chamber pressure of 500.38 psig and at an equivalence ratio of 0.8. There are two modes for calculating the flow of the combustion products through the nozzle. By default, the code runs performs the calculations by assuming the flow through the nozzle is in a shifting equilibrium. This assumes that at any point in the nozzle, the flow is always in equilibrium as it expands through the nozzle and the temperature and pressure are changing. This tends to over predict the I_{sp} computed because the flow generally will travel too quickly through the nozzle as the temperature decreases to be able to complete all the chemical reactions in order to be in chemical equilibrium. The other option is to choose the frozen flow mode of calculation. This assumes the chemical composition is static as the gas flow expands through the nozzle. The gas can be designated as frozen at the nozzle inlet, the nozzle throat, or the nozzle exit. For this research, the gas flow is assumed to be frozen at the combustion chamber. Although it is common to assume frozen flow at the throat, there is little difference in assuming frozen flow at the throat or the nozzle inlet. However, setting frozen flow at the throat requires the nozzle area ratio to be set in the input file. This is undesirable since the experimental data that was compared with the theoretical data was adjusted to not include any pressure thrust effects, which means the experimental data is for a nozzle expanded to sea level pressure at the exit. It is easier to let the code calculate the required nozzle area ratio, especially when the combustion chamber pressure is changed.

The input file was setup to evaluate the I_{sp} with the nozzle exit pressure set at 14.7 psig. The code was run at two different combustion pressures. The first combustion pressure examined was 150 psig. This pressure was chosen because it was approximately

13

Table 1: Combustion Chemical Species Mole Fractions, Beeswax/O2, α = 0.8

Species	Mole Fraction
H	0.038
H_2	0.076
HO	0.078
HO_2	0.00017
H_2O	0.307
H_2O_2	0.000012
O	0.022
O_2	0.035
HCOOH	0.0000023
CHO	0.000016
CO	0.297
CO_2	0.145

in the middle of the range of the experimental combustion chamber pressures achieved during testing. This allowed for a valid comparison between the theoretical data and the experimental data. The second combustion pressure chosen was 500.38 psig (3.45 MPa). This allows for comparison to previously published data for traditional fuel/oxidizer combinations, such as in Reference 1.

The Isp code has a built in library of propellants from which the user may choose. The oxidizers of interest, oxygen and nitrous oxide, already existed in the library, but lard, paraffin, and beeswax were not in the library. These propellants had to be entered into the library manually. The chemical formula, heat of formation, and density and standard temperature and pressure were entered into the library for each propellant. Lard and paraffin were straightforward to enter since the properties are easy to find (24). Beeswax was not so easy to find exact information on, so extra effort was required to produce the information needed. Beeswax is a complex substance used in beehives for the construction of honeycomb (25). The worker bees in the hive secrete beeswax from their abdomens and then combined with propolis to make the honeycomb. Propolis is a substance made of resins that bees extract from the buds of trees. Beeswax is a complex mixture of various esters, hydrocarbons, free acids, alcohols, and other substances (26-28). The exact chemical composition is dependent on what type of bee produces the beeswax and the type of pollen consumed by the bees. In general, most beeswax is made up primarily of three main constituents. Cerotic acid ($CH_3(CH_2)_{24}COOH$) is the most prevalent free acid and makes up approximately 12% of beeswax. Triacontanol ($CH_3(CH_2)_{29}CH_3$) is an ester that makes up roughly 65% of beeswax. The third major component of beeswax is myricyl palmitate ($CH_3(CH_2)_{14}COO(CH_2)_{12})CH_3$), which is

approximately 23% of beeswax. Using these three components and their respective

contributions, a general chemical formula can be estimated to be $C_{46}H_{92}O$. The data for

lard, beeswax, and paraffin needed for use in the code is listed in Table 2 (24). The range

of equivalence ratios examined was 0.2 – 3. This was achieved by running the propellant

combinations at a series of oxidizer to fuel ratios that resulted in the desired range of

equivalence ratios base on the stoichiometric oxidizer to fuel ratios. The stoichiometric

oxidizer to fuel ratios for the fuel/oxidizer combinations are listed in Table 3.

The stoichiometric ratios were computed by balancing the fuel components with

the exhaust products in the chemical formulas for complete combustion and then

performing an oxygen balance on each equation.

Table 2: Physical Data on Solid Fuels at Standard Temperature (24)

Fuel	Chemical Formula	Heat of Formation (kcal/mol)	Density (g/cc)
Beeswax	$C_{46}H_{92}O$	-197.858	0.961
Lard	$C_{15}H_{26}O_6$	-249.9	0.649
Paraffin	$C_{20}H_{42}$	-110.42	0.9

Table 3: Stoichiometric Oxidizer to Fuel Ratios By Mass

Propellants	Stoichiometric Oxidizer to Fuel Ratio
Beeswax + Oxygen	3.32
Beeswax + Nitrous Oxide	9.13
Lard + Oxygen	1.96
Lard + Nitrous Oxide	5.39
50/50 Lard/Paraffin + Oxygen	2.71
50/50 Lard/Paraffin + Nitrous Oxide	7.45
Beeswax + 5% Al + Oxygen	3.19
Beeswax + 10% Al + Oxygen	3.08
Beeswax + 15% Al + Oxygen	2.96
Beeswax + 20% Al + Oxygen	2.83

The following chemical equations for the combustion were used:

$$C_{46}H_{92}O(s) + 68.5O_2(g) \rightarrow 46CO_2(g) + 46H_2O(g) \tag{4}$$

$$C_{46}H_{92}O(s) + 137N_2O(g) \rightarrow 46CO_2(g) + 46H_2O(g) + 137N_2(g) \tag{5}$$

$$C_{15}H_{26}O_6(s) + 18.5O_2(g) \rightarrow 15CO_2(g) + 13H_2O(g) \tag{6}$$

$$C_{15}H_{26}O_6(s) + 37N_2O(g) \rightarrow 15CO_2(g) + 13H_2O(g) + 37N_2(g) \tag{7}$$

$$C_{15}H_{26}O_6(s) + 1.07C_{20}H_{42}(s) + 51.33O_2(g) \rightarrow 36.53CO_2(g) + 35.6H_2O(g) \tag{8}$$

$$C_{15}H_{26}O_6(s) + 1.07C_{20}H_{42}(s) + 10265N_2O(g) \rightarrow 36.53CO_2(g) + 35.6H_2O(g) + 10265N_2(g) \tag{9}$$
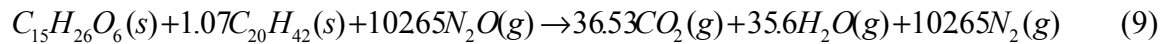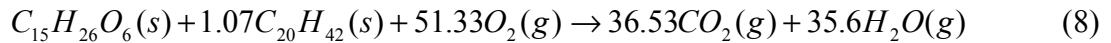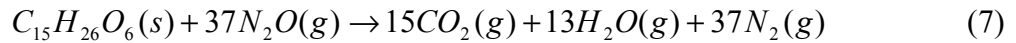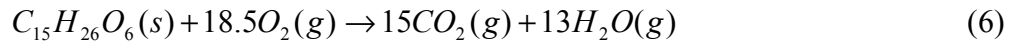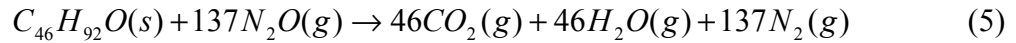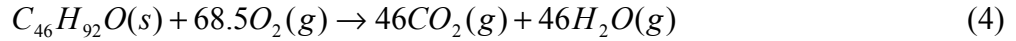
Eqs. 4 and 5 represent the combustion of beeswax with oxygen and nitrous oxide,

respectively. Similarly, Eqs. 6 and 7 represent the combustion of lard. Eqs. 8 and 9

illustrate the combustion of a mixture of 50% lard and 50% paraffin. For the addition of

aluminum, various percentages of aluminum by weight were added to the beeswax. A

range of 5% - 20% of aluminum by mass was chosen for analysis (2).

III. ANALYTICAL RESULTS

III.I Results for $P_c = 150$ psig

The first set of analytical data was examined at a combustion chamber pressure of 150 psig in order to allow for comparison with the experimental data. Individual plots of temperature, specific impulse, ratio of specific heat, and combustion products molecular mass vs. equivalence ratio are given in Appendix A. Table 4 below shows the maximum temperature and vacuum specific impulse for each of the fuel/oxidizer combinations that were analyzed. Vacuum specific impulse is the resulting Isp if the rocket was exhausting into a vacuum as opposed to the atmosphere. There are several conclusions that can be gleaned from Table 4. Beeswax with the addition of aluminum has the highest maximum temperature, with the temperature increasing as the percentage of aluminum increases. Beeswax, the lard/paraffin mixture, and lard with oxygen have the next highest temperatures, in that order. It is worth noting that adding 20% aluminum by mass only increases the maximum temperature by 118 K over no aluminum. Beeswax, the lard/paraffin mixture, and lard with nitrous oxide have the next lowest maximum temperatures, respectively. These relationships can be seen in Figure 2. It can be determined from Figure 2 that the maximum temperature occurs at an equivalence ratio of approximately 0.8.

It should be noted that the temperatures listed in Table 4 are the temperatures in the combustion chamber and not at the nozzle exit. The temperature at the nozzle exit will be much less than the chamber temperature due to expansion through the nozzle. For example, the combustion chamber temperature for a typical equivalence ratio (i.e. 0.3) in the experimental testing would be approximately 1657 K as read from Figure 2.

18

Table 4: Temperature and Specific Impulse Results, Pc = 150 psig

Propellants	Maximum Temperature (K)	Maximum Isp (s)
Beeswax + Gaseous Oxygen	3462	267
Lard + Gaseous Oxygen	3355	250
50/50 Lard/Paraffin + Gaseous Oxygen	3416	260
Beeswax + Nitrous Oxide	3237	237
Lard + Nitrous Oxide	3168	231
50/50 Lard/Paraffin + Nitrous Oxide	3210	234
Beeswax + 5% Al + Gaseous Oxygen	3482	266
Beeswax + 10% Al + Gaseous Oxygen	3518	266
Beeswax + 15% Al + Gaseous Oxygen	3549	268
Beeswax + 20% Al + Gaseous Oxygen	3580	269
Paraffin + Gaseous Oxygen	3447	223
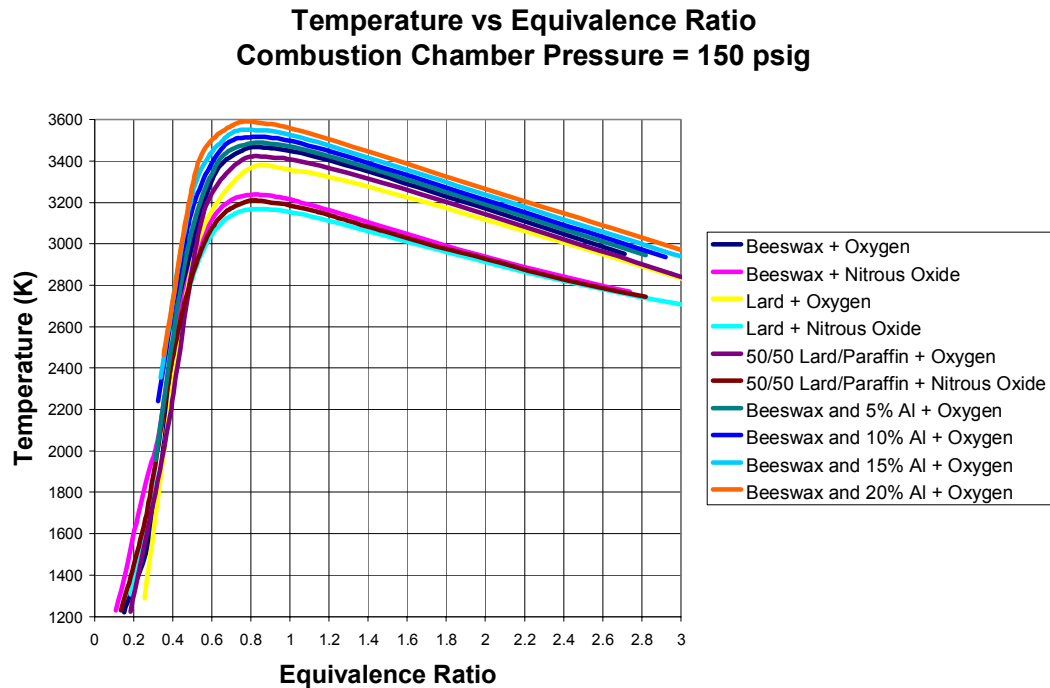
Figure 2: Comparison of Temperature vs. Equivalence Ratios, P_c = 150 psig

At this same equivalence ratio, the ratio of specific heats is approximately 1.3 from Appendix A. Based on the expansion ratio of the nozzle, the exit plane Mach number is approximately 2.3. Using these parameters and assuming frozen flow in the nozzle, the ratio of combustion chamber temperature to exit plane temperature can be calculated from Eq. 10:

$$\frac{T_0}{T_e} = 1 + \frac{\gamma - 1}{2} M_e^2 \tag{10}$$

where T_0 is the combustion chamber temperature, T_e is the exit temperature, M_e is the exit plane Mach number, and γ is the ratio of specific heats (29). In this example, the resultant ratio of chamber temperature to exit temperature is 1.8. This yields an exit plane temperature of approximately 920 K.

Figure 3 shows a similar comparison between the fuel/oxidizer combinations for vacuum specific impulse. It is interesting to note the behavior when aluminum is added to beeswax and burned with oxygen. The I_{sp} is virtually the same with no aluminum added as with any level of aluminum addition considered. Previous analysis has shown that addition of aluminum to traditional hybrid solid fuels actually decreases the specific impulse because the molecular weight of the exhaust products is increased, which negates the increase in the temperature (2).

When determining the specific impulse of an ideally expanded rocket motor, the main driver is the exhaust velocity. Eq. 11 shows the dependence of the exit velocity on the chamber temperature and the molecular mass of the combustion products

Vacuum Specific Impulse vs Equivalence Ratio
(Frozen Flow, P_c = 150 psig)
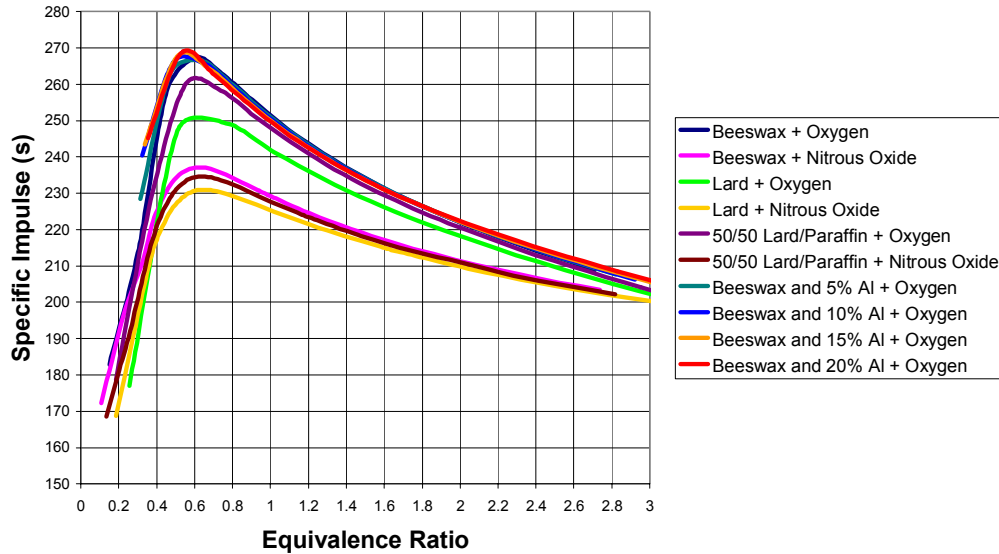
Figure 3: Comparison of Vacuum Specific Impulse vs. Equivalence Ratio, P_c = 150 psig

$$V_e = \sqrt{\frac{2\gamma R_u T_0}{(\gamma-1)M}\left\{1-\left(\frac{P_e}{P_0}\right)^{\frac{\gamma-1}{\gamma}}\right\}} \qquad (11)$$

where V_e is the nozzle exit velocity, γ is the ratio of specific heats, T_0 is the combustion

chamber temperature, M is the combustion products average molecular mass, R_u is the

universal gas constant, P_e is the nozzle exit plane pressure, and P_0 is the combustion

chamber pressure. For our case, the maximum I_{sp} occurs at an equivalence ratio of

approximately 0.6. This is roughly the optimal equivalence ratio to operate a rocket

motor (1). It is interesting to note that as more aluminum is added, the equivalence ratio

where the maximum I_{sp} occurs tends to shift to the left. The reason the equivalence ratio

where the maximum I_{sp} occurs is shifted to the left as compared to where the maximum

21

chamber temperature occurs is due to Eq. 11. Eq. 11 is a function of chamber

temperature, molecular mass of the combustion products, and the ratio of specific heats.

Figures 4 and 5 show the behavior of the average molecular mass of the combustion

products and the ratio of specific heats as a function of the equivalence ratio for beeswax

and oxygen, respectively. The molecular mass clearly increases as the equivalence ratio

increases. The ratio of specific heats decreases as the equivalence ratio increases.

However, the change in the absolute value is not significant enough to overcome other

terms in Eq. 11. It is the combination of these factors that shifts the equivalence ratio to

the left for the maximum Isp. The best way to illustrate this is to plot the ratio of the

combustion temperature to the molecular mass of the combustion products. This is the

dominant term in Eq. 11 for determining where the maximum Isp occurs.

Combustion Products Molecular Mass vs Equivalence Ratio
Beeswax and Oxygen (P$_c$ = 150 psig)
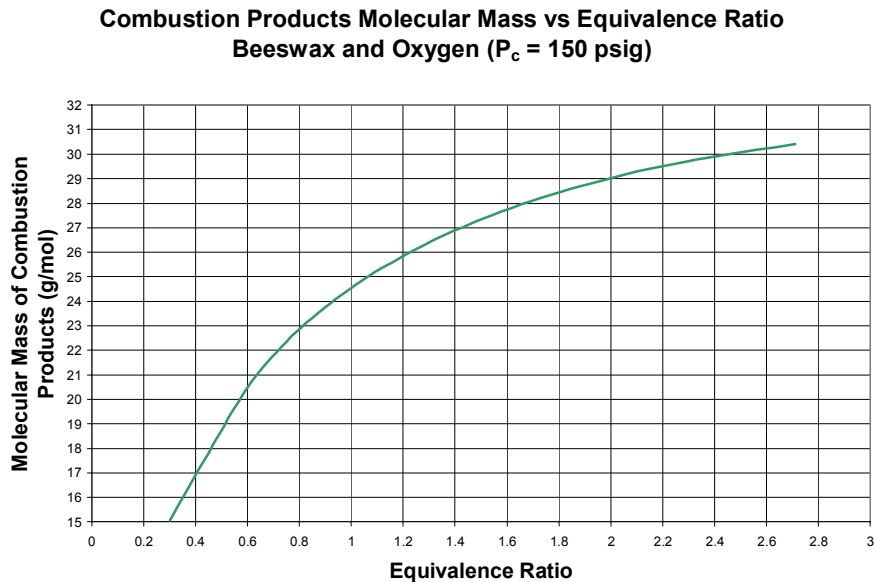
Figure 4: Molecular Mass vs. Equivalence Ratio, P$_c$ = 150 psig

Ratio of Specific Heats vs Equivalence Ratio
Beeswax and Oxygen (P$_c$ = 150 psig)
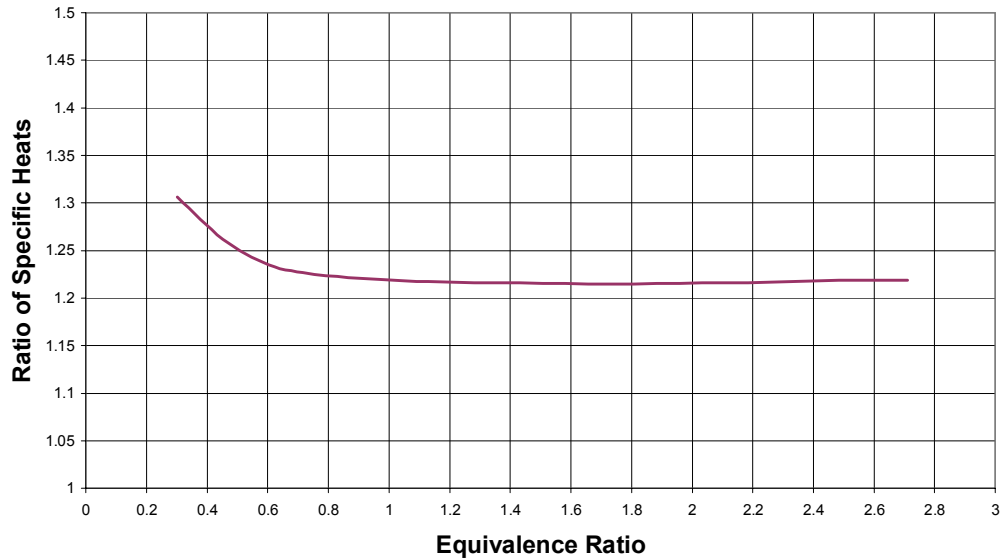
Figure 5: Ratio of Specific Heats vs. Equivalence Ratio, P$_c$ = 150 psig

As can be seen from Figure 6, the maximum of the ratio of temperature to molecular

mass occurs at an equivalence ratio of approximately 0.6. This is exactly where the I$_{sp}$

curve is at its maximum.

From Figure 7, we can see the behavior of the ratio of specific heats vs

equivalence ratio for various propellant combinations. The combinations using nitrous

oxide have the highest values. Several trends are noticeable in the figure. As the

percentage of aluminum increases, the ratio of specific heats decreases. The curve of the

lard/paraffin mixture with oxygen is almost identical to the beeswax plus 5% aluminum

with oxygen curve. The curve for lard plus oxygen is also very close to the curve for

beeswax plus 10% aluminum with oxygen.

23
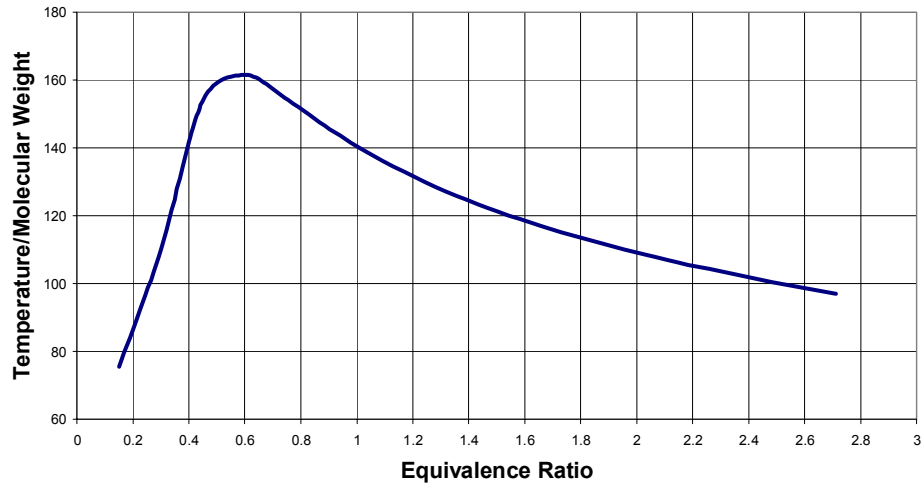
Figure 6: Ratio of Temperature to Molecular Mass vs. Equivalence Ratio, $P_c = 150$ psig

Figure 7: Comparison of Ratio of Specific Heats, $P_c = 150$ psig

In Figure 8, the average molecular mass of the combustion products are shown versus equivalence ratio for various propellant combinations. As expected, the molecular mass increases as the addition of aluminum to beeswax increases from zero to 20%. The three curves for nitrous oxide as the oxidizer behave somewhat differently than those for oxygen. These curves seem to be asymptotically approaching a value between 29 and 30 g/mol as the equivalence ratio increases. It is unclear from the range of equivalence ratios studied here if the molecular mass of the fuel/oxidizer combinations using oxygen will asymptotically approach some value as the equivalence ratio continues to increase.

Combustion Products Molecular Mass vs Equivalence Ratio
(P_c = 150 psig)
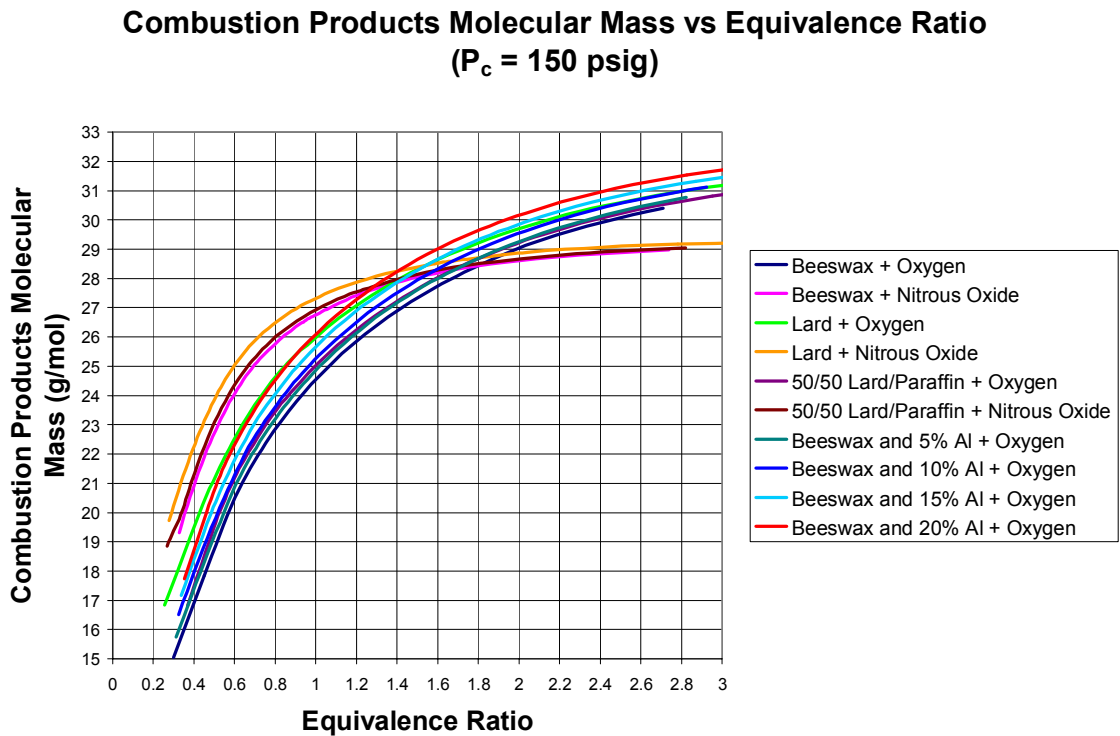
Figure 8: Comparison of Molecular Mass, P_c = 150 psig

III.II Results for P_c = 500.38 psig

A second set of analytical data was calculated for a combustion chamber pressure of 500.38 psig (3.45 MPa) to allow for comparison to previously published data for more traditional hybrid rocket motors. In addition to the change in combustion chamber pressure, the nozzle exit pressure was changed to 2.0 psig to match the conditions that the data in Reference 1 were calculated for. Appendix B contains plots for temperature, vacuum specific impulse, ratio of specific heats, and molecular mass of the combustion products. The traditional hybrid propellant combinations used for comparison were HTPB/hydrogen peroxide, HTPB/LOX, and HTPB/nitrogen tetroxide. These three oxidizers are good oxidizers but have significant safety and handling issues (2). The hydrogen peroxide considered is 90 % hydrogen peroxide and 10% water. Hydrogen peroxide is toxic and a fire hazard. LOX is cryogenic, not easily storable, difficult to handle, and an explosive hazard. Nitrogen tetroxide is the most common storable oxidizer in the U.S., but has toxic fumes.

A limited validation study was performed to evaluate the accuracy of the Isp code. Three propellant combinations were examined: kerosene/LOX, liquid hydrogen/LOX, and UDMH/LOX. The maximum temperature and sea level specific impulse were found at a combustion chamber pressure of 1000 psig from Reference 30. The Isp code was used to calculate the maximum temperature and sea level specific impulse at the same combustion chamber pressure. A summary of the results can be seen in Table 5. The largest difference (3.8%) was in the maximum temperature of liquid hydrogen/LOX.

Table 5: Known vs. Calculated Maximum Temperatures and Sea Level Isp

Propellant Combination	Kerosene/LOX	Liquid Hydrogen/LOX	UMDH//LOX
Optimal O/F Ratio	2.29	5.0	1.38
Known Max. Temperature (K)	3540	3425	3460
Isp Code Max. Temperature (K)	3577	3295	3460
% Difference in Temperature	1.0	3.8	0.4
Known Max. Isp (sec)	289	381	297
Isp Code Max. Isp (sec)	285	378	299
% Difference in Isp	1.4	0.8	0.7

The maximum temperatures and vacuum specific impulses for the analyzed fuel/oxidizer combinations are shown in Table 6. The same trends are evident in the data at 500.38 psig as in the data at 150 psig. The average temperature increase due to increasing the chamber pressure from 150 psig to 500.38 psig was 168.9 K. The corresponding average increase in the vacuum specific impulse was 52.5 s. These are relatively small increases when compared to the large increase in the combustion chamber pressure. The comparison of the temperatures in Table 6 is shown in Figure 9. The propellant combinations using oxygen as the oxidizer resulted in higher temperatures than when using nitrous oxide. Regardless of the oxidizer, beeswax produced the highest temperature and lard produced the lowest except for HTPB/hydrogen peroxide and HTPB/nitrogen tetroxide. As the amount of aluminum added to the beeswax increases, the temperature increases. Similarly to the data at a pressure of 150 psig, the maximum temperature at 500.38 psig occurs at an equivalence ratio of approximately 0.8. Also shown in Table 6 are other propellant combinations. Maximum temperatures for liquid oxygen combined with kerosene and liquid hydrogen are shown as taken from reference 1. Also shown is the maximum temperature of paraffin with gaseous oxygen, beeswax with liquid oxygen, and UDMH with liquid oxygen as computed using the Air Force Specific Impulse Code. These temperatures are all in the range of 3500 K to 3630 K, and are very similar to the temperatures given for the non-conventional propellants analyzed in this study. These results support the validity of the maximum combustion chamber temperatures presented in Table 5 for the propellant combinations considered here.

The results for the vacuum specific impulse behave similarly to the temperature, except the maximum occurs at an equivalence ratio of 0.6. The propellant combinations

Table 6: Temperature and Specific Impulse Results, P_c = 500.38 psig

Propellants	Maximum Temperature (K)	Maximum Isp (s)
Beeswax + Gaseous Oxygen	3650	327
Lard + Gaseous Oxygen	3524	308
50/50 Lard/Paraffin + Gaseous Oxygen	3600	303
Beeswax + Nitrous Oxide	3365	286
Lard + Nitrous Oxide	3288	280
50/50 Lard/Paraffin + Nitrous Oxide	3328	271
Beeswax + 5% Al + Gaseous Oxygen	3670	312
Beeswax + 10% Al + Gaseous Oxygen	3711	328
Beeswax + 15% Al + Gaseous Oxygen	3747	328
Beeswax + 20% Al + Gaseous Oxygen	3783	330
Paraffin + Gaseous Oxygen	3630	307
Beeswax + Liquid Oxygen	3606	326
Traditional Propellants		
HTPB + Hydrogen Peroxide	2802	298
HTPB + Liquid Oxygen	3669	318
HTPB + Nitrogen Tetroxide	3450	297
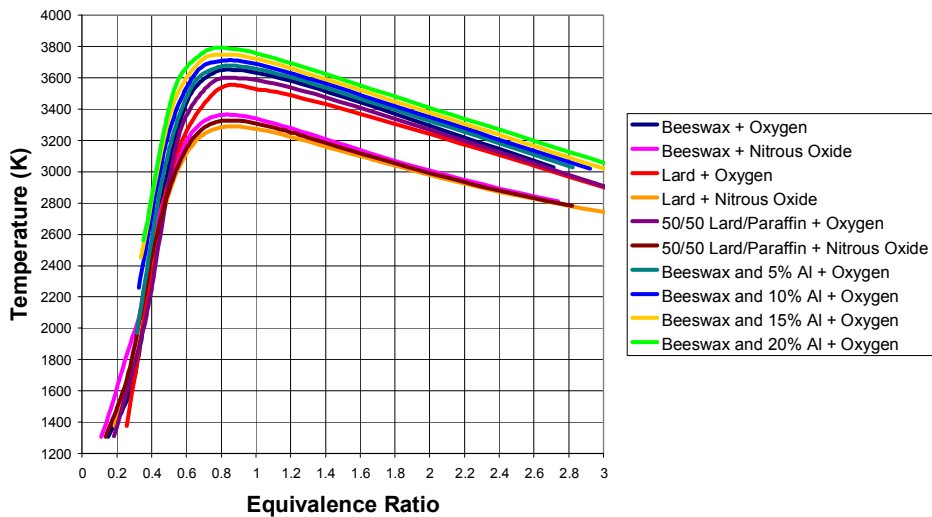
Figure 9: Temperature vs. Equivalence Ratio, Pc = 500.38 psig

using oxygen had higher vacuum specific impulse values than when using nitrous oxide. Beeswax had the highest vacuum specific impulse followed by the lard/paraffin mixture, and then lard. When 5% aluminum was added to the beeswax, it reduced the specific impulse by 15 s. When the amount of aluminum is increased to 10% and 15%, the specific impulse rises to 1 s above the value achieved with no aluminum. At 20% aluminum, the specific impulse rises to 3 s about the value achieved with no aluminum. These trends can be seen in Figure 10.

While the contribution of aluminum shows the potential for slight improvements in the vacuum specific impulse, the negative effects of using aluminum would likely negate this advantage. When using an aluminized propellant, such as in solid rocket motors, there is significant nozzle erosion due to impingement of aluminum oxide particles with the nozzle walls. If severe enough, this erosion can cause failure of the
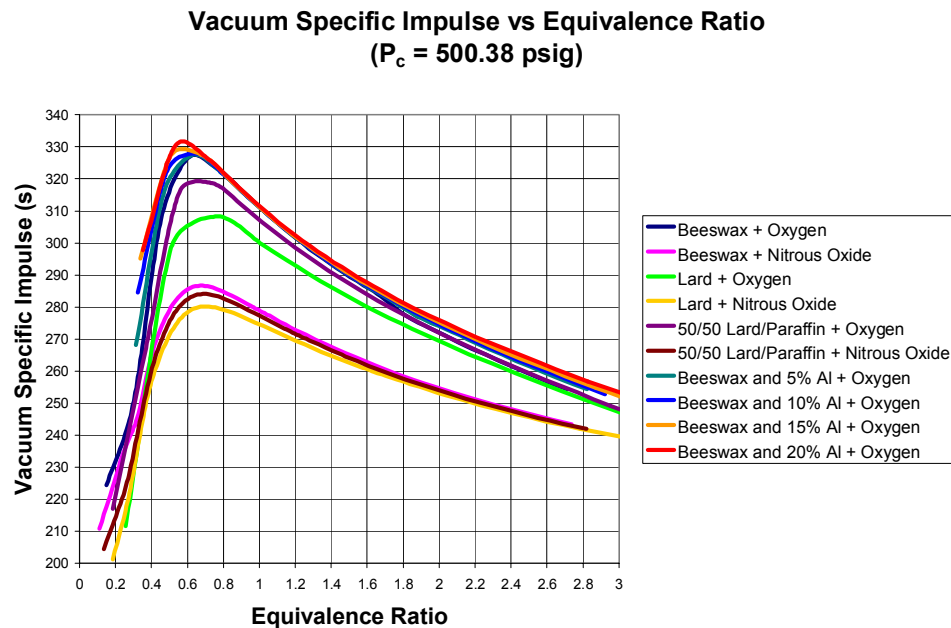
Figure 10: Vacuum Specific Impulse vs. Equivalence Ratio, Pc = 500.38 psig

30

nozzle. Another effect is that using an aluminized propellant usually results in two-phase flow in the nozzle. As the gas flow expands through the nozzle, the temperature of the gas can decrease considerably depending on the expansion ratio of the nozzle, which could results in liquid droplets condensing out of the gas flow. The presence of liquid droplets in the exhaust flow reduces the specific impulse of the rocket. This is due to the energy available to accelerate the gas flow being absorbed by the heavier liquid droplets. These effects are not reproduced by the Isp code, but should be considered when adding aluminum to a propellant.

The HTPB/LOX combination has a higher maximum temperature than all of the propellant combinations analyzed except when aluminum is added to beeswax. The difference between the maximum temperature for HTPB/LOX and beeswax/oxygen is only 19 K. However, the maximum specific impulse for beeswax/oxygen is 9 s higher than for HTPB/LOX. Beeswax/oxygen produces higher chamber temperatures and specific impulses than either HTPB/hydrogen peroxide or HTPB/nitrogen tetroxide. When comparing the propellant combinations using nitrous oxide as the oxidizer, all three have a lower maximum temperature than HTPB/LOX and HTPB/nitrogen tetroxide. All three combinations have a higher temperature than HTPB/hydrogen peroxide. When the maximum vacuum specific impulse is compared, all the propellant combinations using nitrous oxide produced lower specific impulses than the three traditional propellant combinations using HTPB.

These results indicate that beeswax/oxygen should produce the best performing hybrid rocket motor when compared to the traditional hybrid rocket propellants. While the performance between beeswax/oxygen is very close to HTPB/LOX, using gaseous

oxygen is much more convenient than using LOX. There are several factors to consider when evaluating what propellants to use: performance, toxicity, ease of handling, and public acceptability. Given the small performance differences between the propellants considered here, beeswax and gaseous oxygen compare well as potentially new hybrid rocket motor propellants.

IV. DESCRIPTION OF EXPERIMENTAL PROGRAM

<u>IV.I Description of Test Facility</u>

The hybrid rocket test facility is located on the University of Tennessee Agricultural Research Land site just south of the University of Tennessee campus in Knoxville, Tennessee. The test facility consists of a test stand, a storage building, and a safety wall. Figure 11 illustrates the setup of the test site. The safety wall was constructed to act as a barrier to protect individuals in case of a mishap. The wall is constructed of pressure treated wood and filled with sand. Its dimensions are ten ft. long by two and a half ft. thick by six ft. high. The interior of the wall contains approximately six tons of sand. The storage building is used to securely store the test stand, power generator, oxidizer and propane tanks, and other test equipment. Due to the remote nature of the test site, a generator is used to provide electricity for the instrumentation, electric solenoids, and computers.

The test stand consists of a support cage containing the rocket motor mounted on a transportable steel table as illustrated in Figure 12. The solid fuel is formed in a steel cylinder which has a 3 in. outer diameter, is 0.25 in. thick, and is 10 in. long. The combustion port diameter of all motors tested was 0.5 in. The cylinder is held in place by six, 3/8 in. diameter bolts. At the inlet end, there is a steel injector end cap which houses the spark plug for ignition. The oxidizer and propane lines both feed into the steel inlet end cap. When the test is initiated, solenoid valves on the propane and oxidizer lines are both opened, and the spark plug is fired. A flow diagram of the test setup can be seen in Figure 13.

33
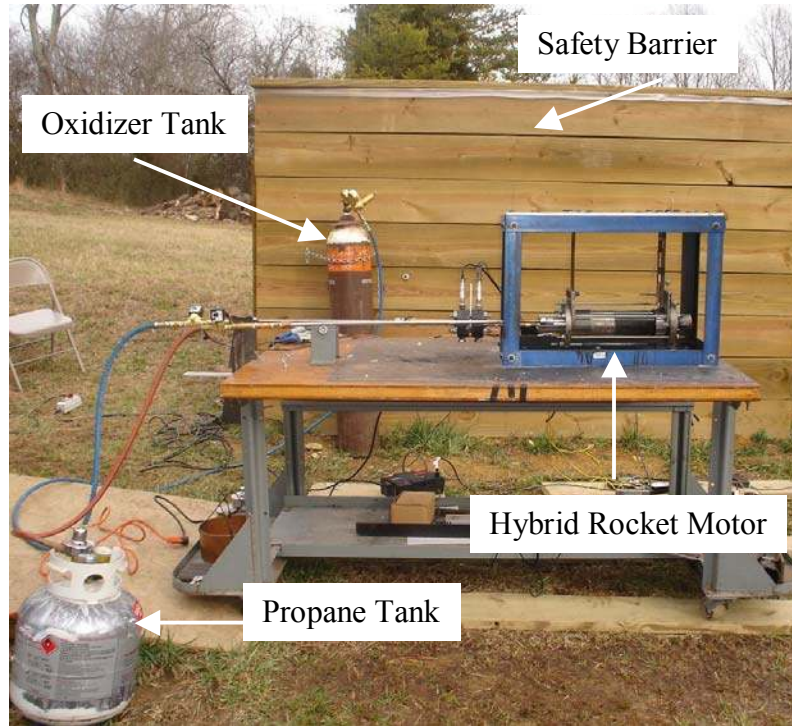
Figure 11: Test Site Setup
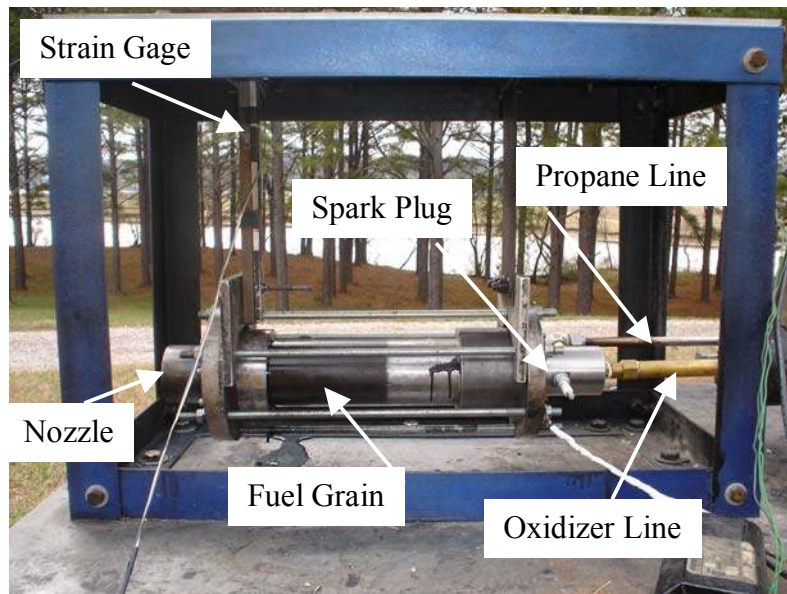
Figure 12: Test Stand
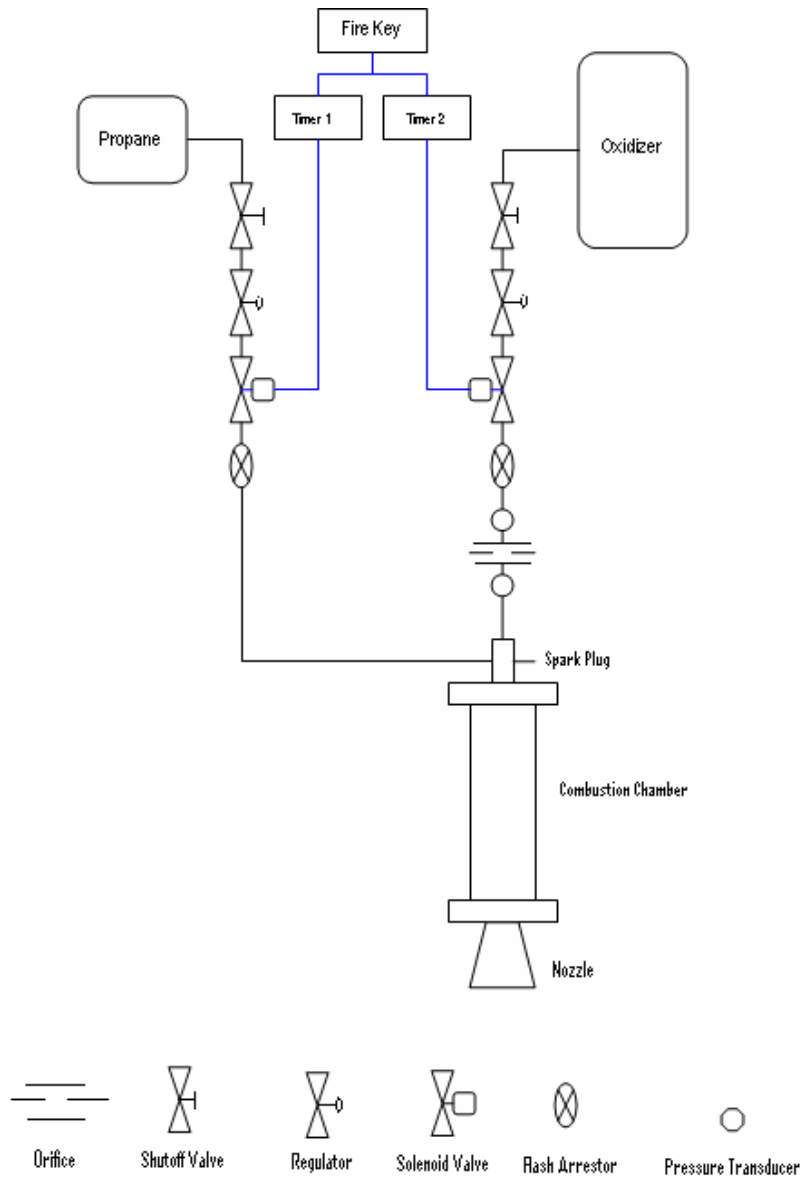
Figure 13: Flow Diagram of Hybrid Rocket Motor

The propane/oxidizer mixture is ignited by the spark plug and provides the initial heat of vaporization to the fuel. The propane solenoid valve and spark plug are both controlled by a single timer, and they are typically on for 0.5 s. The oxidizer solenoid is controlled by a separate timer, which typically runs for 5 to 7 s. At the end of the test, the timer automatically closes the oxidizer valve. The propane is supplied at 80 psig, and the oxidizer is supplied in a range of 200-500 psig by a regulator. The nozzle end cap houses a converging-diverging nozzle made of graphite. As indicated in Figure 3, a strain gage is attached to the aft cantilever support beam in order to measure thrust during the testing. The strain gage is calibrated before every test to determine the relationship between the voltage output of the strain gage and the thrust produced by the rocket motor. Calibrating the strain gage every test eliminated the need to determine the effect of environmental conditions (i.e. ambient temperature) on the thrust measurements. The calibration was accomplished by placing weights in a bucket which loaded the strain gage and then recording the corresponding voltages (see Figure 14 for an illustration of the calibration setup). The range of weights used in the calibration covered the range of thrust values measured during the testing.

Figure 14: Calibration Setup

Figure 15 shows an example of a test calibration. The curvefit from the calibration data

was used to convert the voltages from the strain gage to forces. Pressure in the

combustion chamber is measured using the pressure transducer positioned downstream of

the orifice plate, which is just upstream of the oxygen inlet into the combustion chamber.

A restrictor plate was added after problems arose with combustion occurring on the inlet

surface of the fuel grain, which led to burning along the outside of the fuel grain. The

pressure transducers used were Omega PX603s which have an accuracy of $\pm$ 0.4% of the

full span, which was 1000 psig. Prior experimentation has shown that the pressure

measured downstream of the orifice plate is identical to the pressure measured at the

nozzle end of the combustion chamber (30). Unfortunately, due to budget restrictions,

the pressure difference across the orifice plate to compute the oxidizer mass flow rate had

to be determined using the same pressure transducers.

Calibration Curve
Test 169

$$y = 516.33x - 3.4076$$
$$R^2 = 0.9907$$
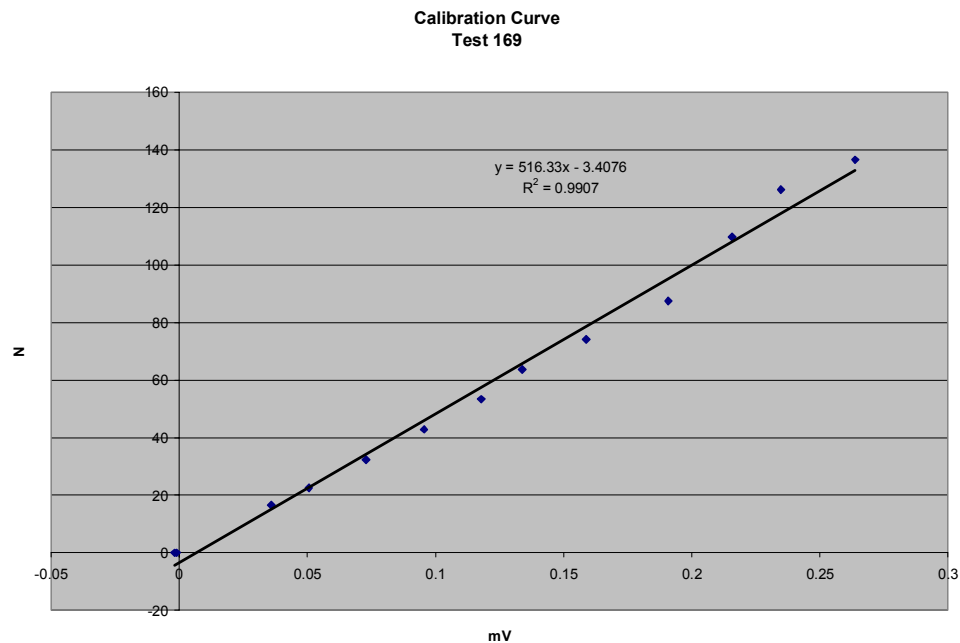
Figure 15: Example of Calibration Curve

37

The nozzle is a converging-diverging type designed to have an exit pressure of 14.7 psig for a combustion chamber pressure of approximately 150 psig. For ease of fabrication, the nozzle uses a simple conical design. It is constructed out of graphite to prevent degradation due to the high temperature. The nozzle is 2.0 in. long with the converging section being 0.53 in. long and a diverging section that is 1.47 in. long. The inlet, throat, and exit diameters are 1.4 in., 0.35 in., and 0.53 in., respectively. The ratio of the exit area to the throat area is 2.312, which results in an exit Mach number of approximately 2.3, assuming a value of 1.3 for the ratio of specific heats. The goal of the nozzle design is to reduce the effect of pressure thrust on the thrust data.

IV.II Mass Flow Rate Uncertainty

Table 7 shows the uncertainty analysis of the oxidizer mass flow rate for test 176 as an example. The absolute value of the range of uncertainties between the two worst case scenarios in the measurement of the mass flow rate is 18 – 28%. Due to this significant uncertainty, the equivalence ratios computed in this study also have a large amount of uncertainty. Due to the large uncertainty in the oxidizer mass flow rate measurement, an attempt was made to evaluate the uncertainty more accurately. A test was run with only oxidizer flowing through the system at an average upstream pressure of 106 psig for approximately 44.5 s. The change in mass of the oxidizer tank during the test was 1.9 kg ± 0.1 kg resulting in an average oxidizer mass flow rate of 0.043 kg/s ± 0.002 kg/s. The oxidizer mass flow rate calculated from the pressure transducer data was 0.038 kg/s, which resulted in a difference of 11% ± 4.7%. This indicated that the actual uncertainty in the oxidizer mass flow rate is less than the theoretical uncertainty due to the pressure transducers. The other source of uncertainty is the possible spallation of

solid particles or liquid droplets of fuel exiting the nozzle without being burned. The ejection of this unburned fuel increases the calculated regression rate without contributing significantly to the thrust produced. Table 8 shows the uncertainties in the instrumentation used in the experimentation. All of the instrumentation was wired into a Minilab 1008 A/D converter and connected to a laptop via USB cable. The Minilab 1008 has 8 channels of 12-bit analog input; however only three channels were used: two for the pressure transducers and one for the strain gage. The data was collected by the laptop computer using the Hewlett Packard Visual Engineering Environment (HP VEE) software. Mass measurements of the fuel grains were taken on a digital scale with 1 gram resolution before and after each test.

Table 7: Oxidizer Mass Flow Rate Uncertainty Estimate for Test 176

	Upstream Pressure (psig)	Downstream Pressure (psig)	Pressure Difference (psig)	Oxidizer Mass Flow Rate (kg/s)	% Difference
Low Case	219	210	9	0.0237	28
Experimental Value	223	206	16	0.0331	N/A
High Case	227	202	25	0.0392	18

Table 8: Uncertainties in Instrumentation

Instrument	Accuracy
Scale	1 gram resolution
Strain Indicator	0.1% (full scale)
Timers	1% (set scale)
Pressure Transducers	0.4% (full scale)

IV.III Testing Procedure

The beeswax fuel grains were produced by melting down bulk beeswax bricks and pouring the beeswax into the steel cylinders. The standard yellow beeswax was purchased from the Southeast Texas Honey Company. The cylinders were placed in wooden stands which hold the cylinders vertically and hold a polished steel rod firmly in the center of the cylinder. The steel rod, which is 0.5 in. diameter, is for forming the combustion port in the grain. The wooden base is constructed to produce a space at the end of the grain 1.875 in. long to act as an aft mixing chamber. The purpose of the aft mixing chamber is to allow the gasified propellants to complete the combustion process as much as possible before exiting the motor. If the nozzle entrance were immediately at the end of the fuel grain, it is unlikely that the combustion process would be complete. The common range of length-to-diameter (L/D) ratios for the aft mixing chamber is 0.5 - 1.0 (1). In this research, the aft mixing chamber had a L/D of 0.75. The liquid beeswax was poured in the cylinder to the top, and a metal cap was placed on top to hold the steel rod in the center while the beeswax cooled. The beeswax was allowed to cool and solidify at room temperature. The cylinder was removed from the wooden stand, and the steel rod hammered out. The fuel grain was then inspected for cracks, and if cracks are present, the grain was melted down, and the fabrication process was repeated.

The testing procedure was established to ensure safety of the experimentation and to eliminate mistakes that could result in a test failure. A test supervisor, range safety supervisor, and calibration supervisor are designated prior to the test. The test supervisor has overall responsibility for the safety of the testing. The calibration supervisor is responsible for the calibration of the strain gage. The range safety supervisor is

40

responsible for certifying that the area is clear before the test is initiated. The test stand is rolled out of the storage building, and the wheels are blocked to prevent the table from moving during a test. Once the test stand is secured, the generator is started, and all electrical systems (instrumentation, solenoid valves, computers, etc.) are setup. A fire extinguisher is placed on the personnel side of the safety barrier in case of fire during a test. The fuel grain is weighed, and the weight is recorded. The inlet section is then examined for any traces of fuel that could possibly cause a fire during a test. If any fuel is present, the section is disassembled and cleaned before the test can be run. Then the propane and oxidizer lines are inspected for leaks. The flow restrictor plate is then installed in the inlet section. The restrictor plate has a hole the same diameter as the combustion port (0.5 in.). The purpose of the restrictor plate is to confine the oxidizer flow to the combustion port. The fuel grain is inserted into the test stand, and the bolts are tightened evenly to prevent leakage during the test. At this point, all personnel except for the test supervisor and calibration supervisor are evacuated to behind the safety wall. The test supervisor pressurizes the oxidizer and fuel lines by opening the supply valves. The calibration supervisor then calibrates the strain gage. Once the calibration is completed, the test supervisor ensures the oxidizer regulator is set to the desired pressure and verifies that the propane and oxidizer timers are set properly. The calibration supervisor then evacuates to the other side of the safety wall. The spark plug is then connected, and the video recording systems is started by the test supervisor. The test supervisor moves behind the safety wall, and the data recording system is activated. The range safety supervisor then informs the test supervisor when the area is clear for the test. The firing switch is plugged in, the firing switch is switched from safe to fire mode, and

then the fire button is pressed by the test supervisor to initiate the test. When the test

terminates, the firing switch is turned back to safe and is unplugged. The firing switch is

only plugged in for the duration of the test to prevent inadvertent opening of the solenoid

valves. The video recording system and data recording system are both stopped. The test

supervisor approaches the test stand and disconnects the spark plug. At this point, the

test stand is safe to approach by personnel. After the fuel grain has had at least 5 minutes

to cool down, it is removed from the test stand and weighed, and the weight is recorded.

IV.IV Data Analysis

The regression rate (or burn rate) of the solid fuel is defined as the rate at which

the exposed fuel surface is burned during combustion. It is measured in a direction

normal to the fuel surface (1). A time-averaged value for the regression rate in a hybrid

rocket motor can be determined by determining the change in the fuel grain thickness and

divided by the time duration of the test as shown in Eq. 12:

$$\dot{r} = \frac{t_{gi} - t_{gf}}{t_b} \tag{12}$$

where $\dot{r}$ is the regression rate, t_{gi} is the initial fuel grain thickness, t_{gf} is the final fuel

grain thickness, and t_b is the burn time. The initial grain thickness is simply measured

before a test. The average final grain thickness is determined by determining the mass of

the burned fuel and, using the known density of the fuel, calculating the average

thickness based on a change in volume of the fuel grain (16).

The mass flow rate of the oxidizer was approximated using a sonic orifice plate

and two pressure transducers as shown in Figure 16. The Omega pressure transducers

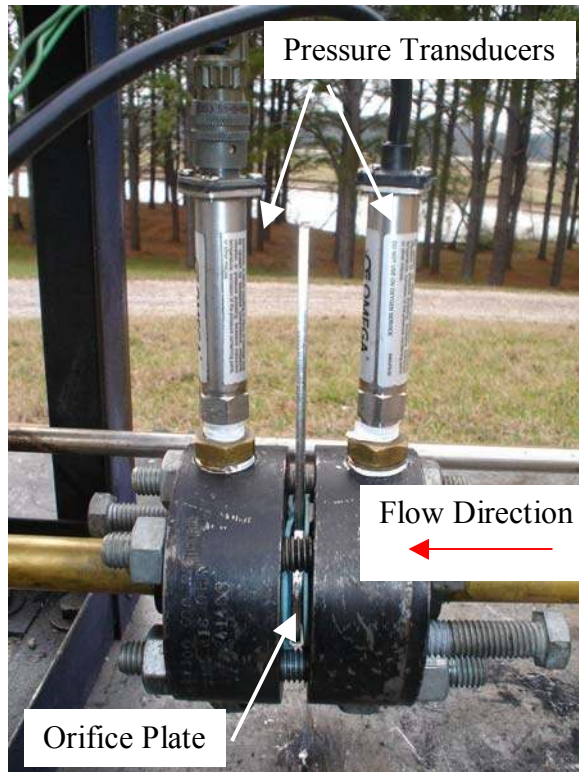have a range of 0-1000 psig and an error of 0.4%. The pressure differential across the

Figure 16: Pressure Transducers and Orifice Plate

orifice is found by measuring the pressure just upstream and immediately downstream of the orifice plate. A MATLAB code was used to create a chart of flow rate versus pressure differential using the average pressure upstream of the orifice plate. The average pressure differential, combined with the value of the upstream pressure is then used to estimate the average flow rate from the chart. Explanation of the code and the code itself can be found in Appendix C. The average mass flow rate of the fuel is estimated as the fuel mass lost during the firing divided by the test duration. A sample of the combustion pressure data is shown in Figure 17. The specific impulse is determined by dividing the total impulse by the weight of the propellant (both fuel and oxidizer) consumed. The total impulse is calculated by numerically integrating the thrust over time for the duration of the test using a simple Riemann squares approximation, and then divided by the weight of the propellant used as shown in Eq. 13:

$$I_{sp} = \frac{\sum_{i=0}^{i=t_b} \frac{1}{2}(T_{i+\Delta t} + T_i) * (t_{i+\Delta t} - t_i)}{g * m_{prop}} \tag{13}$$

where I_{sp} is the specific impulse, T_i is the current thrust value, $T_{i+\Delta t}$ is the thrust at the next time step, t_i is the current time, $t_{i+\Delta t}$ is the time at the next time step, g is the acceleration due to gravity, and m_{prop} is the mass of the propellant consumed during the burn.

The major uncertainty in the specific impulse calculation is due to the uncertainty in the oxidizer mass flow rate during the test. This, in turn, introduces uncertainty in the mass of propellant consumed. The burn time of the test is known to a high degree of certainty, as noted in Table 8. The thrust data is modified to remove any pressure thrust

Combustion Chamber Pressure vs Time
Test 173
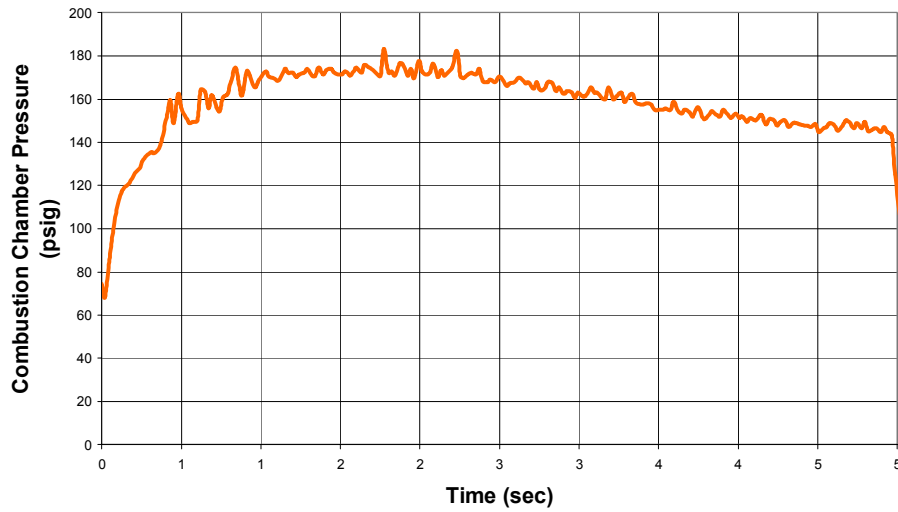
Figure 17: Sample Combustion Chamber Pressure vs. Time Data

contribution to remove any variations in the overall thrust due to the exit pressure not

expanding exactly to atmospheric pressure. An example of the thrust data collected is

shown in Figure 18. This is accomplished by estimating the exit pressure at every point

in time of a test using the combustion chamber pressure and an estimate for the ratio of

the exit pressure and the combustion chamber pressure from compressible flow dynamics

as shown in Eq. 14:

$$p_e(t) = \frac{p_e}{p_c} p_c(t) \tag{14}$$

where $p_e(t)$ is the exit plane pressure as a function of time and $p_c(t)$ is the combustion

chamber pressure as a function of time. Another reason for this thrust correction is for

comparison to the analytical data produced. The ratio of exit pressure to combustion

Thrust vs Time
Beeswax and Oxygen, Test 173
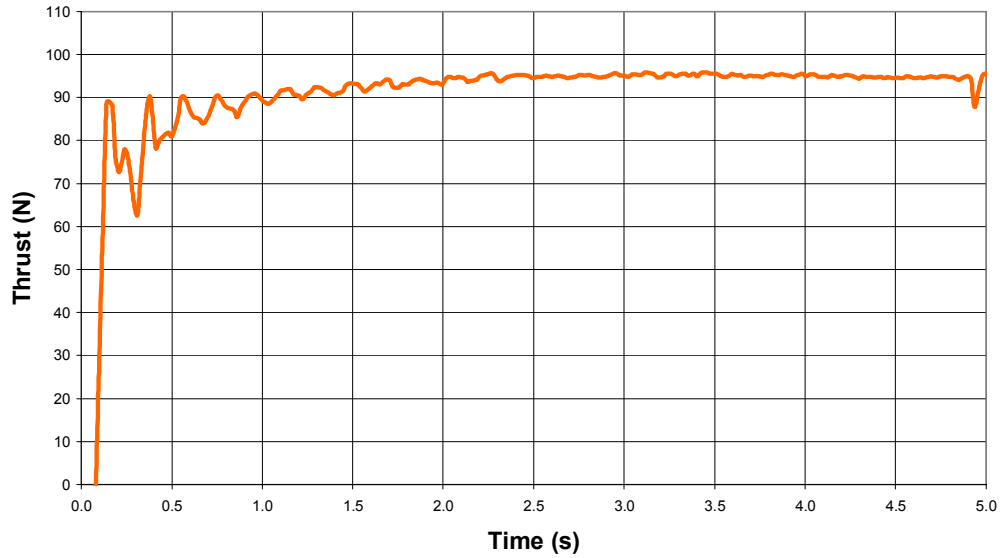
Figure 18: Sample Thrust vs. Time Data

pressure is determined from the nozzle area ratio and the value of the ratio of specific

heats (γ). The nozzle area ratio was computed using Equation 15:

$$\frac{A_e}{A_t} = \frac{\frac{\pi}{4}d_e^{\,2}}{\frac{\pi}{4}d_t^{\,2}} \qquad (15)$$

where A_e is the nozzle exit area, A_t is the nozzle throat area, d_e is the nozzle exit diameter,

and d_t is the nozzle throat diameter. The nozzle area ratio relation is then solved for the

exit Mach number for the nozzle as shown in Equation 16:

$$\frac{A_e}{A_t} = \frac{1}{M_e}\sqrt{\left\{\frac{2}{\gamma+1}\left(1+\frac{\gamma-1}{2}M_e^{\,2}\right)\right\}^{\left(\frac{\gamma+1}{\gamma-1}\right)}} \qquad (16)$$

where M_e is the nozzle exit Mach number. Using the nozzle exit Mach number and the ratio of specific heats, the ratio of combustion chamber pressure to nozzle exit pressure can be calculated as shown in Equation 17:

$$\frac{p_c}{p_e} = \left(1 + \frac{\gamma - 1}{2} M_e^{\ 2}\right)^{\frac{\gamma}{\gamma - 1}} \tag{17}$$

The value of the ratio of specific heats was determined from theoretical analysis of various fuel and oxidizer combinations at the range of equivalence ratios used in the experimental testing. Table 9 shows the values of γ and the ratio of exit pressure to combustion pressure for various fuel/oxidizer combinations for a combustion pressure of 150 psig. The regression rate is determined over a range of equivalence ratios. The equivalence ratio (α) is a measure of whether the fuel/oxidizer combination is rich, lean, or stoichiometric. For hybrid rocket motors, it is defined as the ratio of the actual oxidizer to fuel ratio divided by the stoichiometric ratio of oxidizer to fuel (Eq. 18).

$$\alpha = \frac{\left.\dfrac{O}{F}\right)_{actual}}{\left.\dfrac{O}{F}\right)_{stoichiometric}} \tag{18}$$

Given that the combustion occurs in a diffusion flame and the fuel and oxidizer are consumed at the flame front in the boundary layer where the oxidizer and fuel are at the stoichiometric ratio, the equivalence ratio still has meaning. Between the flame front and the fuel surface is a fuel rich region (31). In the space between the boundary layer surface and the flame front is an oxidizer rich region. The location of the flame front in the boundary layer is determined by the location between these two regions where the

Table 9: Pressure Ratios for Fuel/Oxidizer Combinations

Fuel/Oxidizer	γ	$P_{exit}/P_{combustion}$
Lard/O_2	1.315	0.082
Beeswax/O_2	1.306	0.083
Lard/N_2O	1.306	0.083
Beeswax/N_2O	1.304	0.083

equivalence ratio equals one. In a hybrid rocket, it is important to know the ratio of the oxidizer input to the motor and the resulting fuel that is vaporized from the grain surface. This allows for characterization of the performance of the hybrid rocket motor as a function of a parameter that the user of the rocket motor has physical control over. The main goal of the regression rate analysis is to determine the regression rate as a function a parameter or parameters that are easily controlled or measured and experimentally derived constants. Determining the regression is very important to determining the thrust produced by the motor. This is due to the mass flow rate of the fuel being directly related to the fuel regression rate.   Typical parameters used are total mass flux rate, axial distance along the port, length of the port, combustion chamber pressure, oxidizer mass flux rate, characteristic exhaust velocity, and oxidizer mass flow rate (32). At least eight different possible relations which have been tried, and previous studies have found a very low degree of dependence of regression rate on combustion chamber pressure. However, it has been shown that at the lower end of combustion pressures, there can be a reduction in the regression rate due to the radiation heat transfer dominating (1).

IV.V Costs

The total budget for this research was approximately $4500. This includes the storage building, materials to construct the safety wall, instrumentation, power generator, beeswax, lumber to construct a ramp out of the storage building, and miscellaneous parts (nuts, bolts, etc.). This budget does not include the cost of building the test stand which was constructed during the 1999-2000 school year. It also does not include the cost of items made by the department machine shop or the cost of filling the oxidizer tanks. Table 10 below shows an approximate breakdown of the costs.

Table 10: Research Program Expenses

Item	Cost
Storage Building	$1500
Power Generator	$500
Safety Wall Materials	$1000
Beeswax	$500
Miscellaneous Parts (instrumentation, hardware, electrical equipment, etc.)	$1000

V. EXPERIMENTAL RESULTS AND DISCUSSION

V.I Repeatability Study

A repeatability study was performed to determine how consistently the test stand and instrumentation performed. It is important to determine the level of repeatability in an experimental system to show the reliability of the experimental data. A high level of repeatability improves confidence in the test results. If poor repeatability is observed, test stand problems or instrumentation difficulties could be indicated.

For this study, a total of ten repeatability tests were performed in two sets of five tests.   All of the tests were run with beeswax as the fuel and gaseous oxygen as the oxidizer. The first five tests used an oxidizer supply pressure set by the regulator at 280 psig. The oxidizer supply pressure was chosen for the independent variable in the repeatability study because it is the main variable in the experimental setup that can be controlled. The second set was run at an indicated supply pressure of 500 psig. These two pressures were chosen to determine repeatability across the range of test conditions used in this study. All other conditions were identical in all of the tests. The time for the oxidizer solenoid was set at 5.0 s. The time for the propane solenoid/spark plug timer was set at 0.5 s. The thrust and combustion chamber pressure were recorded and then compared for each set of tests. Not all of the tests were run on the same day. Table 11 shows the ambient temperature on the day for each of the ten tests run.

A summary of the repeatability tests is shown in Table 12. For the tests run at a supply pressure of 280 psig, the combustion chamber pressure results are shown in Figure 19. Several observations can be made from Figure 20. While tests 123, 126, 132, and 136 are fairly close in chamber pressure, test 129 is significantly different.

50

Table 11: Ambient Temperature for Repeatability Tests

Test #	Ambient Temperature (K)
123	294
126	282
129	293
132	278
163	280
168	277
170	279
171	279
176	274
177	274

Table 12: Results for Repeatability Tests

Test #	Avg. Thrust (N)	Avg. Combustion Pressure (psig)
123	37.2	100.0
126	61.9	117.1
129	50.6	96.2
132	55.9	112.1
163	66.3	117.8
168	170.4	237.9
170	160.2	229.2
171	148.4	229.7
176	115.1	223.2
177	108.9	233.5

Also, test 126 shows a significant spike in pressure during the ignition phase. Overall, the average pressure for the five tests was approximately 102 psig with a standard deviation of 11 psig.

The thrust data for the five tests run at a supply pressure of 280 psig is shown in Figure 20. The first observable characteristic is the significant ignition transients. The first 0.5 s of each test show a large spike in the thrust which didn't begin to damp out until 1.5 s. Tests 129 and 132 were close in value and shape. These two tests are the two steadiest of the five tests. Test 126 has an oscillation with a period of approximately 1.0 s. Test 123 has an oscillation with a period of roughly 1.0 s. and an amplitude of approximately 35 N. This test is significantly different from the other four tests. Test 163 shows a general decreasing thrust during the test, but has a thrust value roughly 10 N lower than test 129. The average thrust of the fives tests was approximately 54 N with a standard deviation of 11 N.
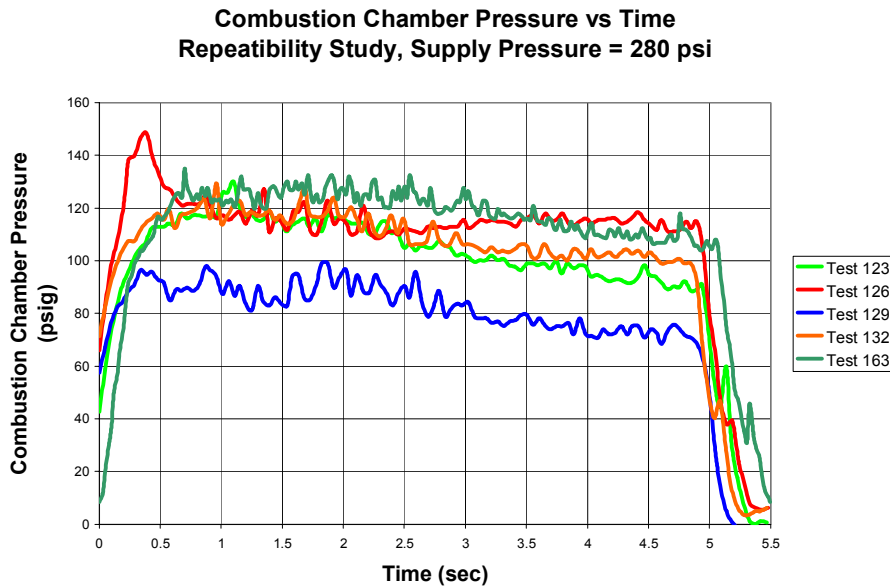

Figure 19: Comparison of Combustion Pressures, Supply Pressure = 280 psig

Thrust vs Time
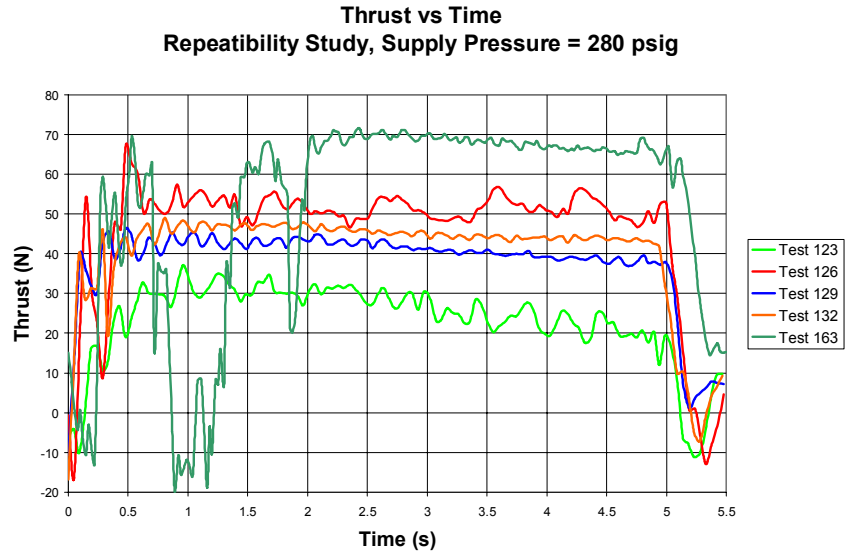**Repeatibility Study, Supply Pressure = 280 psig**

Figure 20: Comparison of Thrust, Supply Pressure = 280 psig

The combustion chamber pressure results for the five tests run with a supply pressure of 500 psig are illustrated in Figure 21. All five tests were very close in value of the pressure and trend. The average combustion chamber pressure of the fives tests was approximately 215 psig with a standard deviation of 5 psig. Overall, the combustion chamber pressure was very consistent during these five tests.

Figure 22 shows the thrust curve comparison of the five repeatability tests run with an oxidizer supply pressure of 500 psi. Compared to the combustion pressure, the thrust curves show much more dispersion. There is a large gap between tests 168, 170, trends, but the values of the thrust vary widely. Test 170 has an increasing thrust versus and 171 and tests 176 and 177. Tests 168, 171, 176, and 177 show similar constant thrust time trend, which is significantly different from the other four tests. The average thrust of the five tests was approximately 140 N and the standard deviation was 27 N. Another characteristic to note is the ignition transients and the time it took for them to damp out.

54

Figure 21: Comparison of Combustion Pressures, Supply Pressure = 500 psig
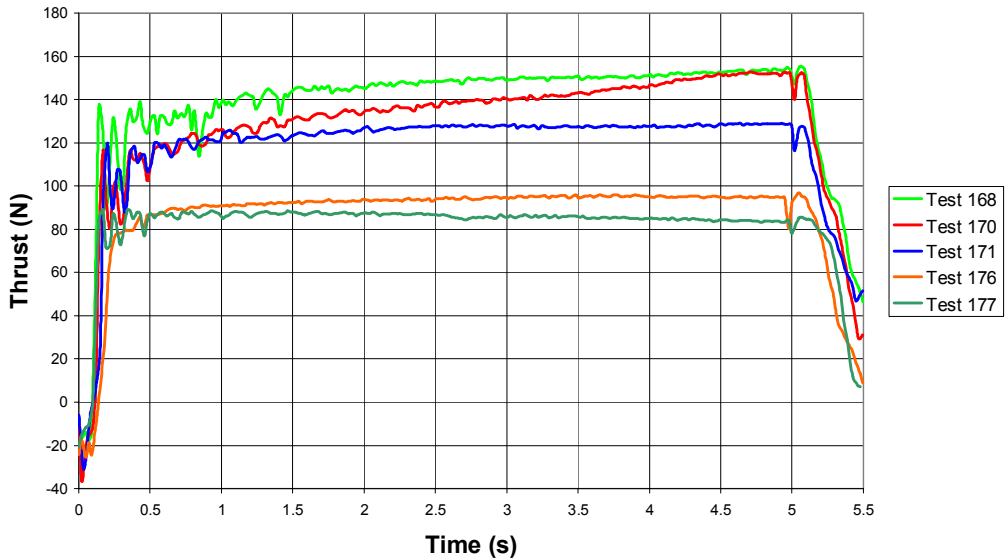

Figure 22: Comparison of Thrust, Supply Pressure = 500 psig

Tests 176 and 177 damped out the quickest. Tests 170 and 171 have very similar ignition transients despite the fact that test 170 has an increasing thrust and test 171 has a constant thrust. Test 168 had the largest ignition transients of the five tests. However, it should be noted that the ignition transients are much less severe at the higher supply pressure due to much more stable combustion.

Due to the oscillations in the thrust data, an attempt was made to determine the natural frequency of the test stand. An impulse was applied to the test stand and the response was measured. There were three such tests. The time response data from the strain gage was analyzed using a fast Fourier transform (FFT). The average natural damped frequency of the three tests was approximately 6.6 Hz.

There are several conclusions from these results. The combustion pressure becomes more repeatable as the supply pressure increases. The problems in the pressure data with the tests run at low supply pressures could be due to combustion instabilities caused by the low combustion pressures. The spikes in tests 126 and 171 are due to inconsistencies in the ignition process. This shows that the ignition process using propane and a spark plug is not always uniform. Another possible cause for variances in the value of the combustion pressures could be imprecise setting of the oxidizer supply pressure. It is quite difficult to set the same pressure on the regulator over multiple tests due to the analog pressure indicator. An illustration of this problem is seen in Figure 23. A more accurate (i.e. digital) control on the regulator could reduce some of the differences in the values of the combustion pressure. As with the combustion pressure, the thrust becomes more stable at higher pressures due to more stable combustion at high pressure. However, there is still a wide variance in the values of the thrust even at the

Average Combustion Chamber Pressure vs Oxidizer Supply Pressure
Beeswax and Oxygen

Figure 23: Average Combustion Chamber Pressure vs. Oxidizer Supply Pressure
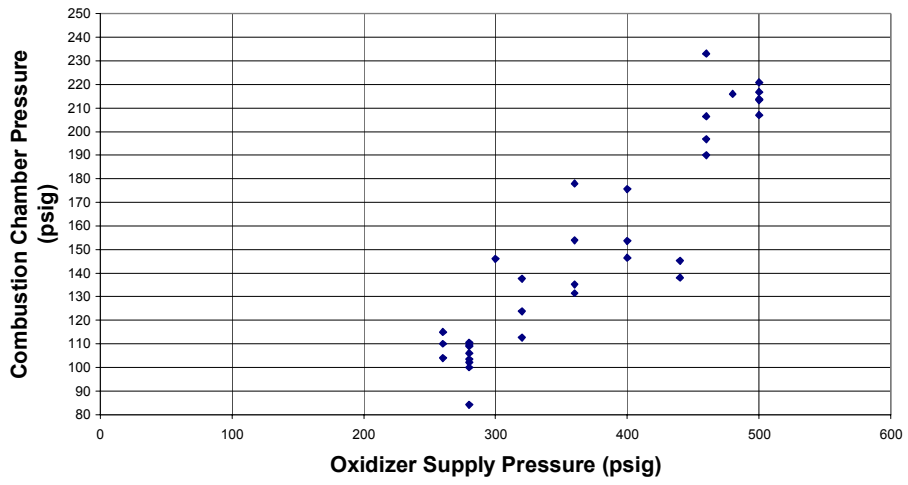
higher combustion pressures. It is apparent that due to the inability to set the supply

pressure on the regulator, this is not the best way to examine repeatability. Therefore, the

supply pressure setting can only be used to choose a general range of test conditions and

the combustion chamber pressures have to be examined after the tests to determine the

actual test conditions. A better way to examine the supply pressure is to plot the pressure

upstream of the orifice plate versus time (see Figures 24 and 25). The average supply

pressure in Figure 24 is approximately 110 psig with a standard deviation of 9 psig. The

average supply pressure in Figure 25 is approximately 230 psig with a standard deviation

of 5 psig. Another way to examine reliability is to examine the entire set of data to look

for general trends. One option is to examine the thrust as a function of the combustion

chamber pressure, as shown in Figure 26. Aside from a few tests, there appears to be a

very linear trend in the data. This would indicate that the test stand produces more

repeatable results than shown earlier. A strong source of variance in the results is the

high uncertainty in the oxidizer mass flow rate calculation. Other sources of differences

could be changes in ambient temperatures, uncertainty in the fuel mass flow rate, and

inconsistencies (i.e air pockets, possible chemical variations between batches of beeswax,

etc.) in the fuel grains.

V.II Beeswax and Nitrous Oxide

As stated in the introduction chapter, one of the oxidizers chosen for examination

was nitrous oxide. It is a commonly used oxidizer and is very safe to handle. Several

tests were run in an attempt to acquire useful data. However, there were significant

problems with the testing. None of the tests were able to achieve stable combustion. The

worst tests failed to achieve any ignition. The best tests achieved some amount of

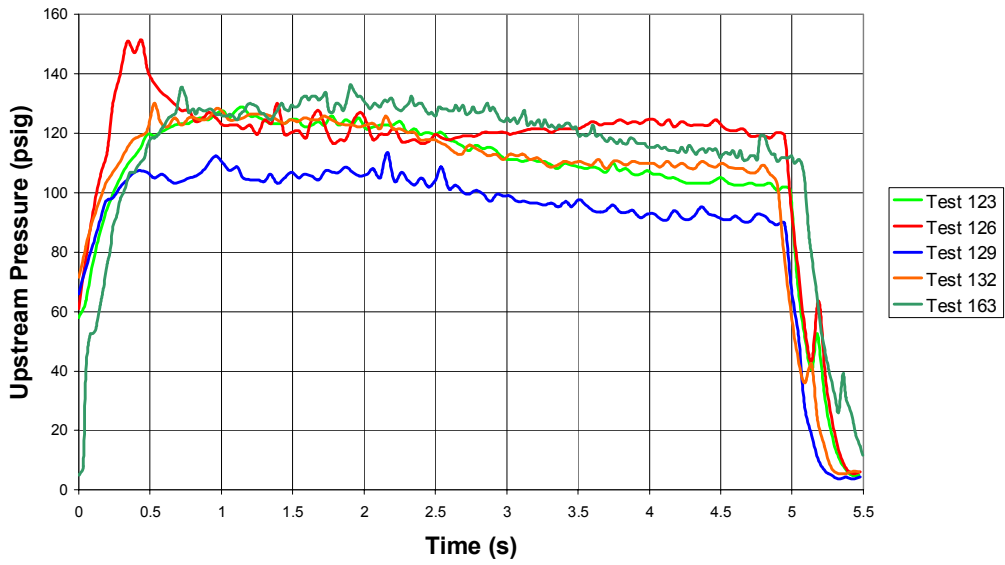Figure 24: Upstream Pressure vs Time, Supply Pressure = 280 psig

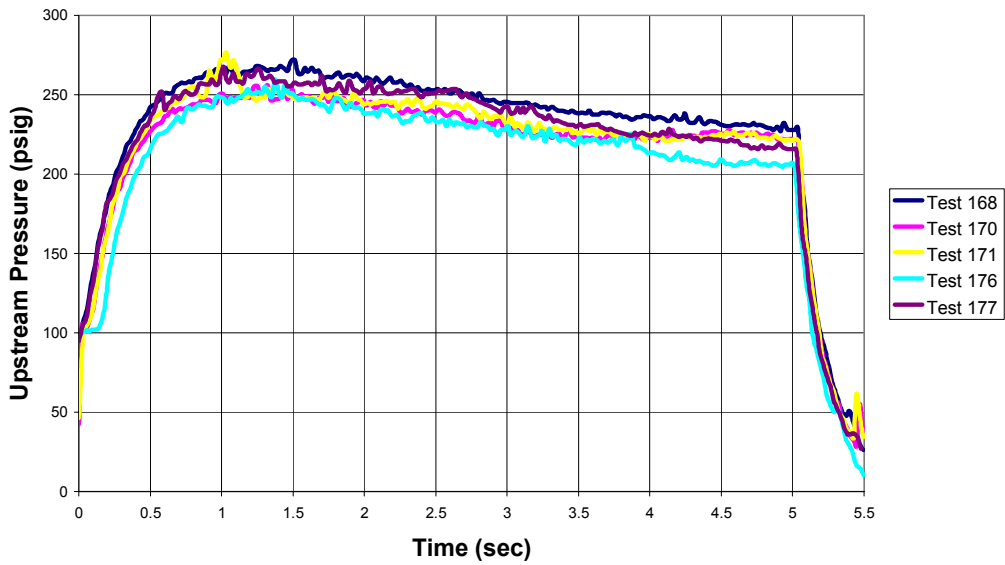Figure 25: Upstream Pressure vs Time, Supply Pressure = 500 psig

59

Average Thrust vs Average Combustion Chamber Pressure
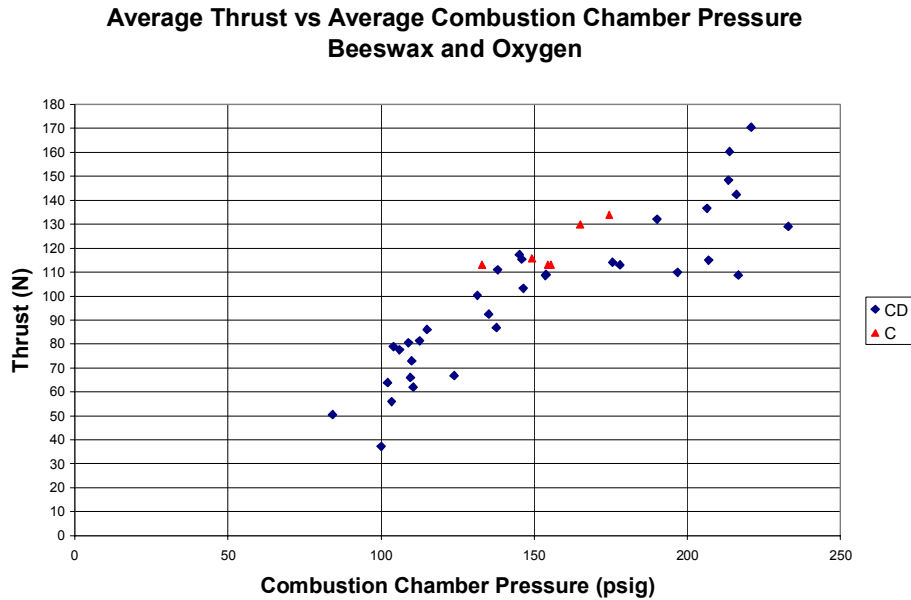**Beeswax and Oxygen**

Figure 26: Average Thrust vs Average Combustion Chamber Pressure

ignition and had significant pulsing during the burn. The exhaust plumes consisted

mainly of smoke with little visible flame. Figure 27 shows some representative results of

the testing. Test 84 was run with an oxidizer supply pressure of 240 psig and the propane

timer was set at 1.0 s. It achieved an average combustion chamber pressure of

approximately 55 psig, but did not achieve stable combustion. At the time, that was near

the limit of the nitrous oxide regulator, so a new regulator was acquired that could deliver

a supply pressure of up to 500 psig. Test 92 was run at a supply pressure of 420 psig, and

the propane timer was increased to 1.2 s. The propane time was increased from 1.0 s to

1.2 s to provide extra initial energy to the fuel grain to improve the ignition process. The

average pressure was approximately 35 psig. Test 95 was run at the same propane time

as test 92, but the supply pressure was increased to 500 psig. The average combustion

pressure increased to only 40 psig. Test 109 was run at a supply pressure of 500 psig, but
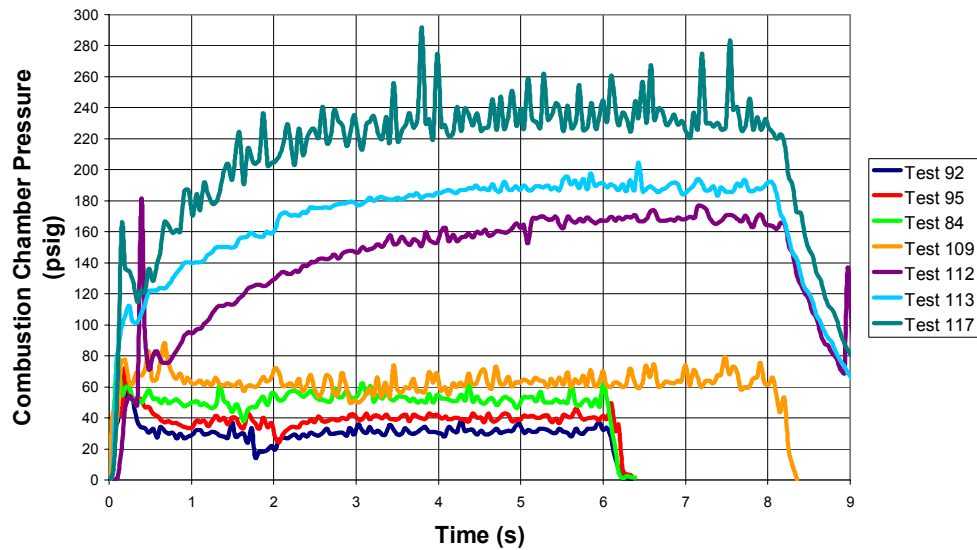
Figure 27: Comparison of Combustion Chamber Pressures for Beeswax and Nitrous

the propane time was increased to 2.0 s. This produced an average pressure of

approximately 60 psig. The length of this test was increased from 6.0 s to 8.0 s in order

to give the ignition process longer to take hold and initiate the combustion process.

However, the pressures achieved in these four tests were too low for stable combustion to

occur. Since the regulator was operating at its maximum discharge pressure, a new

solution to increase the combustion chamber pressure had to be formulated.

An investigation of the characteristic exhaust velocity was initiated. The

characteristic exhaust velocity is a measure of how well the combustion process occurs in

a rocket motor combustion chamber. It is experimentally determined and shown in Eq.

19:

$$c^* = \frac{P_c A_t}{\dot{m}}$$

(19)

where c^* is the characteristic exhaust velocity, P_c is the combustion pressure, A_t is the

nozzle throat area, and $\dot{m}$ is the mass flow rate. A comparison plot of the theoretical

characteristic exhaust velocity for beeswax/O_2 and beeswax/N_2O was examined and is

shown in Figure 28. This was accomplished using the Air Force Specific Impulse code,

which was explained in the Chapter II. The combustion chamber pressure examined was

150 psig, and the exhaust pressure was set at 14.7 psig. As shown in Figure 28, using

nitrous oxide as the oxidizer reduces the characteristic exhaust velocity due to the

presence of nitrogen compared to using pure oxygen as the oxidizer. When the nozzle

was designed, it was designed assuming that oxygen would be the oxidizer. If the

characteristic exhaust velocity is decreased and the mass flow rate is assumed constant,

then the nozzle throat area will have to be decreased in order to achieve the same

combustion chamber pressure as shown in Eq. 20.

$$P_c = \frac{\dot{m}c^*}{A_t} \tag{20}$$

Based on this, a new nozzle was designed for use with nitrous oxide. Due to the

restrictions of the current experimental setup, the nozzle had to be the same length as the

original nozzle. The new throat diameter was 0.14 in. and the new exit diameter was 0.25

in. Test 112 was run with a supply pressure of 340 psig and the propane timer set at 2.0

s. The result was a maximum combustion chamber pressure of 150 psig. This was a

significant increase over the previous four tests. However, this still did not result in

stable combustion, and the motor pulsed during the test. The supply pressure was

increased to 380 psig for test 113, and the maximum combustion chamber pressure was

190 psig. Again, the motor pulsed during the test and never reached steady state
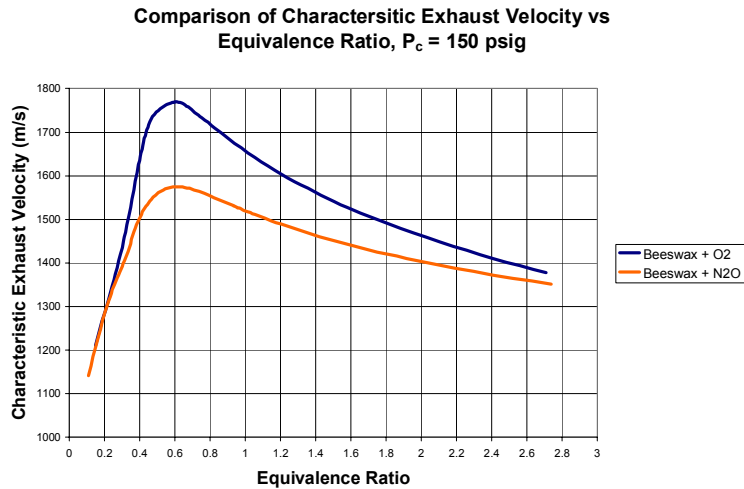
Figure 28: Comparison of Characteristic Exhaust Velocity vs. Equivalence Ratio

combustion. Test 117 was run with a supply pressure of 420 psig, and the maximum

chamber pressure was approximately 235 psig. This test showed significant pulsing, and

the chamber pressure was much less smooth than tests 112 and 113. Given that the new

regulator was again nearing its maximum supply pressure, the next logical step would

have been to design a new nozzle with an even smaller throat diameter. Unfortunately,

the combustion chamber pressure was beginning to approach its maximum allowed value.

It appears that a combustion pressure of higher than 235 psig is required for stable

combustion to be realized. The current test stand needs to be modified or redesigned to

accommodate higher combustion chamber pressures in order to continue this course of

research. Due to these difficulties, no data on regression rate or specific impulse was

collected for beeswax and nitrous oxide. The thrust curves for the tests in Figure 26 are

shown in Figure 29. From the appearance of the exhaust plume, most, it not all, of the

thrust produced was due to the oxidizer blowing through the nozzle and the burning of

the propane during the ignition process. It is unclear why tests 112, 113, and 117 have a

lower thrust level than tests 84, 92, 95, and 109 even though the chamber pressure was higher.

V.III Beeswax and Oxygen: Regression Rate

For the regression rate analysis, the two goals were to compare the regression rate of beeswax and oxygen with other hybrid propellant combinations and to determine an analytical expression for the regression rate. Two of the propellant combinations compared are HTPB/LOX and paraffin/oxygen; Eqs. 21 and 22 show their expressions for regression rate as a function of the oxidizer mass flux rate, respectively (12).

$$\dot{r} = 0.146 G_{ox}^{0.681} \qquad\qquad (21)$$

$$\dot{r} = 0.488 G_{ox}^{0.62} \qquad\qquad (22)$$

Figure 30 shows the results of the regression rate comparison. Beeswax and oxygen have a significantly higher regression rate than HTPB/LOX over the range of oxidizer mass flux rates examined. Based on the experimental data, the regression rate for beeswax/oxygen is at least three times higher than HTPB/LOX. This was similar to results found in previous research into paraffin and oxygen as discussed in chapter one. However, it was surprising to discover that beeswax and oxygen demonstrated a higher regression rate than paraffin and oxygen. The beeswax data shows a wide range of spread, so it is difficult to determine exactly how much higher the regression rate is over that of paraffin. Figure 30 shows that there is significant uncertainty in the mass flux rate due to the uncertainty in the oxidizer mass flow rate. The uncertainty in the regression rate calculation due to uncertainties in the initial port radius, burn time, initial fuel mass, and burned fuel mass was investigated, and the details are presented in Appendix D.
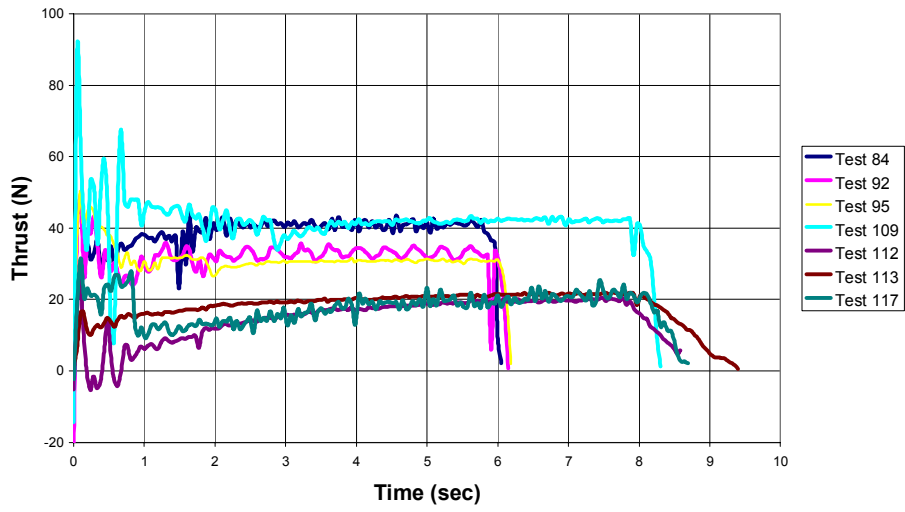
Figure 29: Thrust vs Time, Beeswax and Nitrous Oxide

The average uncertainty in the regression rate over all of the tests was 0.33 mm/s. It should be noted, however, that despite the uncertainty in the oxidizer mass flux rate and regression rate, the regression rate is still significantly higher than HTPB. However, the fact that the regression rate is higher than the traditional hybrid propellants such as HTPB/LOX shows that beeswax should be able to provide a higher thrust hybrid rocket motor using a simple, single port grain geometry.

The next step was to determine an expression for the regression rate. In the literature, there are many different expressions for regression rate as a function of many different variables (32). Several different expressions were examined to evaluate which would best fit the experimental data. One thing to note is all of the beeswax fuel grains tested were the same length, so the length of the combustion port was not considered here
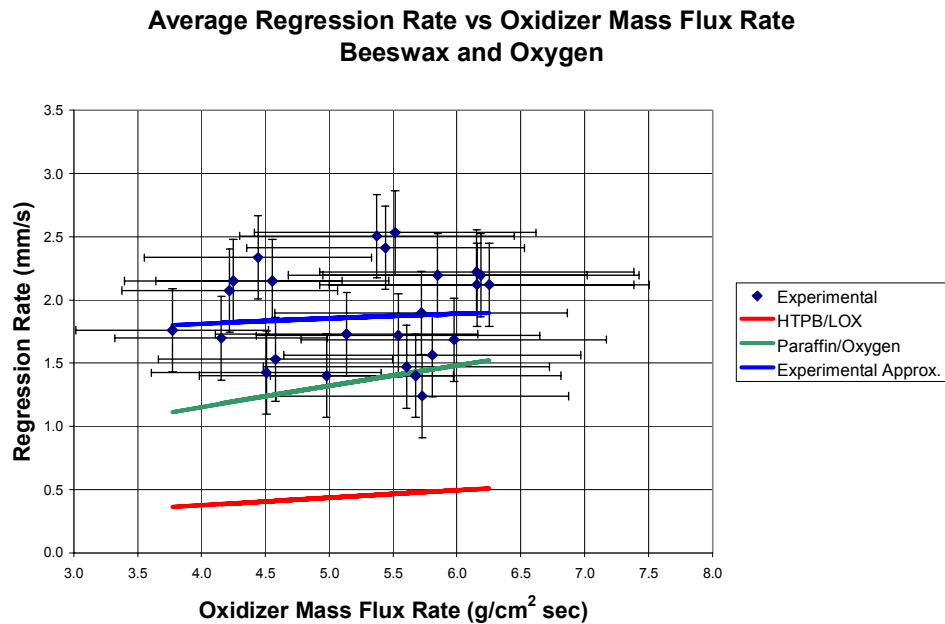

Figure 30: Comparison of Regression Rates

as a dependent variable in the regression rate expressions. This is due to the nature of the

current test stand being unable to accommodate different length fuel grains. To include

the effects of the length of the port, different length fuel grains need to be tested and a

correlation would have to be found. For this study, the regression rate was assumed

constant along the grain length. This does not include the space at the end of the fuel

grain that acts as the aft mixing chamber. All of the expressions examined are the

typically used general power series, shown in Eq. 23:

$$\dot{r} = aX^n \tag{23}$$

where X is the independent variable and a and n are experimentally derived constants

(1,2). Four independent variables were analyzed in this study: oxidizer mass flux rate,

total propellant mass flux rate, combustion chamber pressure, and oxidizer mass flow

rate.

As shown in Eqs. 21 and 22, it is common to examine the regression rate as a

function of the oxidizer mass flux rate. A power series expression from the experimental

data in Figure 30 is shown in Eq. 24:

$$\dot{r} = 1.5731 G_{ox}^{0.1026} \tag{24}$$

where $\dot{r}$ is the regression rate and G_{ox} is the oxidizer mass flux rate. The problem with

this expression is the poor correlation due to the large amount of scatter in the

experimental data. The R-squared value for this correlation is 0.0054. In an attempt to

improve correlation between the regression rate expression and the experimental data, the

total propellant mass flux rate was examined. The total mass flux rate includes the mass

flux of the fuel, which is found using the average mass flow rate of the fuel over the

duration of the test, and the mass flux of the oxidizer. The resulting expression for the

regression rate is shown in Eq. 25

$$\dot{r} = 0.0535 G_{TOT}{}^{1.4855} \qquad (25)$$

where G_{TOT} is the total propellant mass flux rate. This expression has a much better correlation ($R^2 = 0.3642$) than with the oxidizer mass flux rate. When the regression rate is plotted against the total propellant mass flux rate, as in Figure 31, there is a noticeable decrease in the scatter in the data. While the total propellant mass flux rate shows a better correlation than the oxidizer mass flux rate, there are other expressions that have better agreement with the experimental data. A common independent variable used for regression rate expressions in solid rocket motors is the combustion chamber pressure. The expression for regression rate as a function of the combustion chamber pressure is shown in Eq. 26

$$\dot{r} = 0.181 P_c{}^{0.478} \qquad (26)$$

where P_c is the combustion chamber pressure. The reduction in the scatter of the regression rate data when presented against the combustion chamber pressure can be seen in Figure 32. The R-squared value for this correlation is 0.4758. The expression in Eq. 12 was evaluated only using the data shown in Figure 32 that used a converging-diverging nozzle. The data resulting from using a converging nozzle is shown for historical reference only.

The last parameter examined as an independent variable was the oxidizer mass flow rate. Figure 33 shows the regression rate versus the oxidizer mass flow rate. Using the oxidizer mass flow rate showed the least scatter of all of the variables analyzed. When an expression for the regression rate was determined, it showed the best correlation

Figure 31: Regression Rate vs. Total Propellant Mass Flux Rate

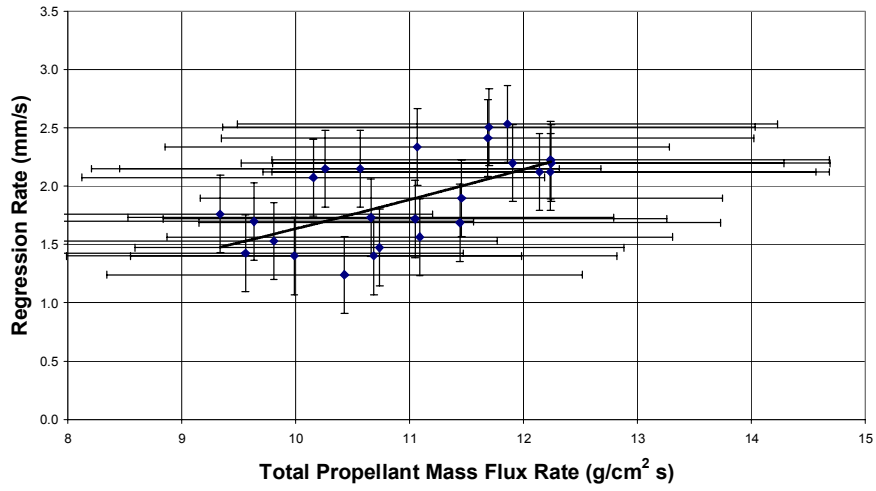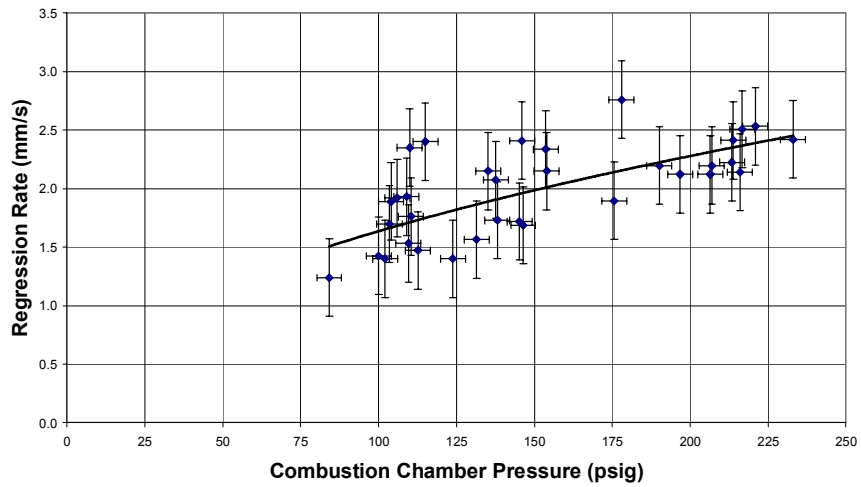Figure 32: Regression Rate vs. Combustion Chamber Pressure

with the experimental data ($R^2 = 0.4876$). The analytical expression is shown in Eq. 27:

$$\dot{r} = 11.815 \dot{m}_{ox}^{\,0.4862} \tag{27}$$

where $\dot{m}_{ox}$ is the oxidizer mass flow rate.

While using the oxidizer mass flow rate has the best correlation, there is still significant scatter in the data. The maximum spread in the regression rate at a given mass flow rate is ± 0.4 mm/s.

There are several possible reasons for the significant scatter in the regression rate data. As stated in Chapter IV, the error from the pressure transducers was $\pm 0.4\%$. While this is sufficient for the measurement of the pressure upstream and downstream of the orifice plate, the mass flow rate is computed from the pressure differential across the orifice plate. When measuring the difference in pressure, a 0.4% error in the transducers begins to have a much more significant effect on the data. This is illustrated in Figure 34.
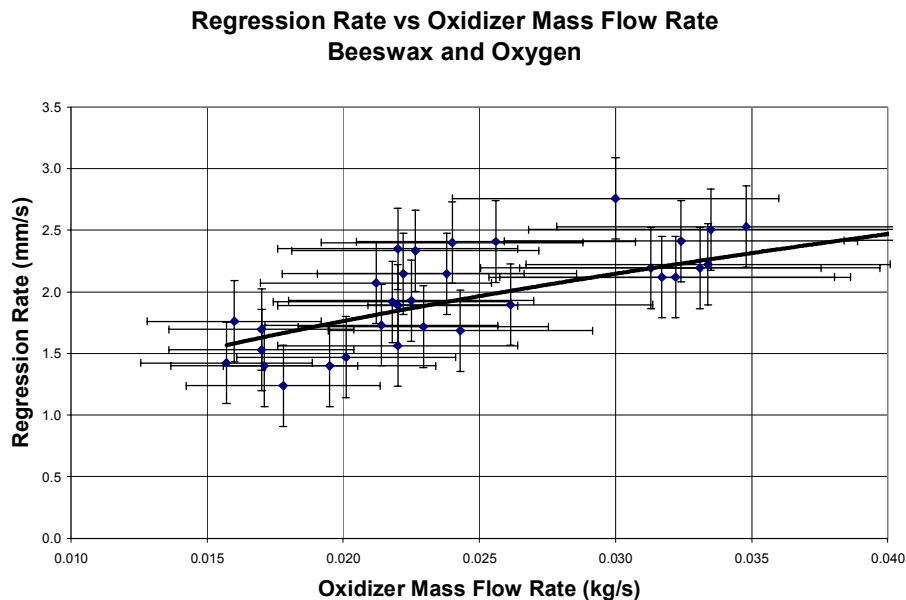

Figure 33: Regression Rate vs. Oxidizer Mass Flow Rate

The pressure differential across the orifice plate is shown versus time for Test 169. This test had an oxidizer supply pressure of 400 psig. Another possible causes for scatter in the data include inconsistencies in the fuel grains due to air pockets formed during the fabrication process. One way to measure this possibility is to examine the initial fuel grain mass measurements. The average initial fuel grain mass was 3.391 kg with a standard deviation of 0.017 kg. Another cause could be the spallation of solid or melted particles of beeswax leaving the motor unburned. This would tend to inflate the measured regression rate, as no attempt to measure the spallation of unburned beeswax was made. Another possibility is errors in the fuel grain mass measurements. As noted earlier, the accuracy of the scale used was ± 1gram. All of the tests were run for the same duration (5.0 s) and the propane was run for the same duration (0.5 s) for all tests. The likely explanation of the errors in the data is a combination of all of these possibilities.
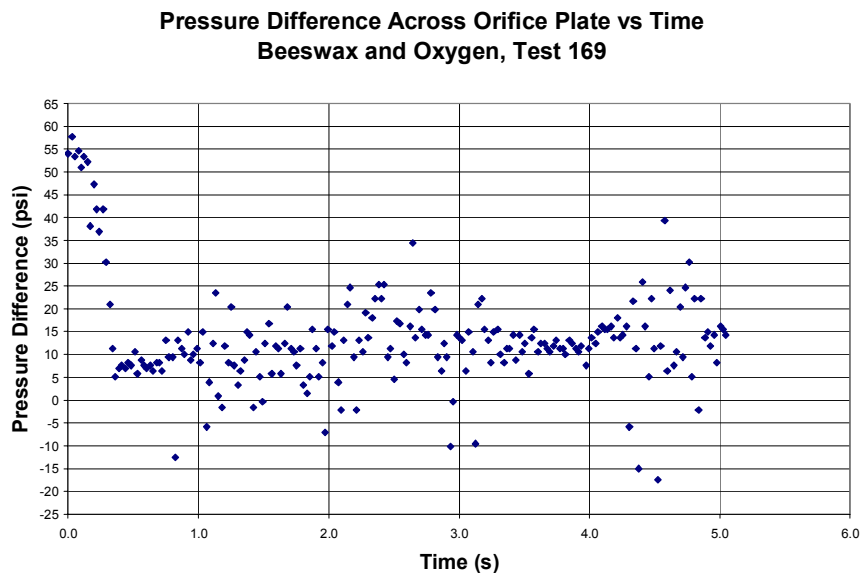

Figure 34: Pressure Difference vs. Time, Test 169

71

V.IV Beeswax and Oxygen: Specific Impulse

The sea level specific impulse for beeswax and oxygen was found by integrating the thrust over the duration of the test to find the total impulse and then dividing by the weight of the propellant burned. The experimental data was used to evaluate the specific impulse, and then the data was compared to a theoretical analysis of the specific impulse. The theoretical data was evaluated at a combustion chamber pressure of 150 psig, and the equivalence ratio was varied. The theoretical seal level specific impulse was computed assuming frozen flow through the nozzle. A plot of the experimental and theoretical specific impulses as a function of equivalence ratio is presented in Figure 35. Several observations can be made from Figure 35. First, a significant variance in the data is apparent. The primary source of scatter is the uncertainty in the equivalence ratio, which is primarily due to uncertainty in the oxidizer mass flow rate. A calculation of the uncertainty in the equivalence ratio was performed and the average uncertainty over all the tests was 0.24. This is illustrated in Figure 35 by horizontal error bars. This again highlights the need for funding to purchase a differential pressure transducer to improve accuracy of the oxidizer mass flow rate. Also, a large number of the tests resulted in a calculated specific impulse greater than the theoretical value. There are several possible reasons for these results. Clearly, there is enough scatter in the data to question the specific impulse data that is above the theoretical curve in Figure 35. The possible sources of uncertainty, in descending order of magnitude, are the oxidizer mass flow rate, the burned fuel mass, the burn time, and the thrust. When all of these are
 accounted for, the average uncertainty over all the tests for the calculated sea level
accounted for, the average uncertainty over all the tests for the calculated sea level

72

specific impulse was 5.6 s. The calculations for the specific impulse uncertainty are shown in Appendix D. Another variable is the combustion pressure. The experimental data was collected over a range of combustion chamber pressures, while the theoretical analysis was conducted for a chamber pressure of 150 psig. However, if the specific impulse is analyzed as a function of the combustion chamber pressure, similar results are observed as shown in Figure 36. There are several reasons one would expect the experimental specific impulse data to be below the calculated theoretical values. The theoretical values do not account for a chemically reacting gas throughout the nozzle. In other words, the computer code assumes the chemical composition of the gas does not change as it flows through the nozzle. This can change the ratio of specific heats and the molecular mass of the exhaust gas which in turn changes the exit velocity. This can represent a loss of specific impulse of 0.5% (2). Also not accounted for in the theoretical
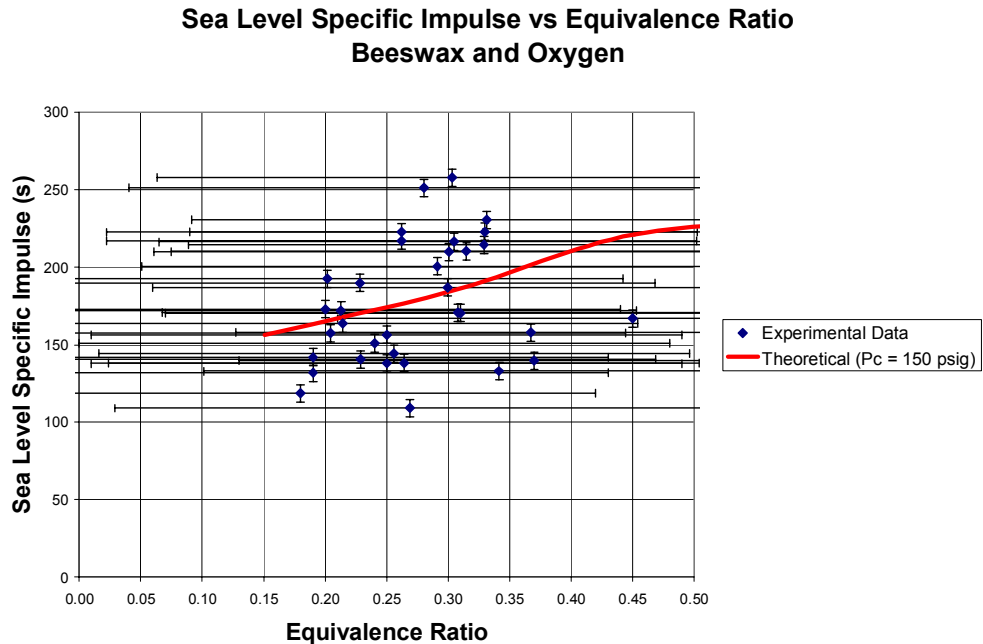

Figure 35: Comparison of Experimental and Theoretical Specific Impulse

analysis are viscous losses in the nozzle, which reduce the exit velocity and in turn reduce the specific impulse. These losses are due to the presence of a boundary layer inside the nozzle, and can reduce the effective exhaust velocity by 0.5% to 1.5% (1). Multiphase flow in the nozzle can also reduce the exit velocity as discussed previously. Having liquid or solid particles in the exhaust can cause a reduction of up to 5% in the specific impulse of the motor. Other losses can be caused by unsteady or oscillating combustion. As shown in the repeatability study earlier, there was unsteady combustion occurring in some of the tests, primarily at lower combustion pressures (2). A final source of reduction in the specific impulse is divergence losses due to the shape of the nozzle. Due to the conical shape of the nozzle, there will be a component of the exit velocity vector in the radial direction. Any component of the exit
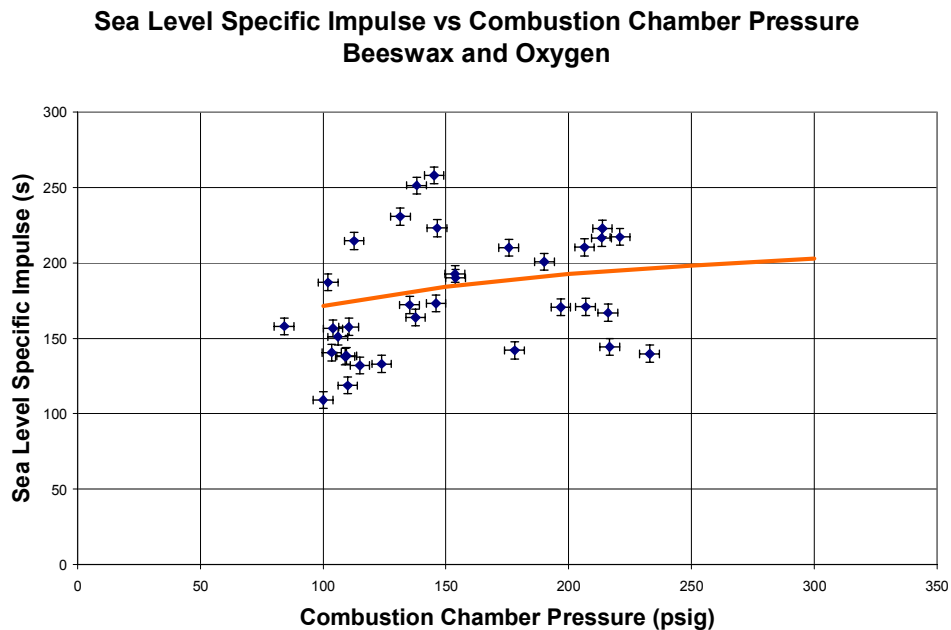

Figure 36: Specific Impulse vs. Combustion Chamber Pressure

74

velocity vector not in the axial direction will result in a loss of specific impulse. This contribution to the losses is a function of the cosine of the nozzle half angle, and can be computed using Eq 28 (1):

$$\lambda = \frac{1}{2}\left(1 + \cos\theta_{cn}\right) \tag{28}$$

where λ is the thrust efficiency and θ_{cn} is the nozzle half angle. The half angle for the nozzle used was 3.54 degrees, which results in a loss of approximately 0.1%. Adding up these losses results in a possible 7.1% reduction in the specific impulse from the theoretical values. Figure 37 shows these losses in relation to the theoretical and experimentally derived results for the specific impulse. Note that this new curve for the specific impulse does not account for possible errors in the propellant mass flow rate or thrust measurements. Ideally, the experimental data would fall very close to, or on, the curve that accounts for the losses. There is also the possibility of unaccounted losses that would be responsible for the discrepancies between the experimental data and the loss-accounted theoretical results.

V.V Beeswax and Oxygen: Thrust

An analysis of the thrust data was conducted to determine a theoretical value for the thrust for a hybrid rocket motor using beeswax and oxygen as propellants. For simplicity, it was assumed the combustion chamber pressure was 150 psig and the equivalence ratio was 0.3. This combustion pressure was chosen because the part of the theoretical analysis used to compare to the experimental data was performed at that pressure. This equivalence ratio was chosen as an average value experienced in the experimental results. For this analysis, it was also assumed to have an ideally expanded

nozzle, which eliminated the exit pressure contribution to the thrust. This reduces the thrust expression to Eq. 29:

$$T = \dot{m} V_e \tag{29}$$

where T is the thrust, $\dot{m}$ is the mass flow rate through the nozzle, and V_e is the nozzle exit velocity. Using an ideally expanded nozzle also allows the use of the relation of the specific impulse to the exit velocity as shown in Eq. 30:

$$I_{sp} = \frac{V_e}{g_0} \tag{30}$$

where I_{sp} is the specific impulse, V_e is the nozzle exit velocity, and g_0 is acceleration due to gravity. Substituting Eq. 30 into Eq. 29 yields an expression for the thrust as shown in Eq. 31.
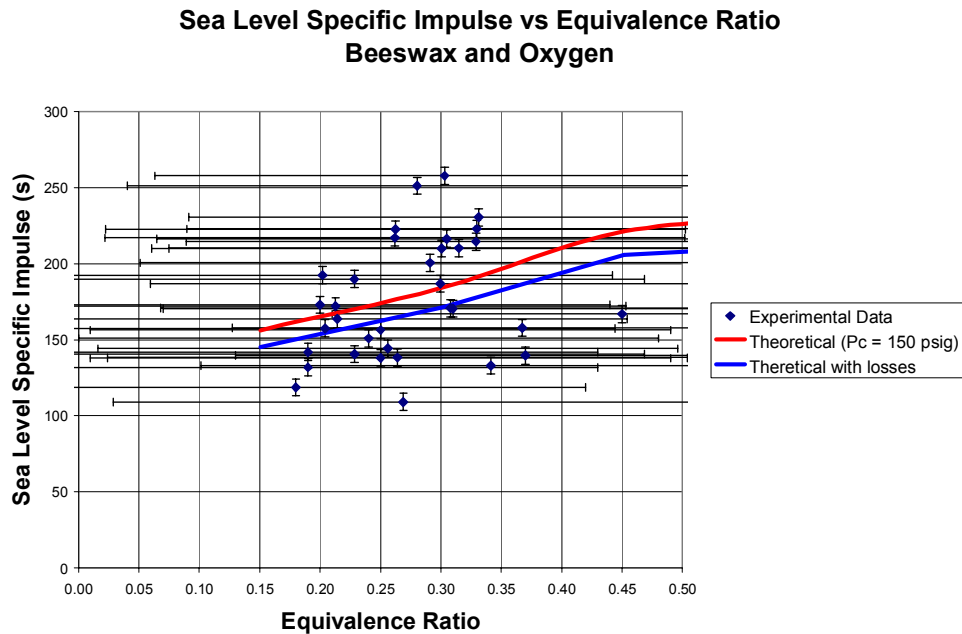
Figure 37: Specific Impulse Including Losses

$$T = \dot{m} I_{sp} g_0 \tag{31}$$

Eq. 31 was used to determine the theoretical values of thrust. From Appendix A, the specific impulse for beeswax/O_2 at an equivalence ratio of 0.3 is 184 s. To correlate with the experimental data, the total approximated propellant mass flow rate from the experimental data was used in Eq. 31. A comparison of the measured average thrust values with their theoretical counterparts is shown in Table 13. It is evident from Table 13 that the experimental values of the thrust are significantly higher than the theoretical estimations. This is likely due to the uncertainty in the propellant mass flow rates used in the ideal thrust calculations. It would appear the true mass flow rates are higher than have been approximated since the actual measured thrust levels are higher than the calculated ideal thrust levels. Higher actual values of equivalence ratio would increase both specific impulse and propellant mass flow rates used in the thrust calculations and more closely match them with the measured thrust values.

Table 13: Comparison of Actual and Theoretical Thrust

Test #	Pc (psi)	Avg. Thrust (N)	Ideal Thrust (N)	% Error
30	149.3	115.8	151.4	23.5
32	155.5	113.0	170.0	33.5
34	154.5	113.0	168.8	33.1
35	146.0	115.5	103.2	11.9
156	146.4	103.2	96.8	6.6
159	153.7	108.6	83.9	29.4
161	145.2	117.4	101.9	15.21
173	153.9	109.1	99.64	9.5

VI. CONCLUSIONS AND RECOMMENDATIONS

VI.I Conclusions

The main objective of this research was to evaluate regression rates for non-conventional bio-derived hybrid rocket propellants and compare them to traditional hybrid rocket motor propellants. Such preliminary work is necessary to produce a hybrid rocket with a high thrust level using a simple, single port geometry. For the tests using beeswax and oxygen, the regression rate was measured and determined to be at least 3 times higher than HTPB/LOX and possibly higher than paraffin/oxygen. For example, at an oxidizer mass flux rate of 4.0 $g/cm^2 s$, HTPB/LOX has a regression rate of 0.4 mm/s, paraffin/oxygen has a regression rate of 1.2 mm/s, and beeswax/oxygen has a regression rate of 1.8 ± 0.33 mm/s. The wide range given for the beeswax/oxygen regression rate is due to scatter in the experimental data. An expression for the regression rate was derived as a function of the oxidizer mass flow rate. Mass flow rate was chosen as the independent variable for the expression because it had the best correlation with the experimental data. Unfortunately this limits the application of the equation to our engine design or one of identical design.

Another objective was to determine experimentally the thrust and specific impulse and compare them to theoretical values to validate the data. This part of the research proved difficult due to mechanical issues resulting in poor thrust data. This led to significant scatter in the thrust data, which in turn produced scatter in the specific impulse data. Calculated experimental sea level specific impulses were both above and below their theoretical levels. Some tests did fall near the theoretical values when losses were accounted for, but many tests were above the theoretical value. The thrust data collection

needs to be improved in order to reduce uncertainty. At a combustion chamber pressure of 150 psig, the experimentally-measured thrust turned out to be higher than the predicted values. The test stand appears to be reliable for combustion pressure measurements, but improvements are needed in the thrust data system. The largest room for improvement is in the measurement of the oxidizer mass flow rate. Due to the significant uncertainties in the oxidizer mass flow rate, the equivalence ratios calculated in this study have a very significant uncertainty and should be viewed accordingly.

When beeswax and nitrous oxide were tested, it was determined that a higher combustion chamber pressure than the test stand can achieve is required for stable combustion. Attempts were made to increase the combustion chamber pressure by redesigning the nozzle, but the pressure limits of the test stand were reached before stable combustion occurred. No data for regression rate or specific impulse was acquired, but this propellant combination is still worth pursuing. A summary of all the tests is presented in Appendix F.

For the analytical model, the goals were to produce theoretical data at a chamber pressure of 150 psig for comparison with the experimental data and at a chamber pressure of 500.38 psig for comparison with published data for traditional hybrid propellants. A set of data at a pressure of 150 psig was created and used to validate the experimental data. A set of data for many different non-traditional hybrid propellants was produced for a pressure of 500.38 psig and compared to traditional hybrid propellants. Beeswax combined with oxygen proved to be the best propellant combination producing a maximum specific impulse of 327 s. Overall, oxygen as the oxidizer produced better performance than nitrous oxide. For the solid fuels examined, beeswax produced the best

results followed by lard. After lard was the 50%/50% mixture of lard and paraffin by mass. When comparing beeswax and oxygen with the traditional hybrid propellants, it had a higher specific impulse than HTPB/LOX, HTPB/hydrogen peroxide, and HTPB/nitrogen tetroxide. A database of propellant properties was created for use by future hybrid rocket motor designers.

Overall, the state of the art in hybrid rocket motor technology was advanced by examining previously not considered non-conventional, bio-derived propellants.

VI.II Recommendations for Further Research

For future research, several improvements to the test stand are recommended. The main recommendation is to improve the oxidizer mass flow rate measurement. For the pressure data used to determine the oxidizer mass flow rate, a differential pressure transducer is recommended to reduce the scatter in the mass flow rate measurements. Unfortunately, the funding was not available to purchase the needed differential pressure transducer. This would improve the correlation for the regression rate expressions. If a differential pressure transducer is not successful, a flow rate meter could be acquired. The effects of ignition transients and oscillations need to be minimized with regard to thrust measurements. A preload could be placed on the system during testing. This could potentially help with the scatter in the data and the damping characteristics. If this is not sufficient to correct the scatter in the data, then the current strain gage setup could be replaced with a load cell. Also, the test stand needs to be able to accommodate higher combustion pressures. The nozzle end cap could be modified to incorporate an o-ring to assist in the containing the pressure. Also, another method for securing the fuel grain in the test stand needs to be developed. The practice of using bolts to secure the fuel grain

81

can only be improved by using stronger bolts. This has limits as the current setup will

not handle bolts much larger than currently used. Another parameter desirable to

measure is the combustion chamber temperature and compare it to the theoretical value.

An internet search was unable to find a thermocouple that could handle the maximum

temperature of roughly 3400K. However, there are thermocouples available that can

measure the nozzle exit plane temperature, and the exit temperature can be used to

estimate the combustion chamber temperature using Equation __. Unfortunately, these

thermocouples are well outside the funding available for this project. A lesser

thermocouple was purchased and an attempt was made to measure the exhaust

temperature. The thermocouple did not collect any data due to the strong oxidizing

environment, but it physically survived the temperature and dynamic pressure. A list of

recommended equipment is included in Appendix E.

For future research, more tests need to be performed to get better correlation for

the regression rate data and thrust data. Improving the thrust data will improve the

resulting specific impulse data. Also, the current research was limited to a range of

equivalence ratios between 0.2 and 0.4. The mass flow rate of the oxidizer system needs

to be increased in order to increase the equivalence ratio. It is desirable to collect data

over a wider range of equivalence ratios. Once these tests are completed, scale-up hybrid

motors will need to be tested in order to determine if the results acquired for lab-scale

motors will translate into flight-sized hybrid rocket motors. One way to assist in

applying the lab scale tests to larger motors is to incorporate the length of the combustion

port into the regression rate expression. To accomplish this, fuel grains of differing

lengths need to be tested. Another area that could be pursued in the experimental phase

is the use of additives to the solid fuels. Aluminum powder could be added to evaluate if it matches the theoretical performance. Another additive that could be used is carbon black. This is often added to solid propellants to reduce radiation heat transfer to the solid fuel grain.

REFERENCES

1. Humble, R., Henry, G., Larson, W., et al, <u>Space Propulsion Analysis and Design</u>, McGraw Hill Companies, Inc., 1995.

2. Sutton, G. and Biblarz, O., <u>Rocket Propulsion Elements</u>, 7th Edition, John Wiley and Sons, Inc., 2001.

3. Sellers, Jerry Jon, Investigation Into Hybrid Rockets and Other Cost-Effective Propulsion System Options for Small Satellite, University of Surrey Ph.D. Thesis, 1996.

4. Wernimont, E.J., and Heister, S.D., "Combustion Experiments in a Hydrogen Peroxide/Polyethylene Hybrid Rocket with Catalytic Ignition", <u>Journal of Propulsion and Power</u>, V 16, No. 2, pp. 318-326, 2000.

5. MARS Advanced Rocketry Society Webpage, http://www.mars.org.uk/bfore.html.

6. Orion Propulsion Latest News Webpage, http://www.orionpropulsion.com/latestnews.php#october2006B.

7. Risha, G. A., Boyer, E., Wehrman, R. B., Kuo, K. K., "Performance Comparison of HTPB-Based Solid Fuels Containing Nano-Sized Energetic Powder in a Cylindrical Hybrid Rocket Motor," AIAA Joint Propulsion Conference., July 7-10, 2002.

8. DeRose, M. E., Pfeil, K. L., Carrick, P. G., and Larson, C. W., "Tube burner studies of cryogenic solid combustion ," AIAA/ASME/SAE/ASEE Joint Propulsion Conference and Exhibit, 33rd, Seattle, WA, July 6-9, 1997

9. Barry, Patrick L., "Candlestick Rocket Ship," Science at NASA Webpage, Jan. 29, 2003, http://science.nasa.gov/headlines/y2003/28jan_envirorocket.htm

10. Reid, Czerne M., "Candle wax is rocket science: Paraffin fuels test launch," Stanford Report, Nov. 5, 2003, http://news-service.stanford.edu/news/2003/november5/rocketwax-115.html

11. Karabeyoglu, Mustafa A., "Transient Combustion in Hybrid Rockets", Stanford University Ph.D. thesis, August 1998.

12. Karabeyoglu, M. A., Cantwell, B. J. and Altman D., "Development and Testing of Paraffin-Based Hybrid Rocket Fuels", 37th AIAA/ASME/SAE/ASEE Joint Propulsion Conference, Salt Lake City, UT, July 8-11, 2001.

13. Karabeyoglu, M. A., Zilliac, G., Cantwell, B. J., De Zilwa, S. R. N. and Castelucci, P., "Scale-up Tests of High Regression Rate Liquefying Hybrid Rocket Fuels", Presented at 41st Aserospace Sciences Meeting and Exhibit, Reno, AIAA paper 2003-1162.

14. De Zilwa, S., Zilliac, G., Karabeyoglu, M. A. and Reinath, M., "Time-Resolved Fuel-Grain Measurement in Hybrid Rockets", 39th AIAA/ASME/SAE/ASEE Joint Propulsion Conference, 20-23 July, 2003, Huntsville, AL.

15. Lydon, M. C., Brown, T. R., "Testing of Paraffin-Based Hybrid Rocket Fuel Using Hydrogen Peroxide Oxidizer," CSGC Undergraduate Space Research Symposium, April 2005.

16. Adams, A., Cline, D., Payne, P., and Rowe, C., "Aerospace Engineering Senior Design Project," University of Tennessee, Spring 2003.

17. Lyne, James E., Naoumov, Viatcheslav I., et al, "First Steps in the Development and Testing of Nontoxic, Bioderived Fuels for Hybrid Rocket Motors," Presented at 43rd AIAA Aerospace Sciences Meeting and Exhibit, Reno, Nevada, January 2005

18. Sietzen, Frank, "The Greening of Rocket Propulsion," Aerospace America, pp. 28-35, July 2005.

19. Covarrunias, Amanda. Toxin Found in Simi Valley's Ground Water, *The Los Angeles Times*, December 5, 2002.

20. The Associated Press, Fuel Chemical Tainting Some Groundwater, *The Salt Lake Tribune*, January 7, 2003.

21. Bowman, Chris, "Aerojet to pay $25 million to settle pollutant lawsuit," The Sacramento Bee, May 17, 2006.

22. The Environmental Working Group. *Rocket Science, Chapter 3*. http://www.ewg.org/reports/rocketscience/chap3.html.

23. Dunn, Bruce P., "Rocket Engine Specific Impulse Program Help File," Dunn Engineering, 2001.

24. Conversations with Dr. Viatcheslav Naoumov, Visiting Professor, University of Tennessee, 2005.

25. New Zealand Beeswax Limited website: http://beeswax.co.nz/index.php?page=info.

26. Akrochem Corpopration, "AKROCHEM® Beeswax - Yellow Refined," Beeswax Fact Sheet, 2007.

27. Bogdanov, Stefan, "Quality and Standards of Pollen and Beeswax," Swiss Bee Research Centre, Bern Switzerland, 2004.

28. Krell, R. "Value-Added Products From Beekeeping," FAO Agricultural Services Bulletin No. 124, Food and Agriculture Organization of the United Nations, Rome, Italy, 1996.

29. John, J. E., Gas Dynamics, Prentice Hall, 2006.

30. Scholes, Joshua, "Bio-derived Fuels for Hybrid Rocket Motors," University of Tennessee Master's Thesis, 2005.

31. Turns, Stephen R., "An Introduction to Combustion: Concepts and Applications," McGraw Hill Companies Inc., 2000.

32. Korting, P., Schoyer, H. and Timnat, Y., "Advanced Hybrid Rocket Motor Experiments", 36th Congress of the International Astronautical Federation, Stockholm Sweden, October 1985.

APPENDICES

APPENDIX A: DATA FOR CHAMBER PRESSURE OF 150 PSIG

Temperature vs Equivalence Ratio: Beeswax and Oxygen
(P_c = 150 psi)
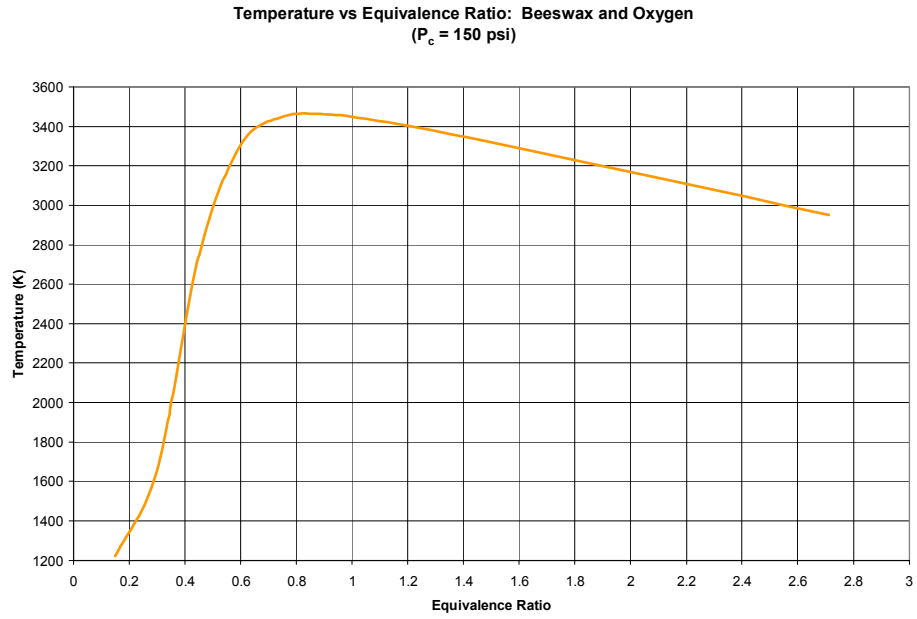
Figure 38: Temperature vs. Equivalence Ratio, Beeswax/Oxygen, P_c = 150 psig

Specific Impulse vs Equivalence Ratio
Beeswax and Oxygen (Pc = 150 psi)
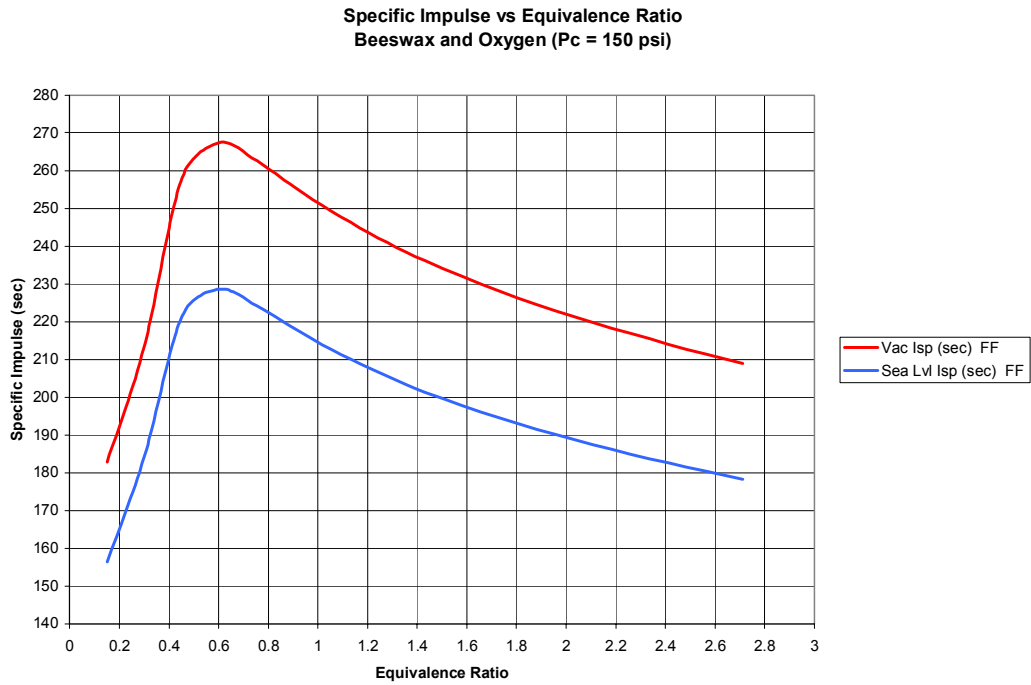
Figure 39: Specific Impulse vs. Equivalence Ratio, Beeswax/Oxygen, P_c = 150 psig

Ratio of Specific Heats vs Equivalence Ratio
Beeswax and Oxygen (P_c = 150 psi)
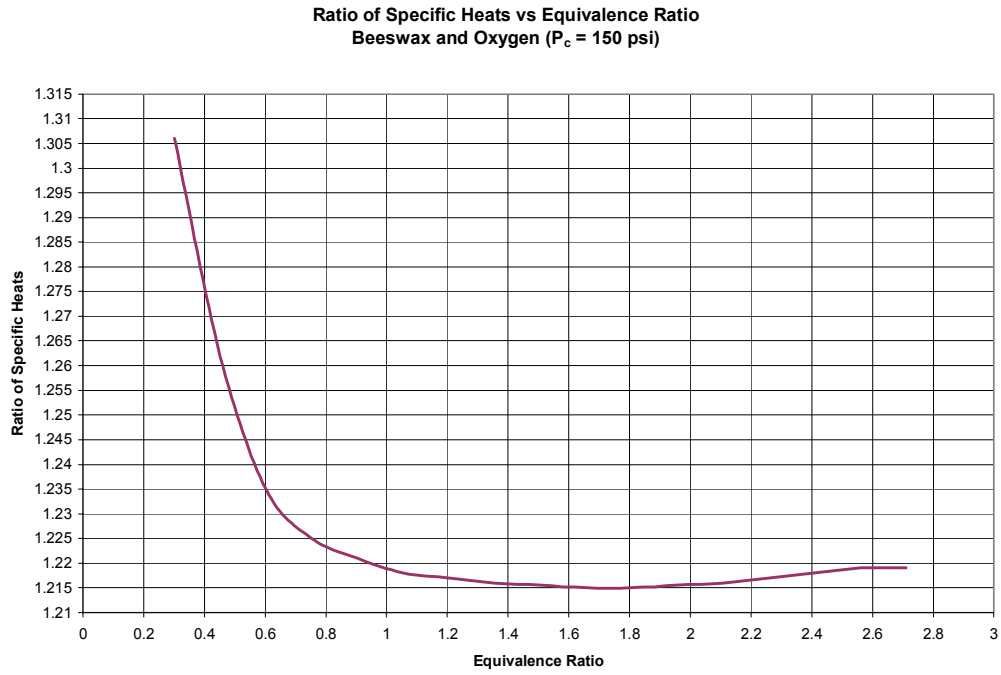
Figure 40: Ratio of Specific Heats vs. Equivalence Ratio, Beeswax/Oxygen, P_c = 150 psig

Combustion Products Molecular Mass vs Equivalence Ratio
Beeswax and Oxygen (P_c = 150 psi)
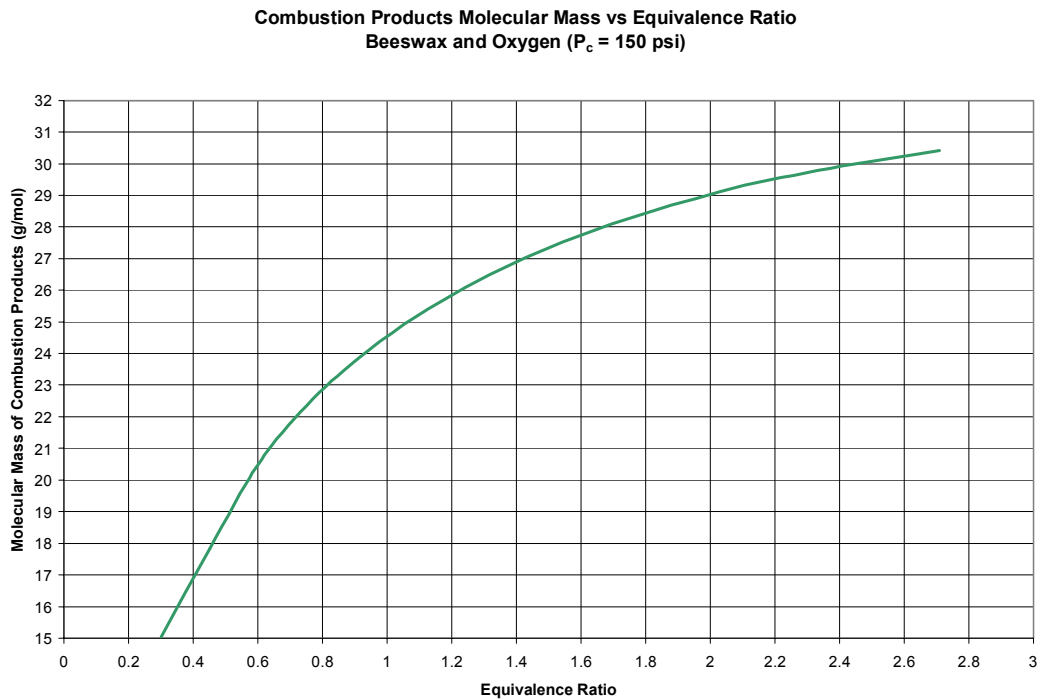
Figure 41: Molecular Mass vs. Equivalence Ratio, Beeswax/Oxygen, P_c = 150 psig

91
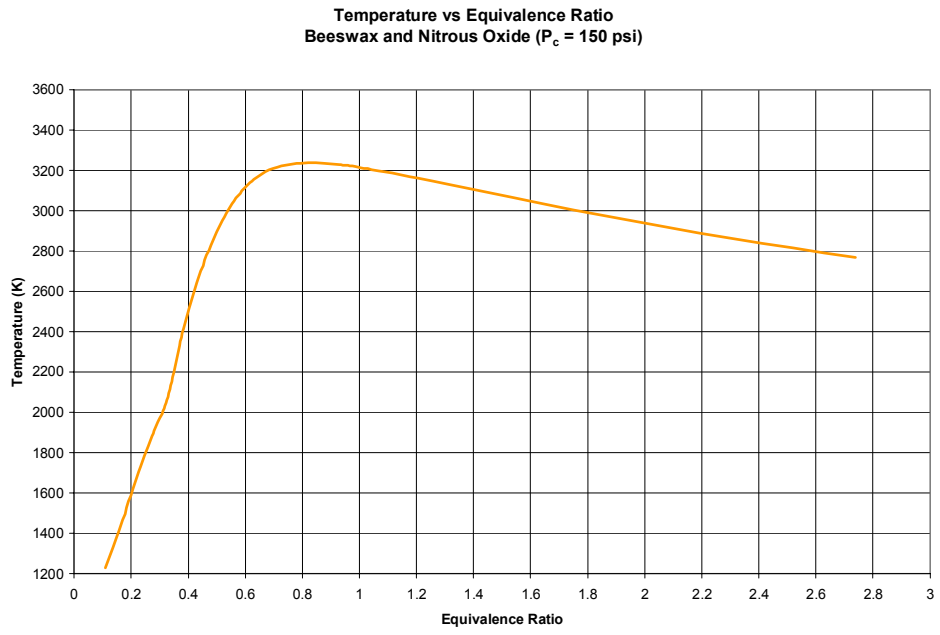
Figure 42: Temperature vs. Equivalence Ratio, Beeswax/Nitrous Oxide, P_c = 150 psig
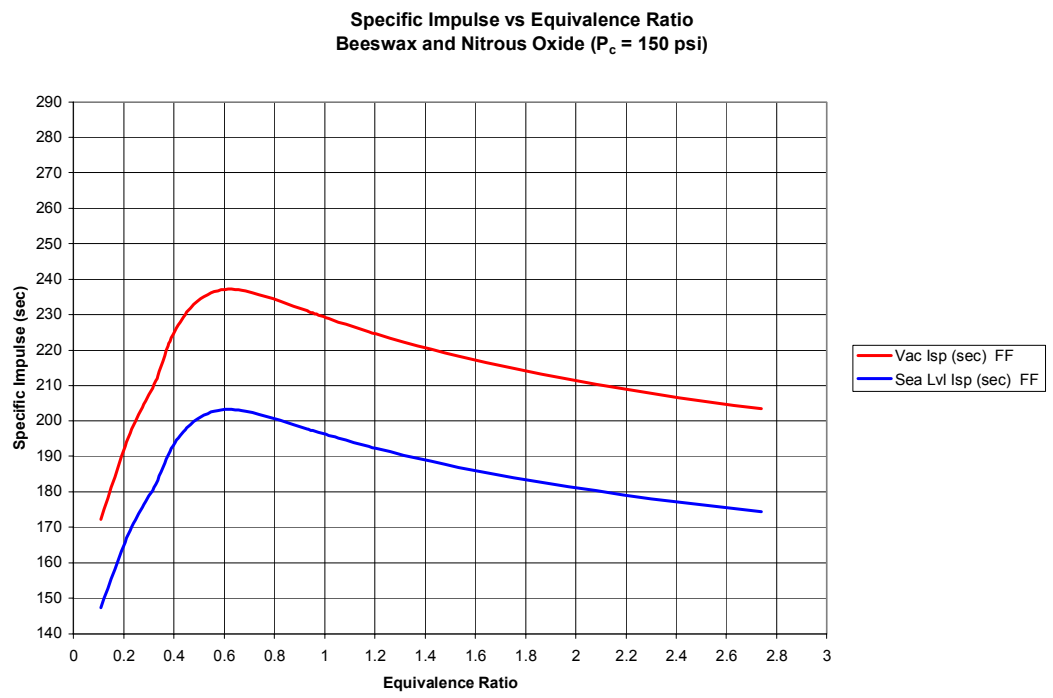
Figure 43: Specific Impulse vs. Equivalence Ratio, Beeswax/Nitrous Oxide, P_c = 150 psig
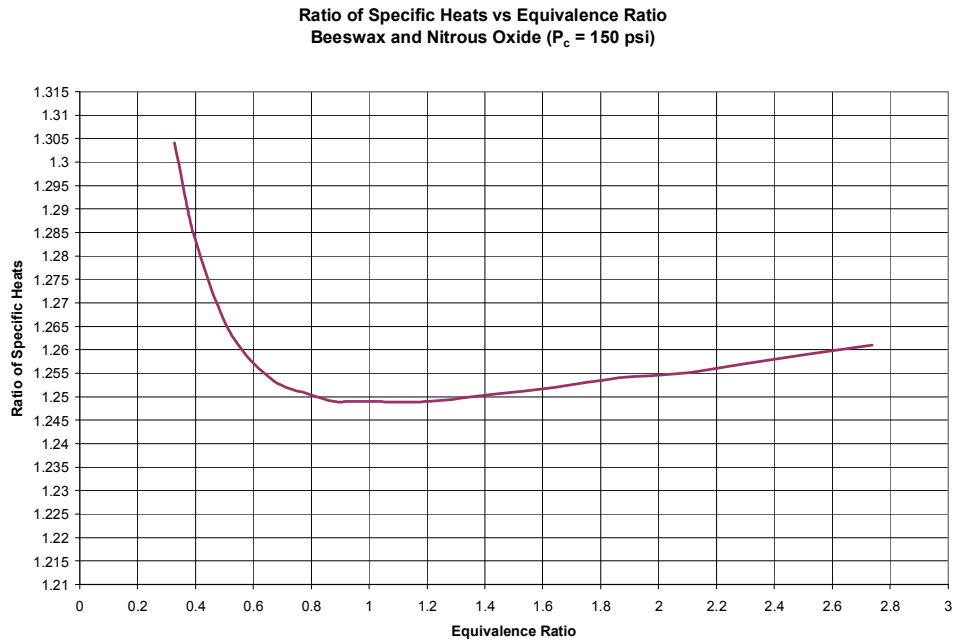
Figure 44: Ratio of Specific Heats vs. Equivalence Ratio, Beeswax/Nitrous Oxide, P_c = 150 psig
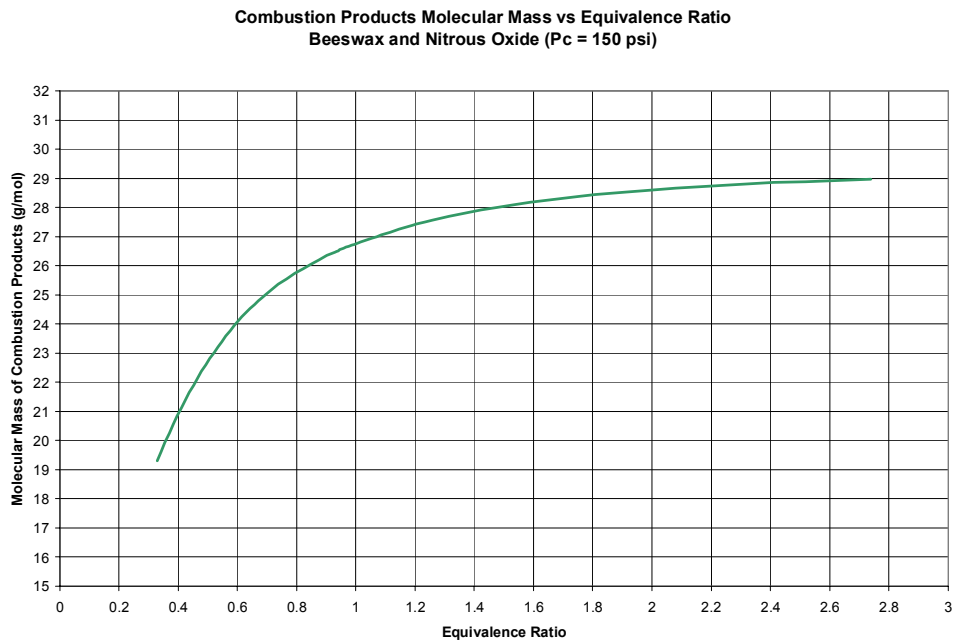
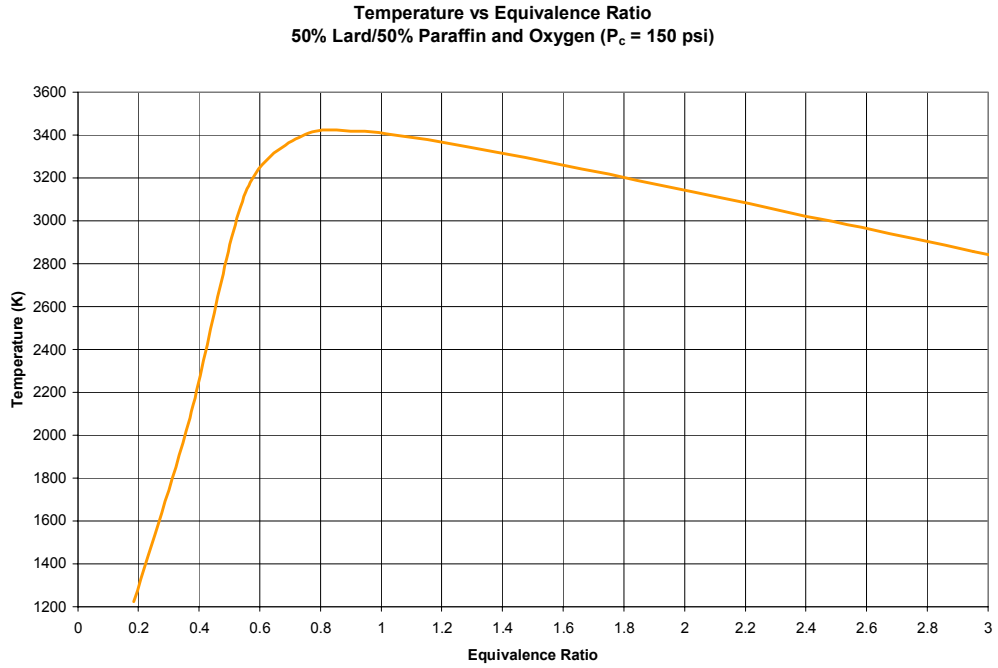Figure 45: Molecular Mass vs. Equivalence Ratio, Beeswax/Nitrous Oxide, P_c = 150 psig

Temperature vs Equivalence Ratio
Lard and Oxygen (P_c = 150 psi)
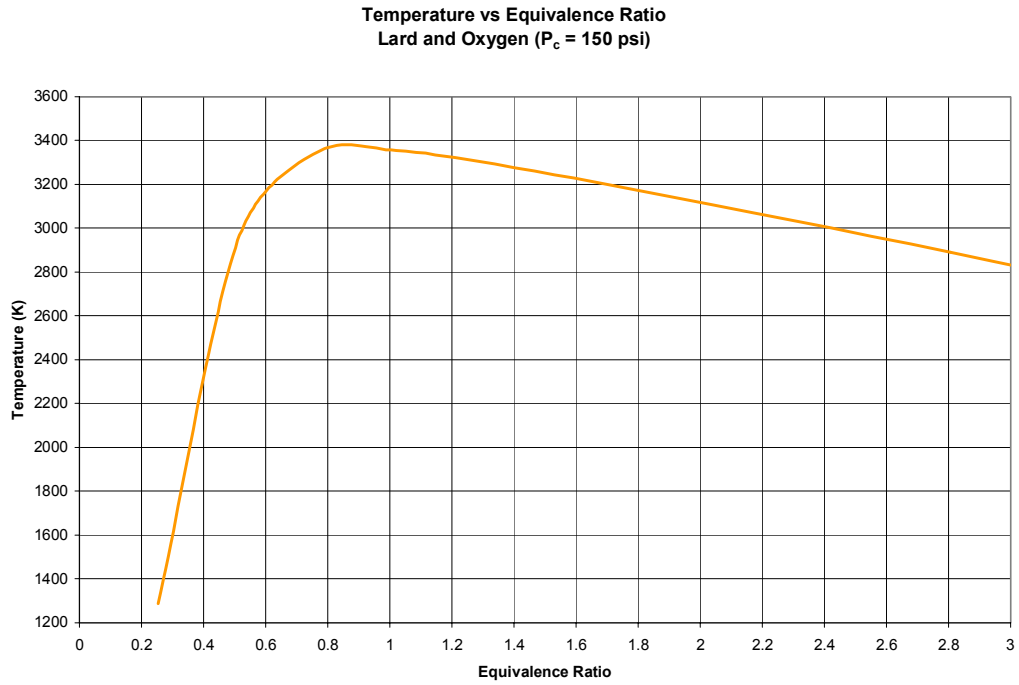
Figure 46: Temperature vs. Equivalence Ratio, Lard/Oxygen, P_c = 150 psig

Specific Impulse vs Equivalence Ratio
Lard and Oxygen (P_c = 150 psi)
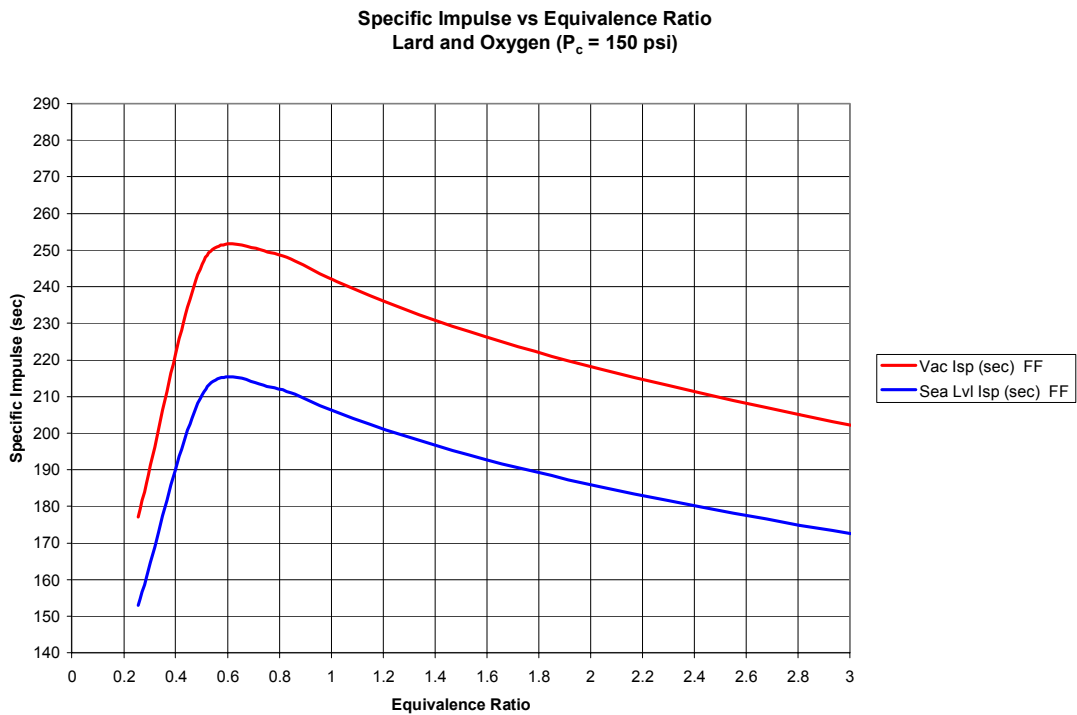
Figure 47: Specific Impulse vs. Equivalence Ratio, Lard/Oxygen, P_c = 150 psig

Ratio of Specific Heats vs Equivalence Ratio
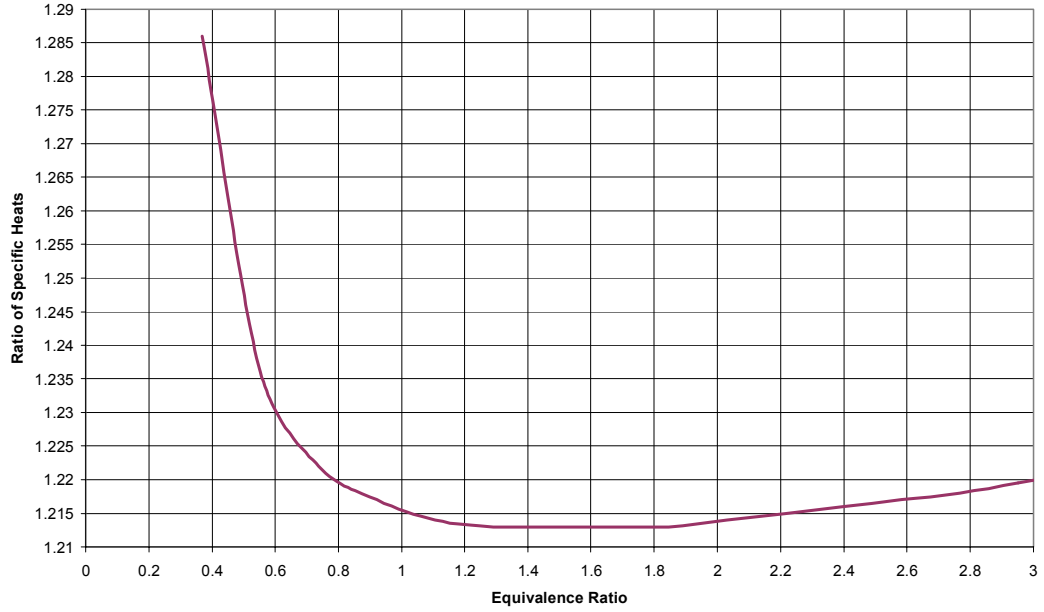**Lard and Oxygen (P$_c$ = 150 psi)**
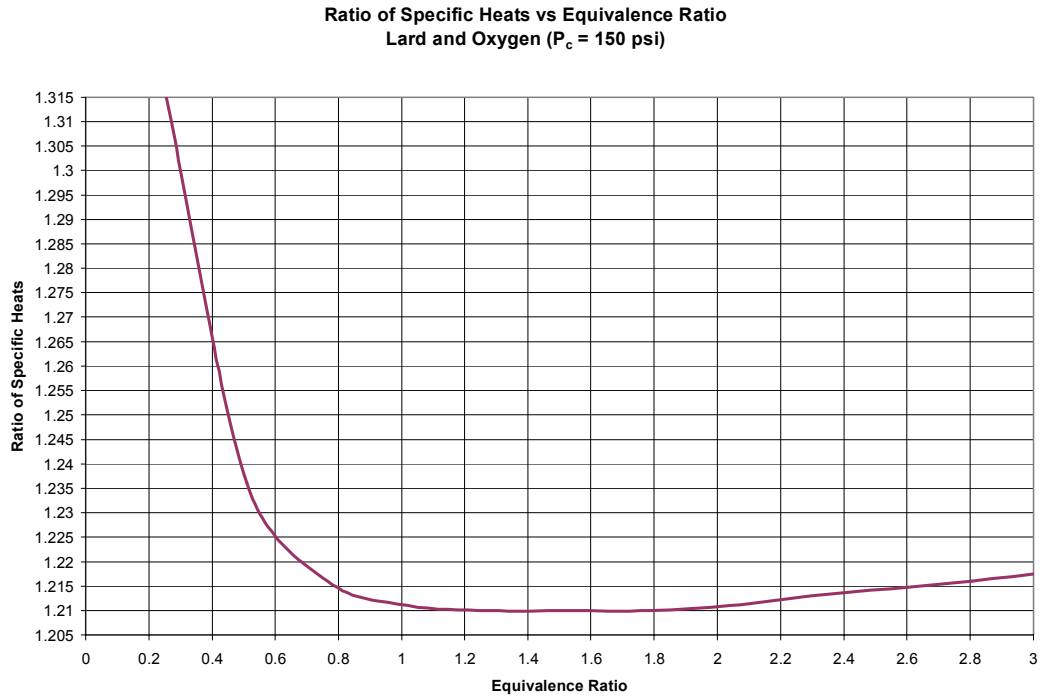
Figure 48: Ratio of Specific Heats vs. Equivalence Ratio, Lard/Oxygen, P$_c$ = 150 psig

Combustion Products Molecular Mass vs Equivalence Ratio
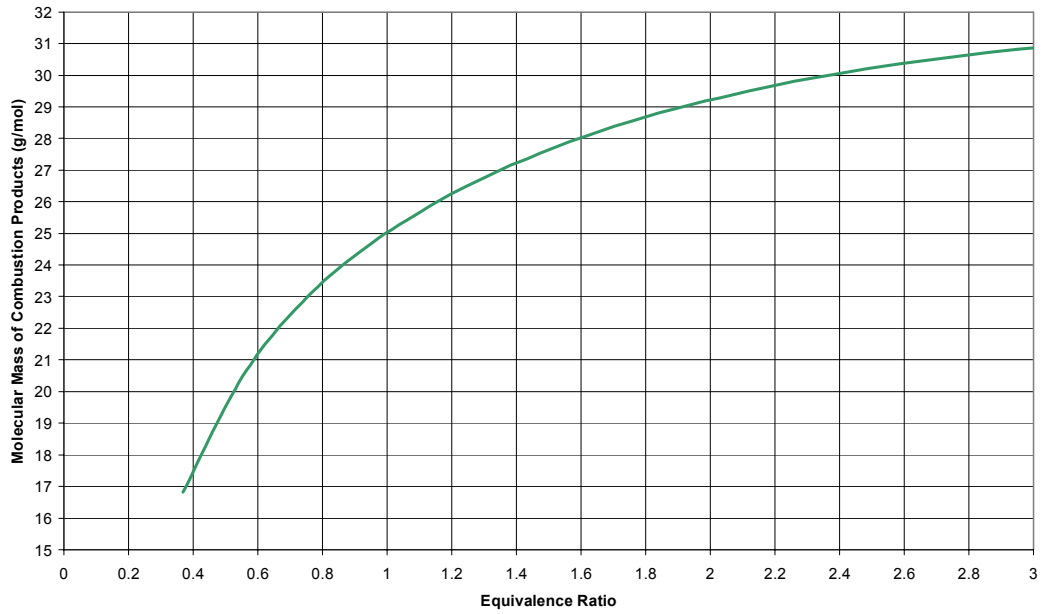**Lard and Oxygen (P$_c$ = 150 psi)**
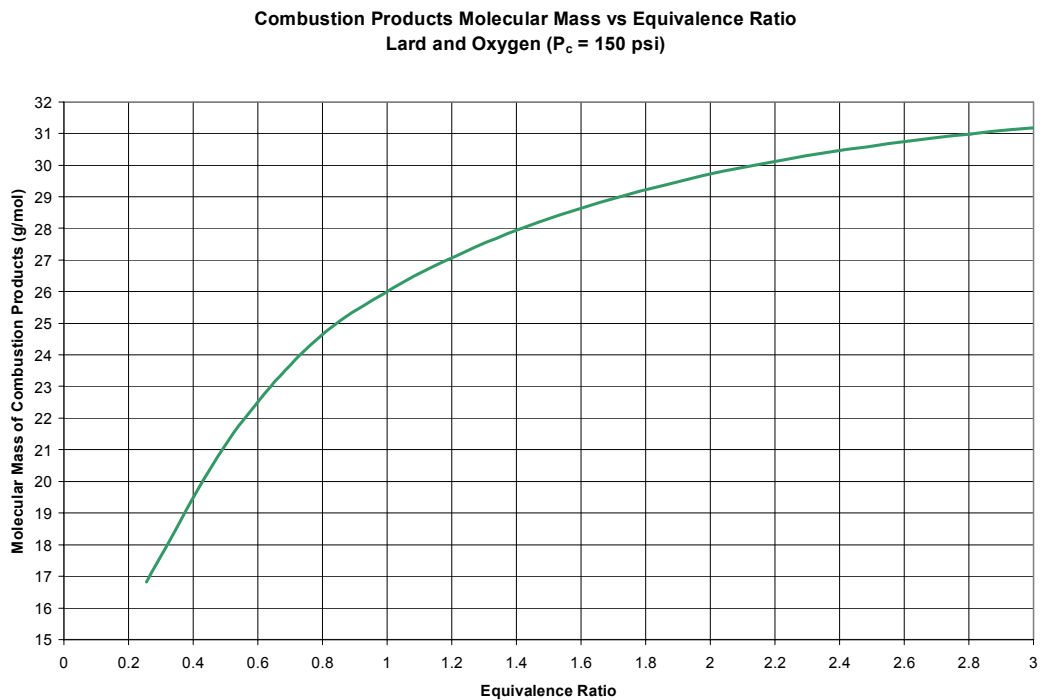
Figure 49: Molecular Mass vs. Equivalence Ratio, Lard/Oxygen, P$_c$ = 150 psig

Temperature vs Equivalence Ratio
Lard and Nitrous Oxide (Pc = 150 psi)
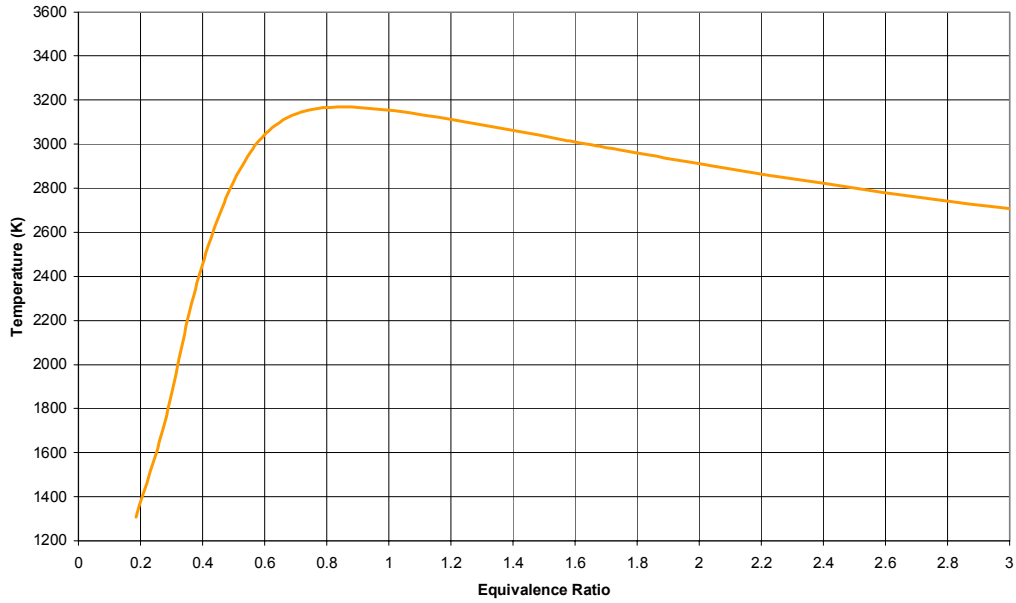
Figure 50: Temperature vs. Equivalence Ratio, Lard/Nitrous Oxide, P_c = 150 psig

Specific Impulse vs Equivalence Ratio
Lard and Nitrous Oxide (P$_c$ = 150 psi)
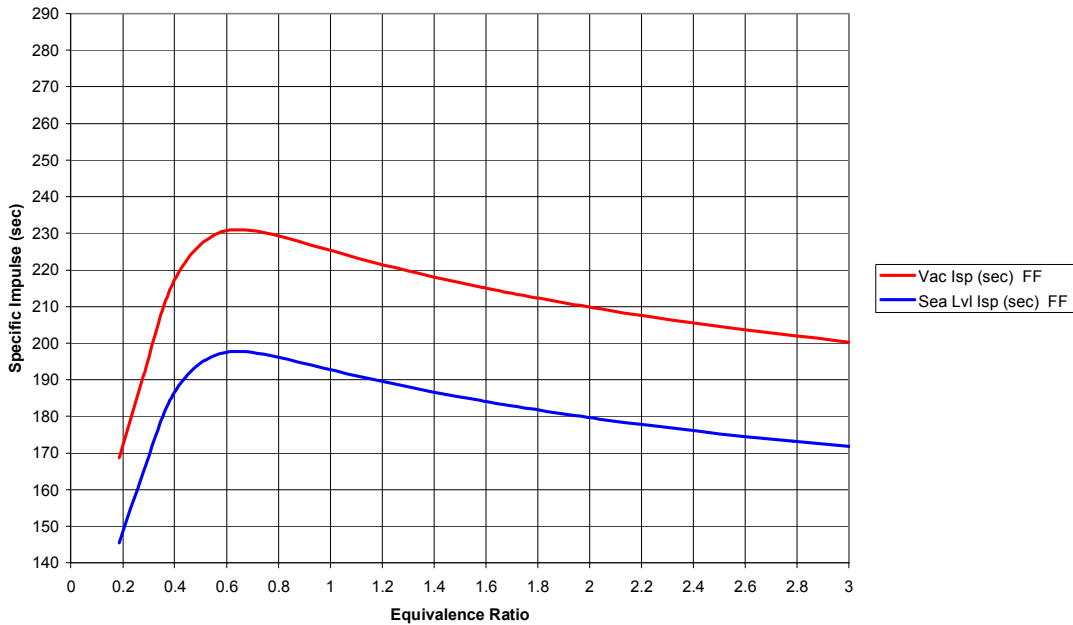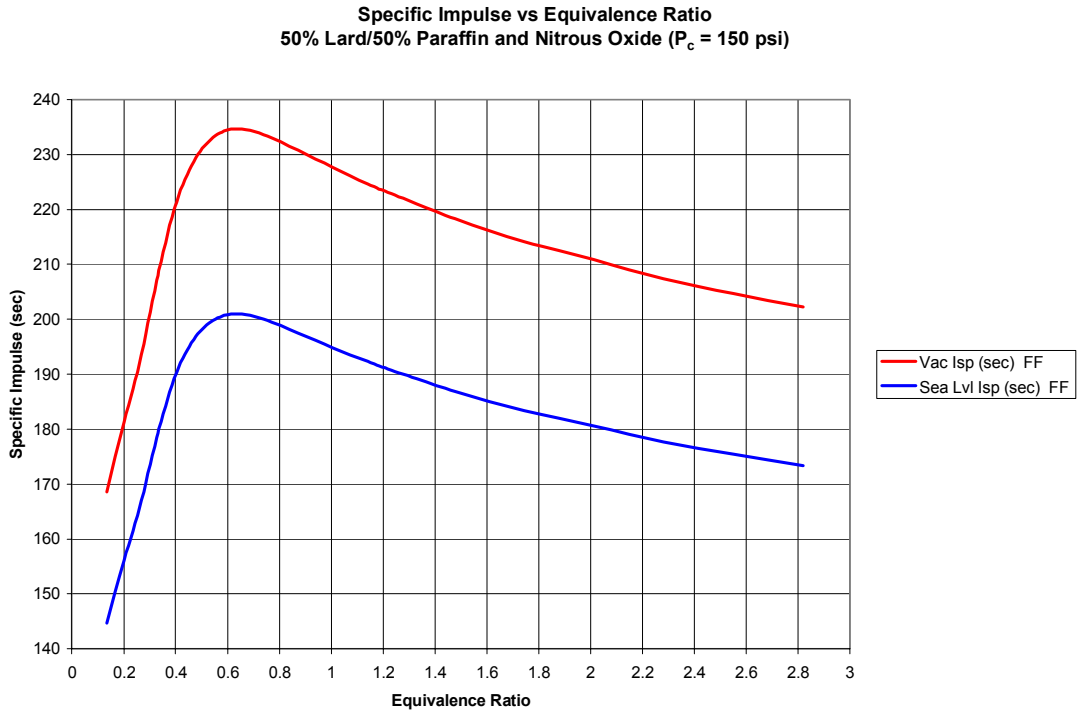

Figure 51: Specific Impulse vs. Equivalence Ratio, Lard/Nitrous Oxide, P_c = 150 psig

96

Ratio of Specific Heats vs Equivalence Ratio
Lard and Nitrous Oxide (P$_c$ = 150 psi)
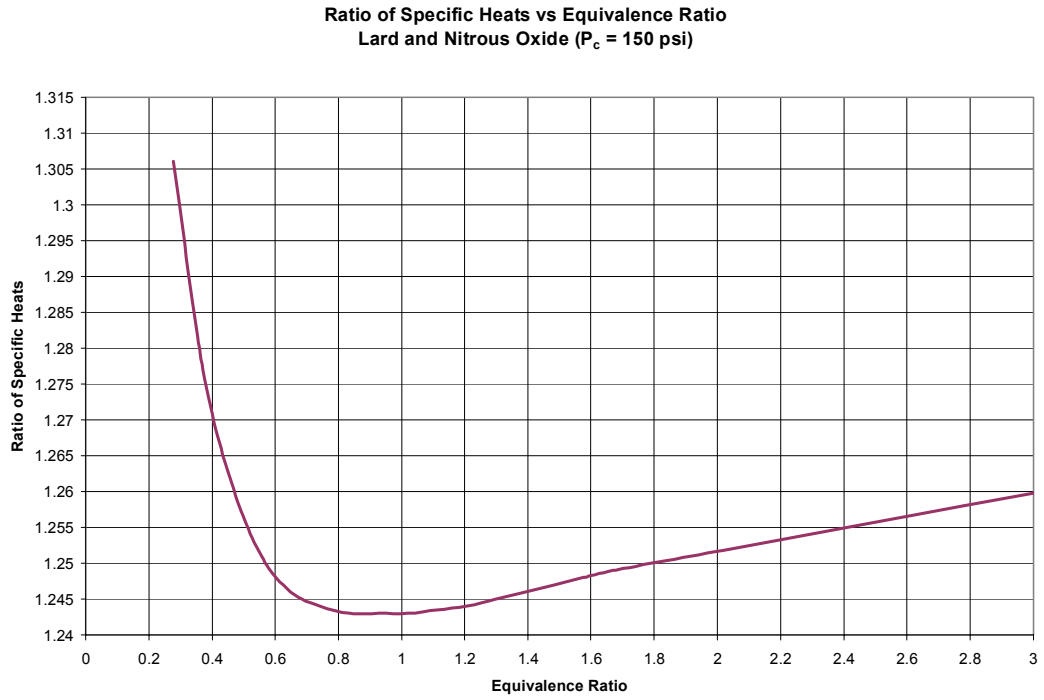
Figure 52: Ratio of Specific Heats vs. Equivalence Ratio, Lard/Nitrous Oxide, P$_c$ = 150 psig

Combustion Products Molecular Mass vs Equivalence Ratio
Lard and Nitrous Oxide (P$_c$ = 150 psi)
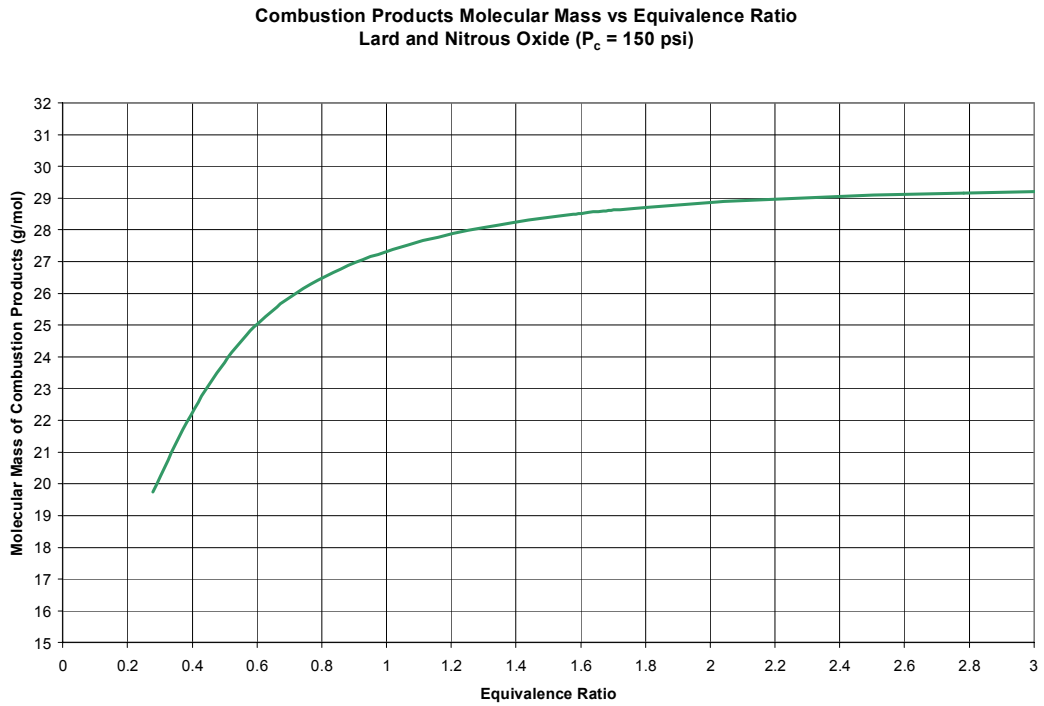
Figure 53: Molecular Mass vs. Equivalence Ratio, Lard/Nitrous Oxide, P$_c$ = 150 psig

Temperature vs Equivalence Ratio
50% Lard/50% Paraffin and Oxygen (P$_c$ = 150 psi)

Figure 54: Temperature vs. Equivalence Ratio, 50/50 LP/Oxygen, P$_c$ = 150 psig

Specific Impulse vs Equivalence Ratio
50% Lard/50% Paraffin and Oxygen (P$_c$ = 150 psi)
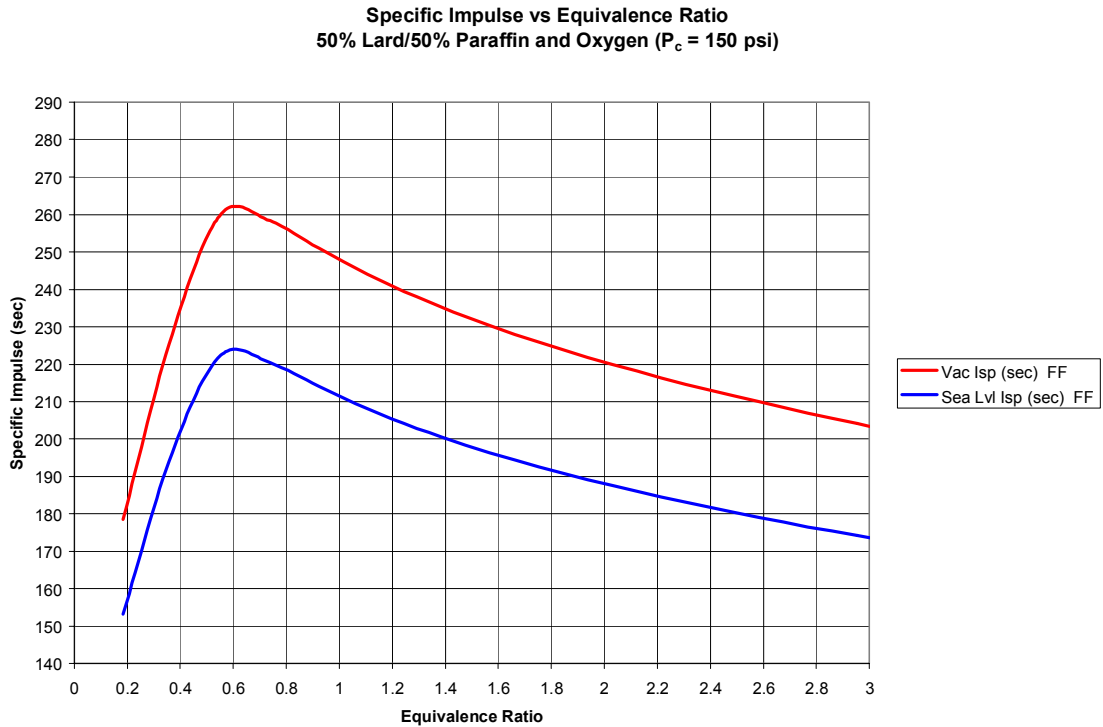
Figure 55: Specific Impulse vs. Equivalence Ratio, 50/50 LP/Oxygen, P$_c$ = 150 psig

Ratio of Specific Heats vs Equivalence Ratio
50% Lard/50% Paraffin and Oxygen (P_c = 150 psi)

Figure 56: Ratio of Specific Heats vs. Equivalence Ratio, 50/50 LP/Oxygen, P_c = 150 psig

Combustion Products Molecular Mass vs Equivalence Ratio
**50% Lard/50% Paraffin and Oxygen (P_c = 150 psi)**

Figure 57: Molecular Mass vs. Equivalence Ratio, 50/50 LP/Oxygen, P_c = 150 psig
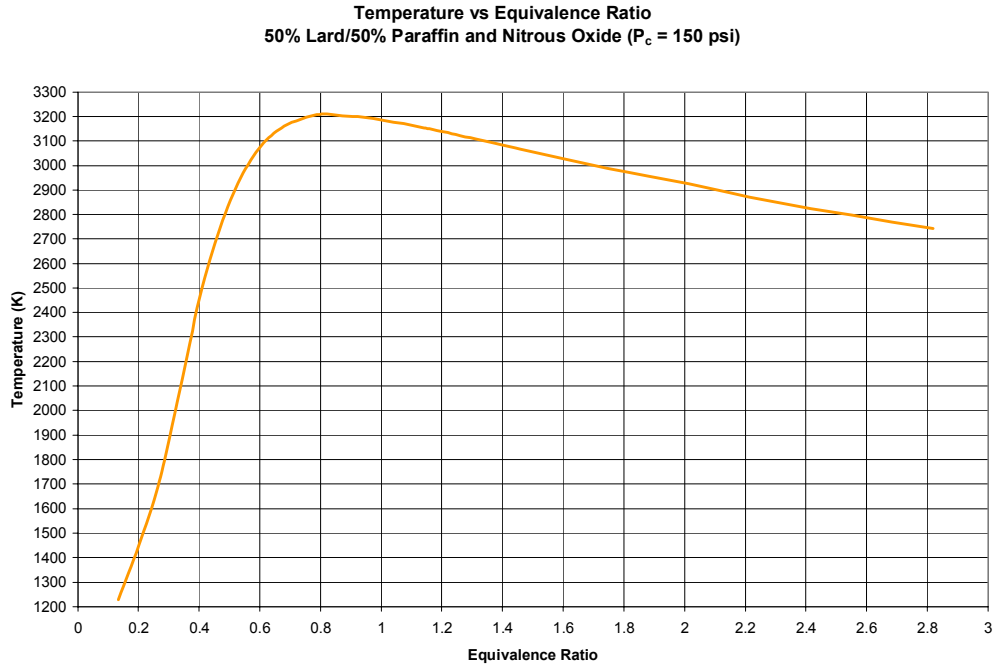
Figure 58: Temperature vs. Equivalence Ratio, 50/50 LP/Nitrous Oxide, P_c = 150 psig

Figure 59: Specific Impulse vs. Equivalence Ratio, 50/50 LP/Nitrous Oxide, P_c = 150 psig

Ratio of Specific Heats vs Equivalence Ratio
50% Lard/50% Paraffin and Nitrous Oxide (P_c = 150 psi)
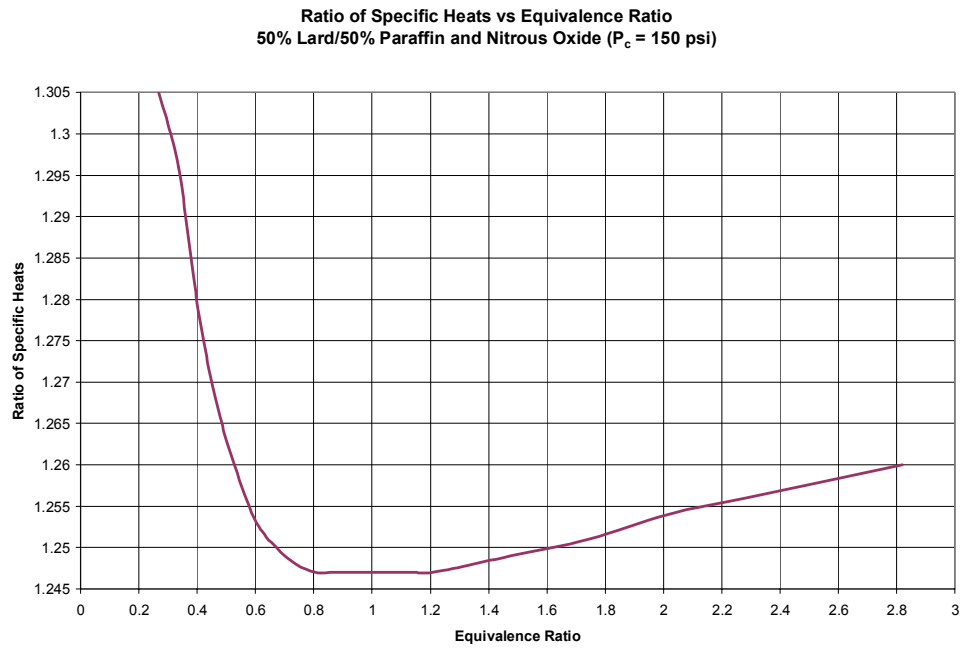
Figure 60: Ratio of Specific Heats vs. Equivalence Ratio, 50/50 LP/Nitrous Oxide, P_c = 150 psig

Combustion Products Molecular Mass vs Equivalence Ratio
50% Lard/50% Paraffin and Nitrous Oxide (P_c = 150 psi)
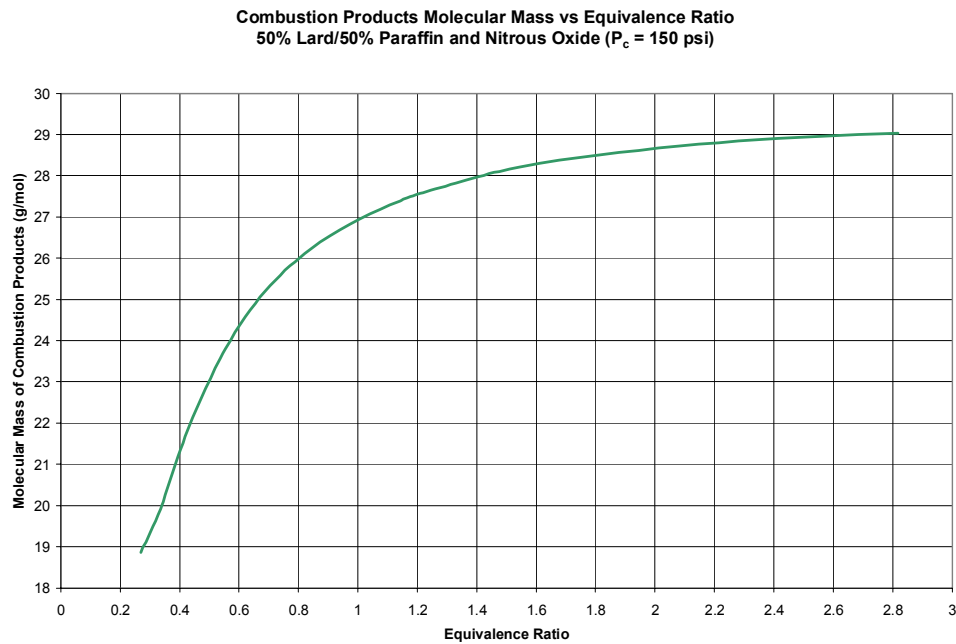
Figure 61: Molecular Mass vs. Equivalence Ratio, 50/50 LP/Nitrous Oxide, P_c = 150 psig

APPENDIX B: DATA FOR CHAMBER PRESSURE OF 500.38 PSIG
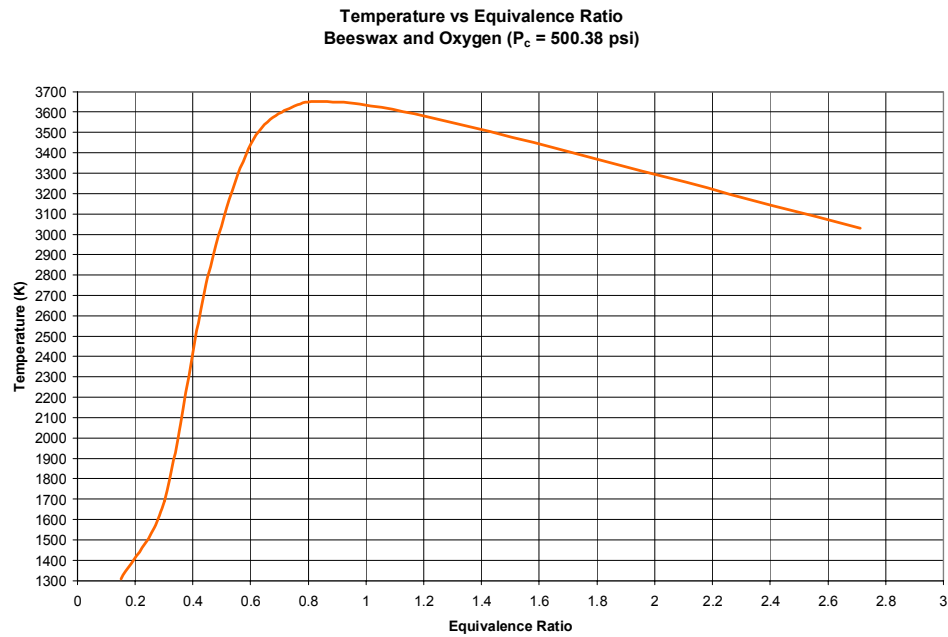
Figure 62: Temperature vs. Equivalence Ratio, Beeswax/Oxygen, P_c = 500.38 psig
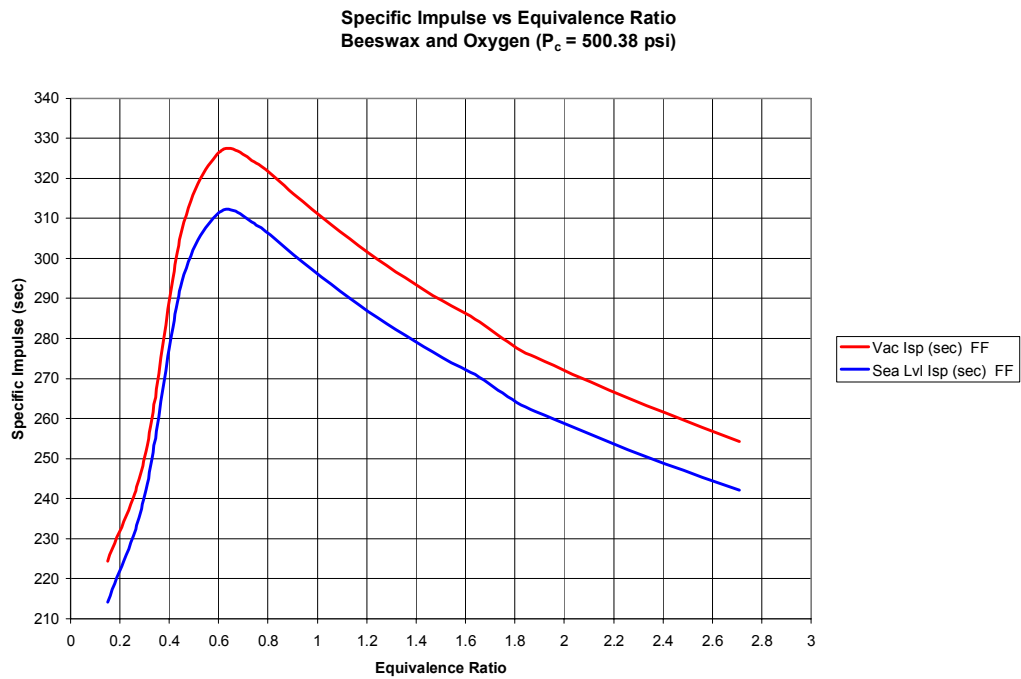
Figure 63: Specific Impulse vs. Equivalence Ratio, Beeswax/Oxygen, P_c = 500.38 psig
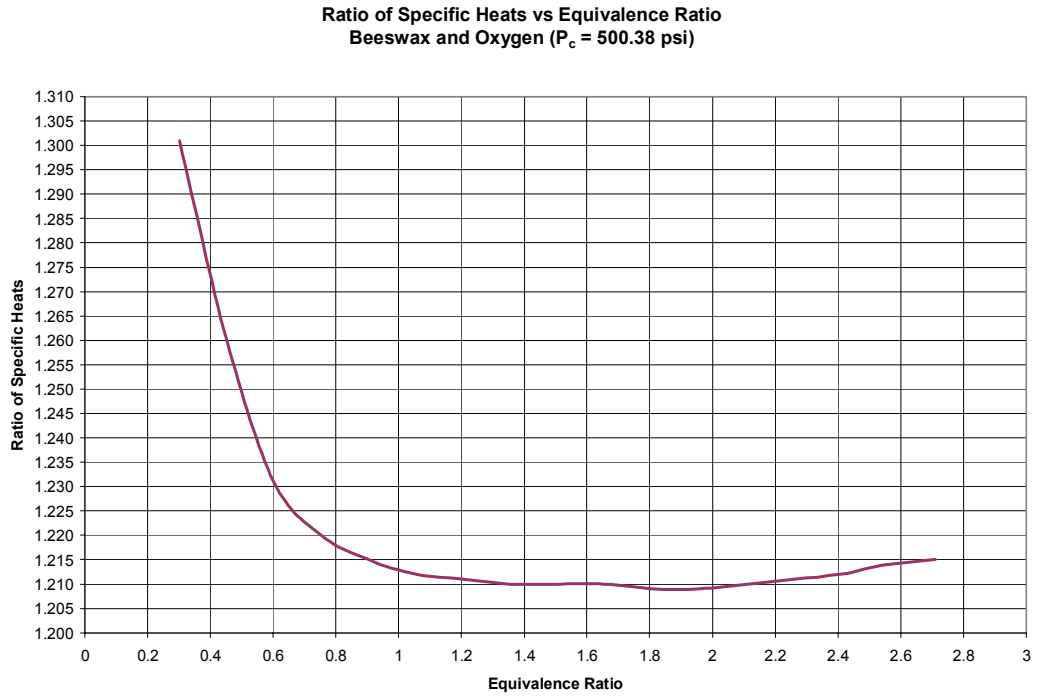
Figure 64: Ratio of Specific Heats vs. Equivalence Ratio, Beeswax/Oxygen, P_c = 500.38 psig
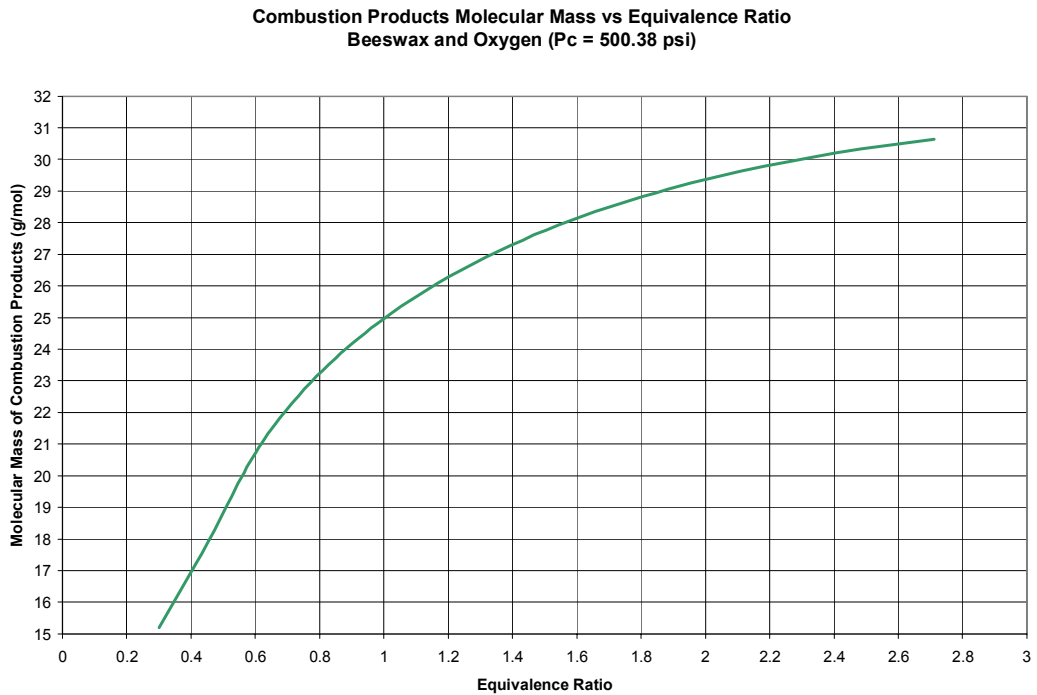
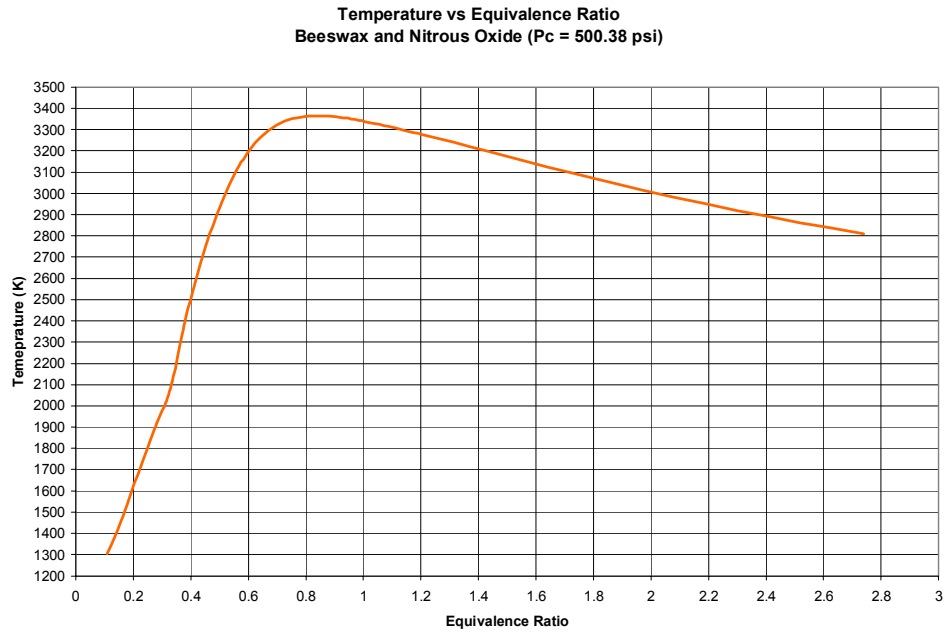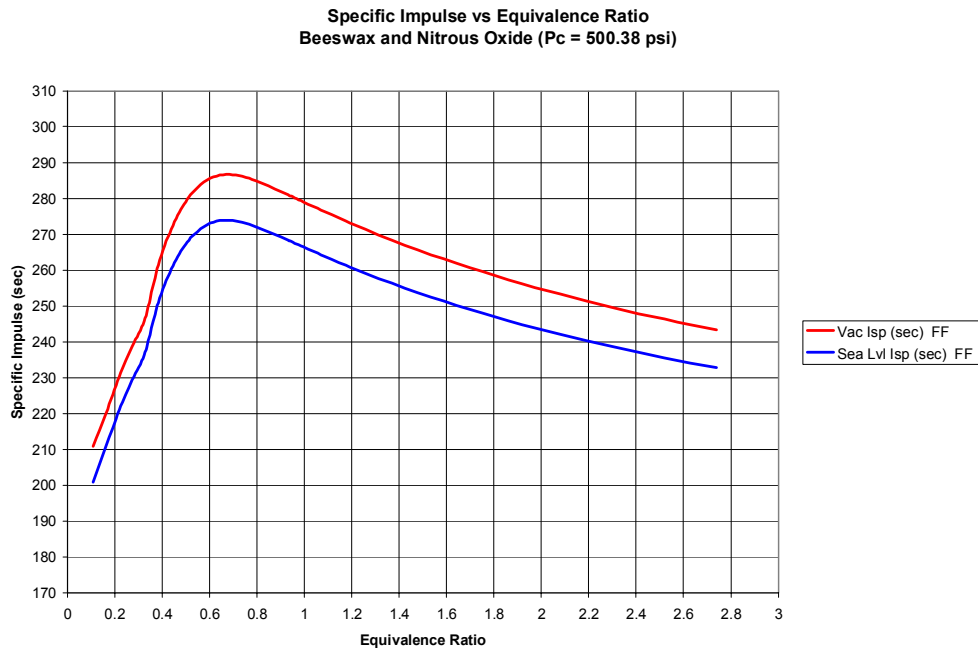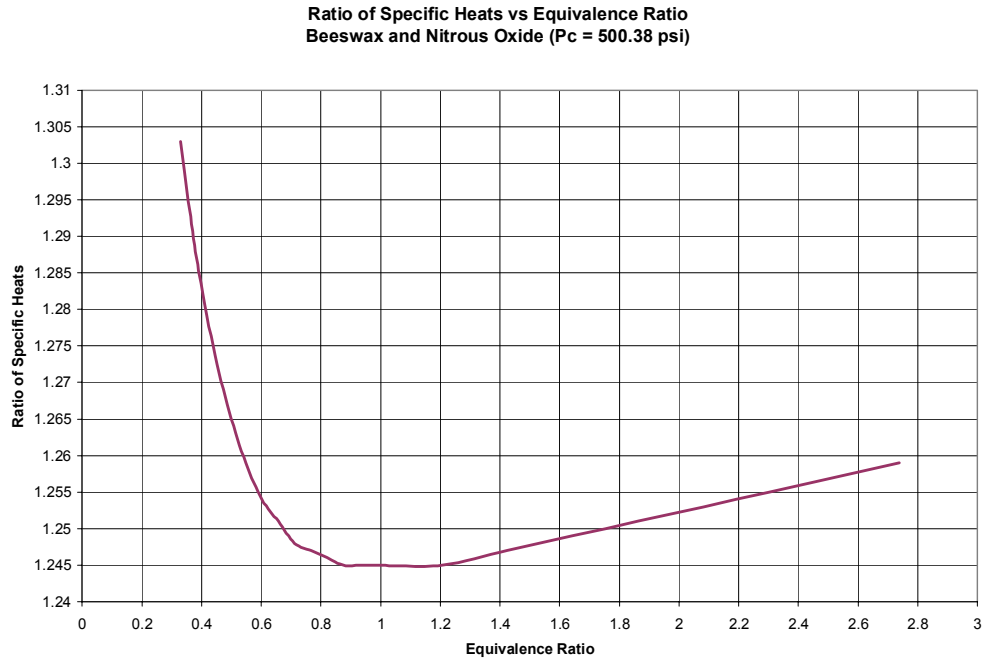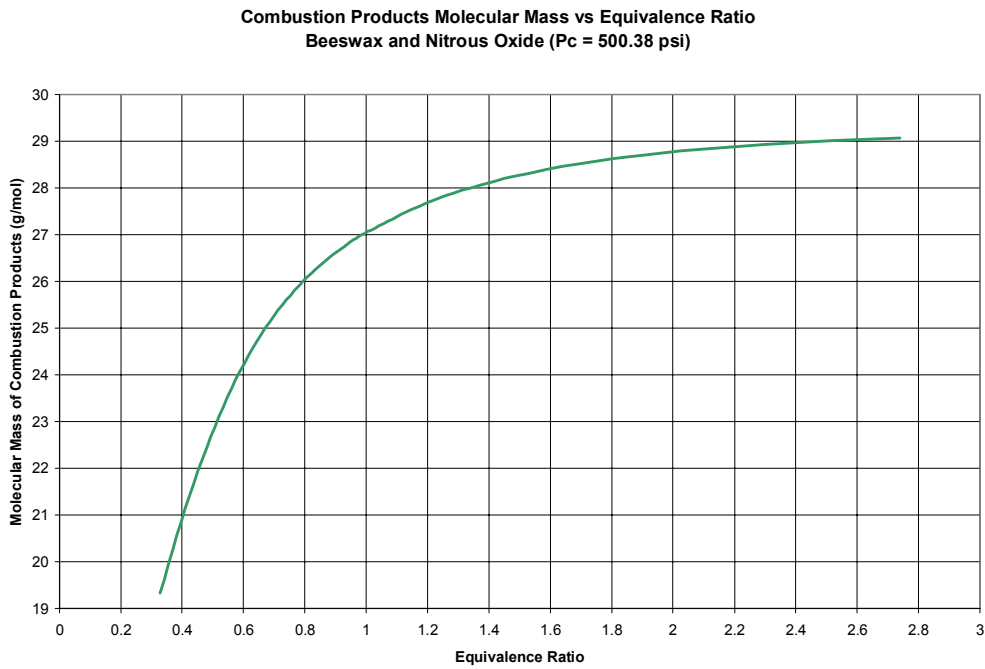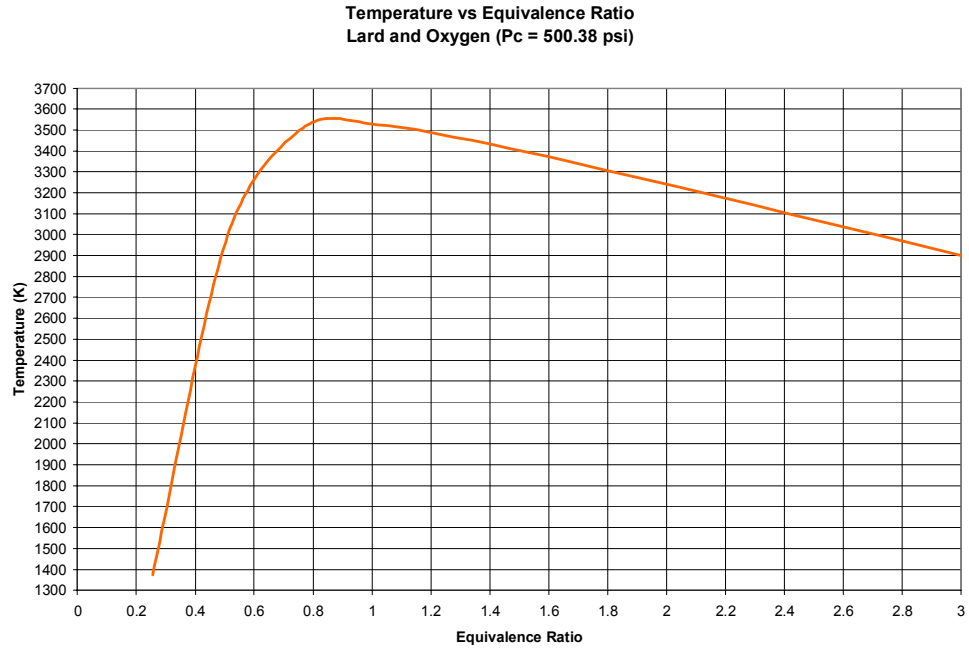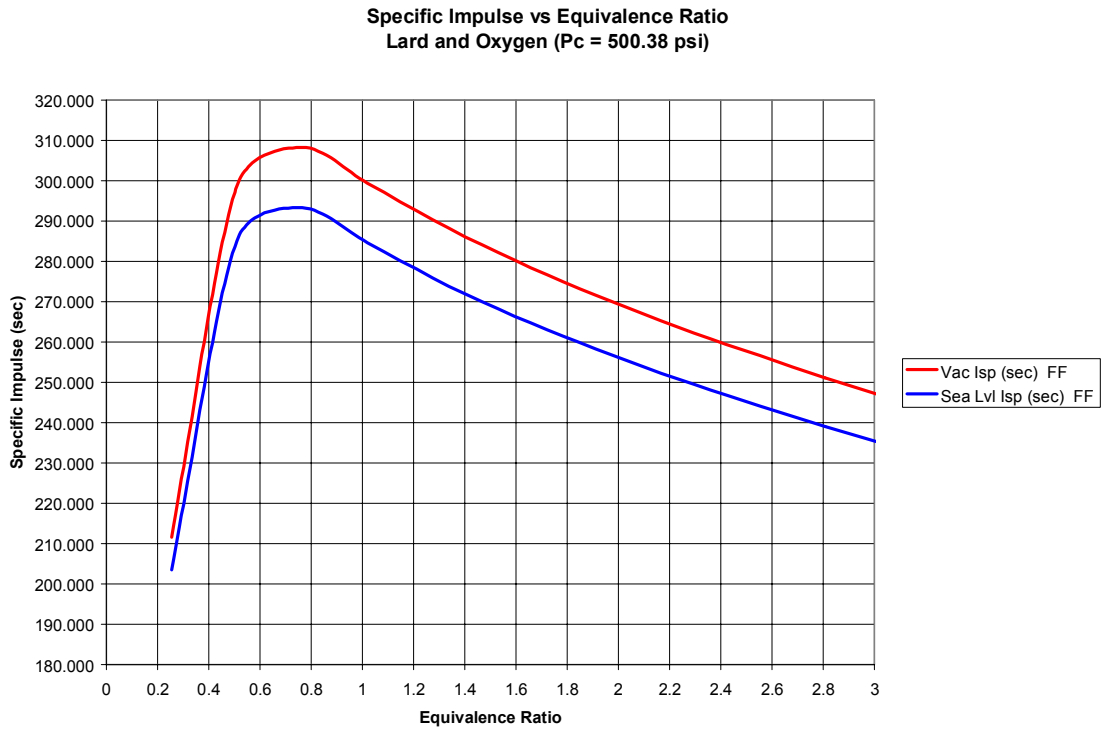Figure 65: Molecular Mass vs. Equivalence Ratio, Beeswax/Oxygen, P_c = 500.38 psig

103

Temperature vs Equivalence Ratio
Beeswax and Nitrous Oxide (Pc = 500.38 psi)

Figure 66: Temperature vs. Equivalence Ratio, Beeswax/Nitrous Oxide, P_c = 500.38 psig

Specific Impulse vs Equivalence Ratio
Beeswax and Nitrous Oxide (Pc = 500.38 psi)

Figure 67: Specific Impulse vs. Equivalence Ratio, Beeswax/Nitrous Oxide, P_c = 500.38 psig

104

Ratio of Specific Heats vs Equivalence Ratio
Beeswax and Nitrous Oxide (Pc = 500.38 psi)

Figure 68: Ratio of Specific Heats vs. Equivalence Ratio, Beeswax/Nitrous Oxide, P_c = 500.38 psig

Combustion Products Molecular Mass vs Equivalence Ratio
Beeswax and Nitrous Oxide (Pc = 500.38 psi)

Figure 69: Molecular Mass vs. Equivalence Ratio, Beeswax/Nitrous Oxide, P_c = 500.38 psig

Temperature vs Equivalence Ratio
Lard and Oxygen (Pc = 500.38 psi)

Figure 70: Temperature vs. Equivalence Ratio, Lard/Oxygen, P_c = 500.38 psig

Specific Impulse vs Equivalence Ratio
Lard and Oxygen (Pc = 500.38 psi)

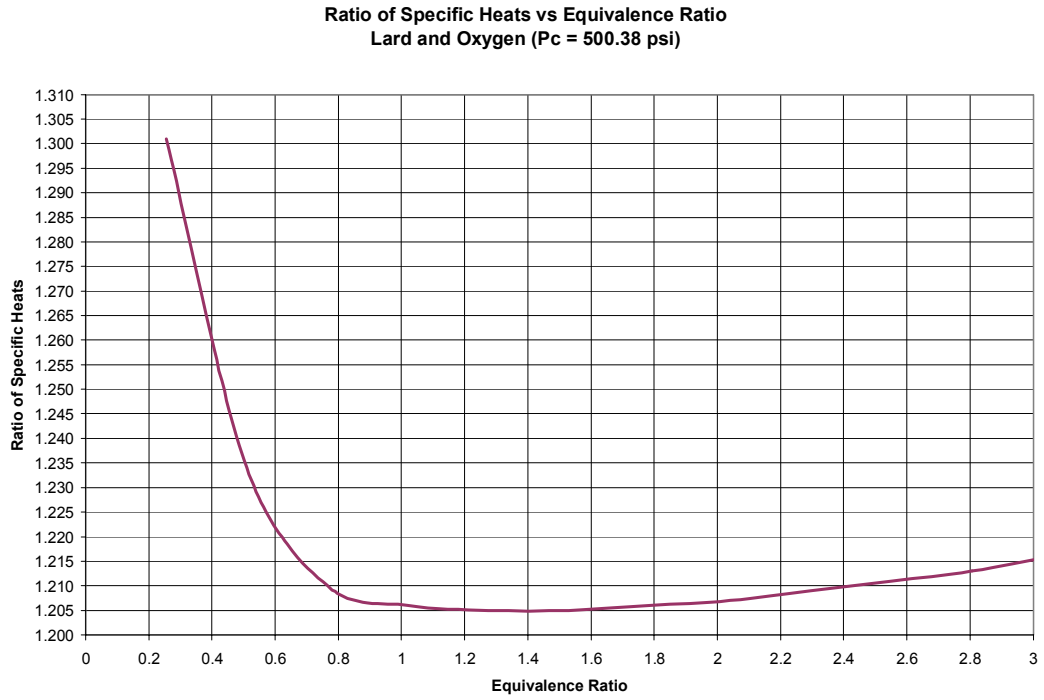Figure 71: Specific Impulse vs. Equivalence Ratio, Lard/Oxygen, P_c = 500.38 psig

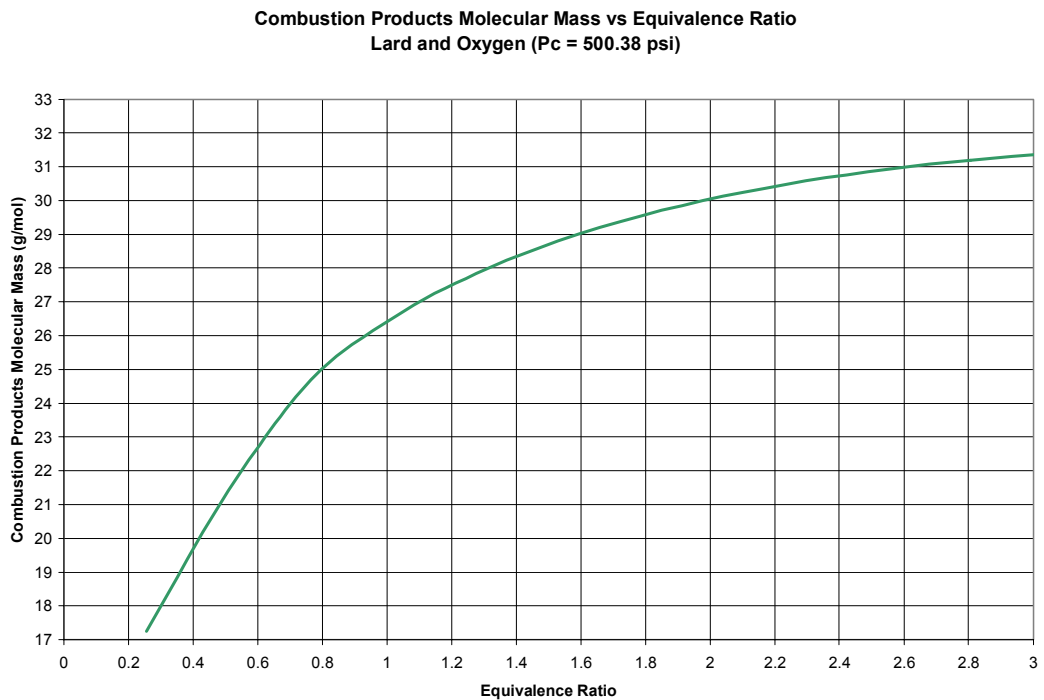**Ratio of Specific Heats vs Equivalence Ratio**
Lard and Oxygen (Pc = 500.38 psi)

Figure 72: Ratio of Specific Heats vs. Equivalence Ratio, Lard/Oxygen, P_c = 500.38 psig

Combustion Products Molecular Mass vs Equivalence Ratio
Lard and Oxygen (Pc = 500.38 psi)

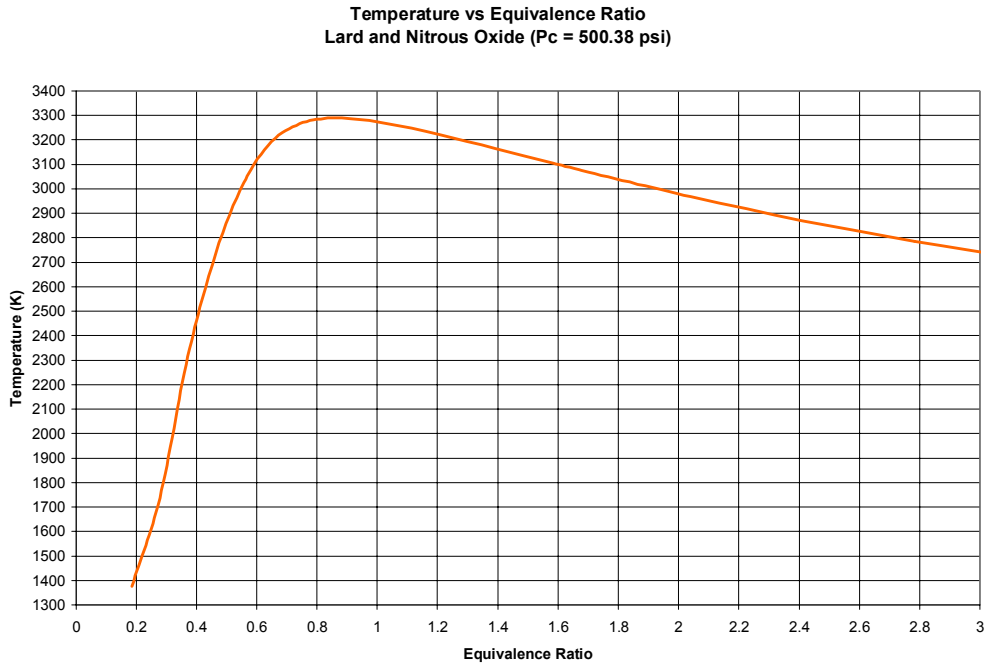Figure 73: Molecular Mass vs. Equivalence Ratio, Lard/Oxygen, P_c = 500.38 psig

Temperature vs Equivalence Ratio
Lard and Nitrous Oxide (Pc = 500.38 psi)

Figure 74: Temperature vs. Equivalence Ratio, Lard/Nitrous Oxide, P_c = 500.38 psig

Specific Impulse vs Equivalence Ratio
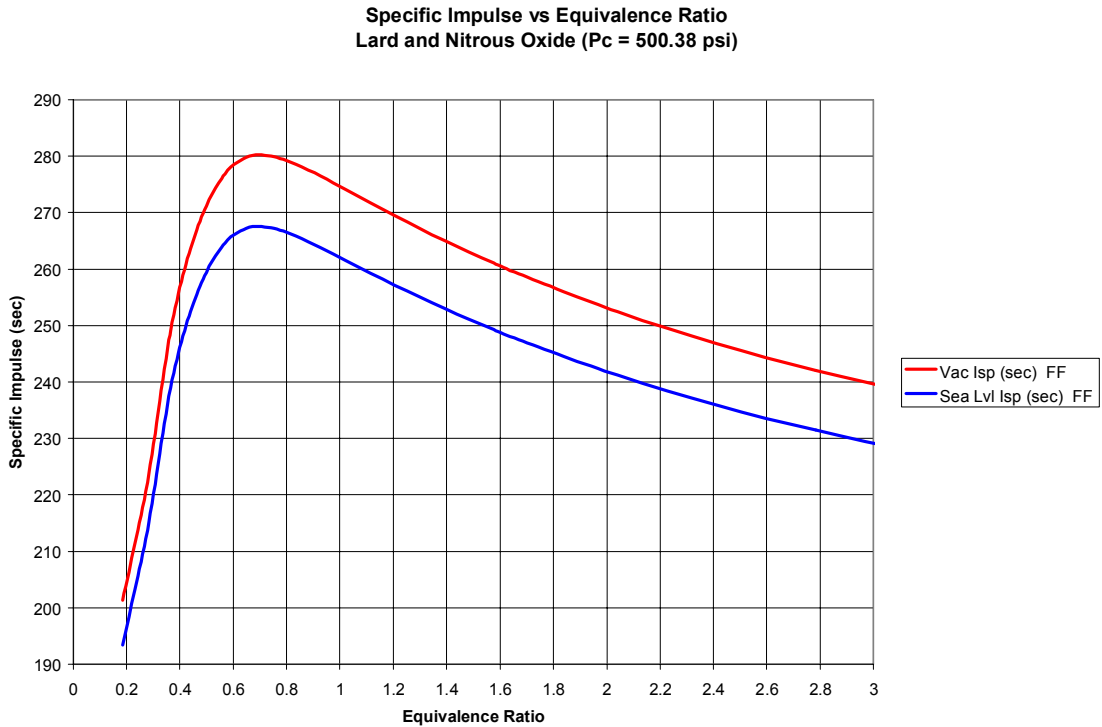**Lard and Nitrous Oxide (Pc = 500.38 psi)**

Figure 75: Specific Impulse vs. Equivalence Ratio, Lard/Nitrous Oxide, P_c = 500.38 psig

Ratio of Specific Heats vs Equivalence Ratio
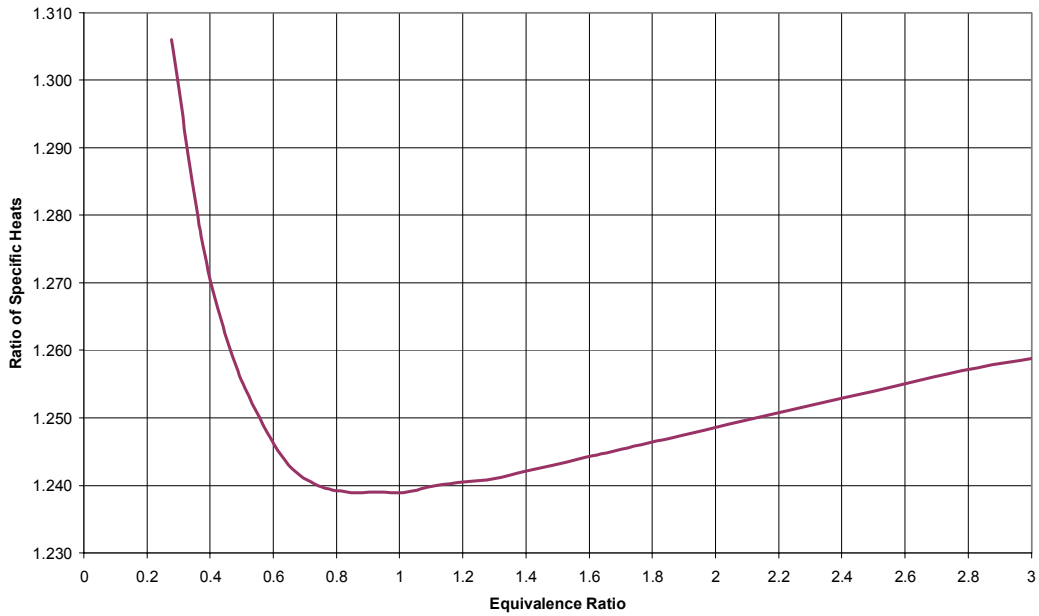**Lard and Nitrous Oxide (Pc = 500.38 psi)**

Figure 76: Ratio of Specific Heats vs. Equivalence Ratio, Lard/Nitrous Oxide, P_c = 500.38 psig

Combustion Products Molecular Mass vs Equivalence Ratio
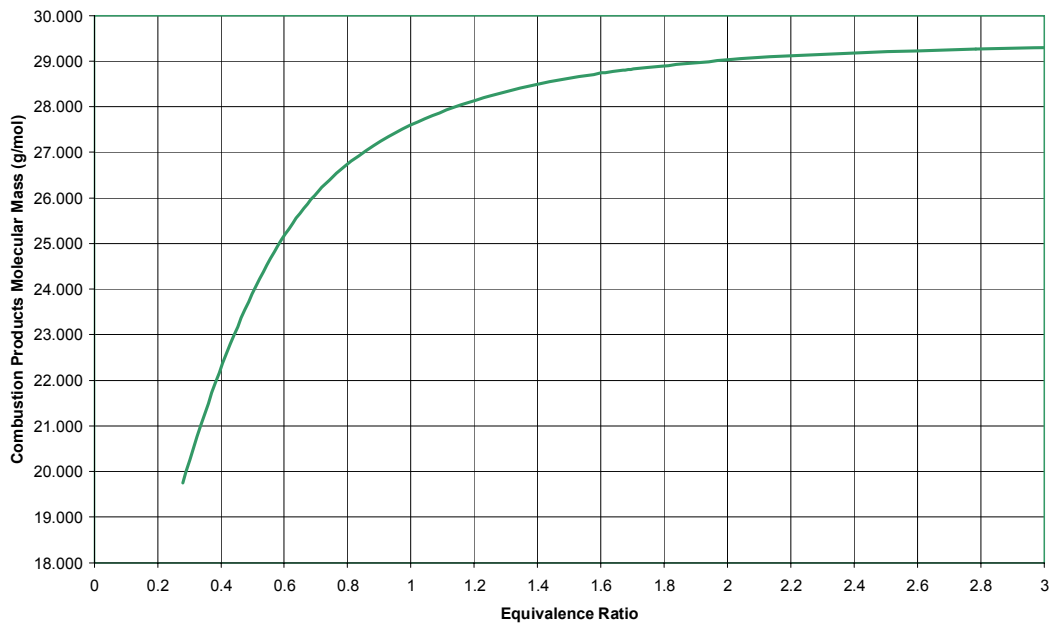**Lard and Nitrous Oxide (Pc = 500.38 psi)**

Figure 77: Molecular Mass vs. Equivalence Ratio, Lard/Nitrous Oxide, P_c = 500.38 psig
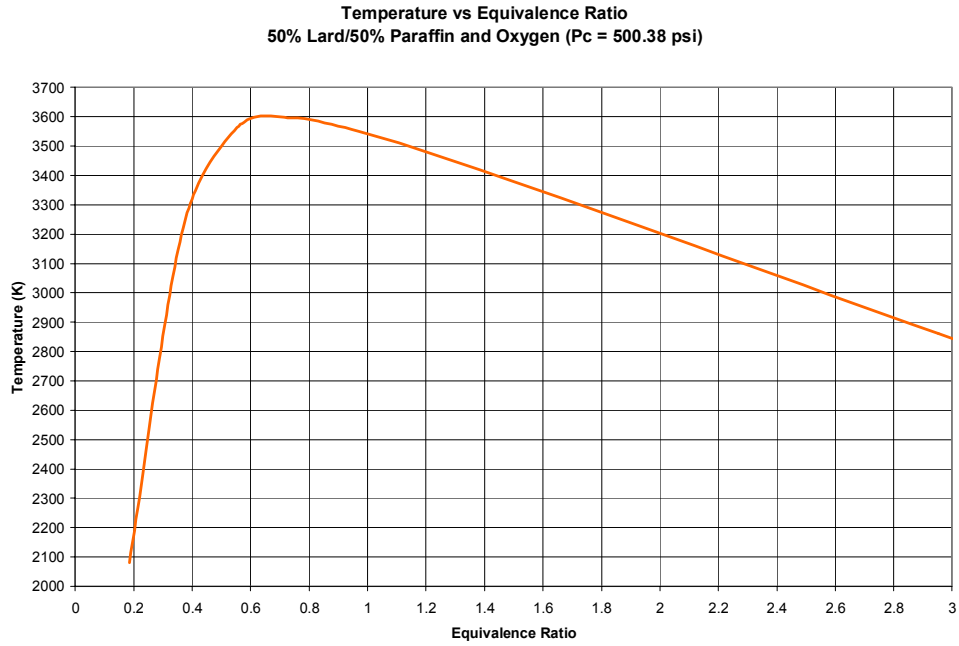
Temperature vs Equivalence Ratio
50% Lard/50% Paraffin and Oxygen (Pc = 500.38 psi)

Figure 78: Temperature vs. Equivalence Ratio, 50/50 LP/Oxygen, P_c = 500.38 psig

Specific Impulse vs Equivalence Ratio
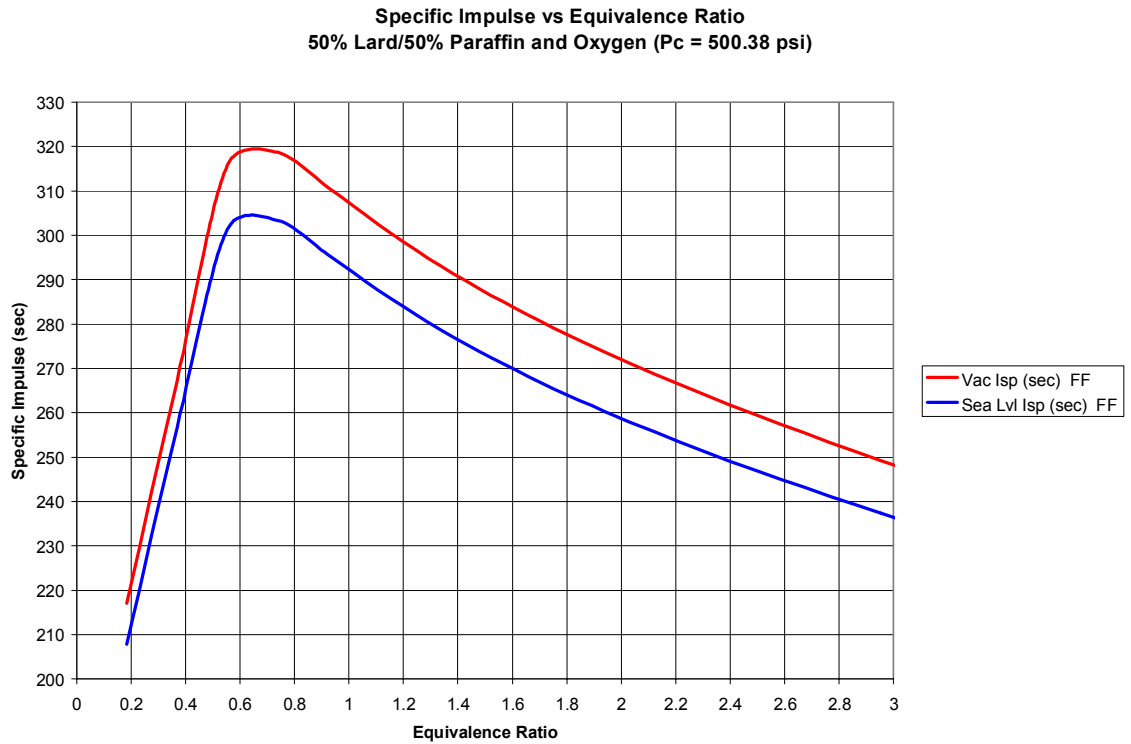**50% Lard/50% Paraffin and Oxygen (Pc = 500.38 psi)**

Figure 79: Specific Impulse vs. Equivalence Ratio, 50/50 LP/Oxygen, P_c = 500.38 psig

110

Ratio of Specific Heats vs Equivalence Ratio
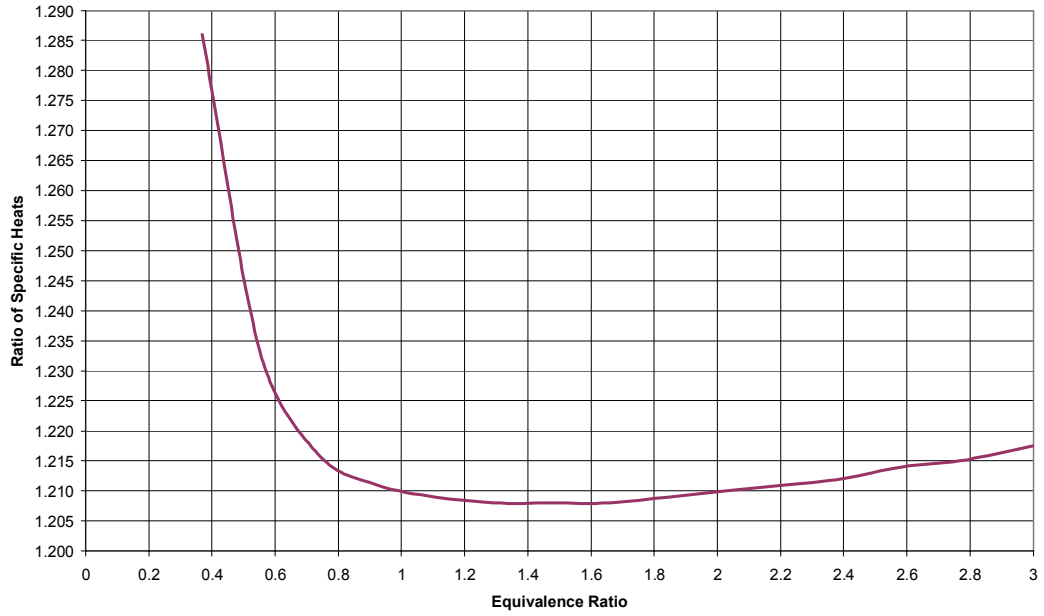**50% Lard/50% Paraffin and Oxygen (Pc = 500.38 psi)**

Figure 80: Ratio of Specific Heats vs. Equivalence Ratio, 50/50 LP/Oxygen, P_c = 500.38 psig

Combustion Products Molecular Mass vs Equivalence Ratio
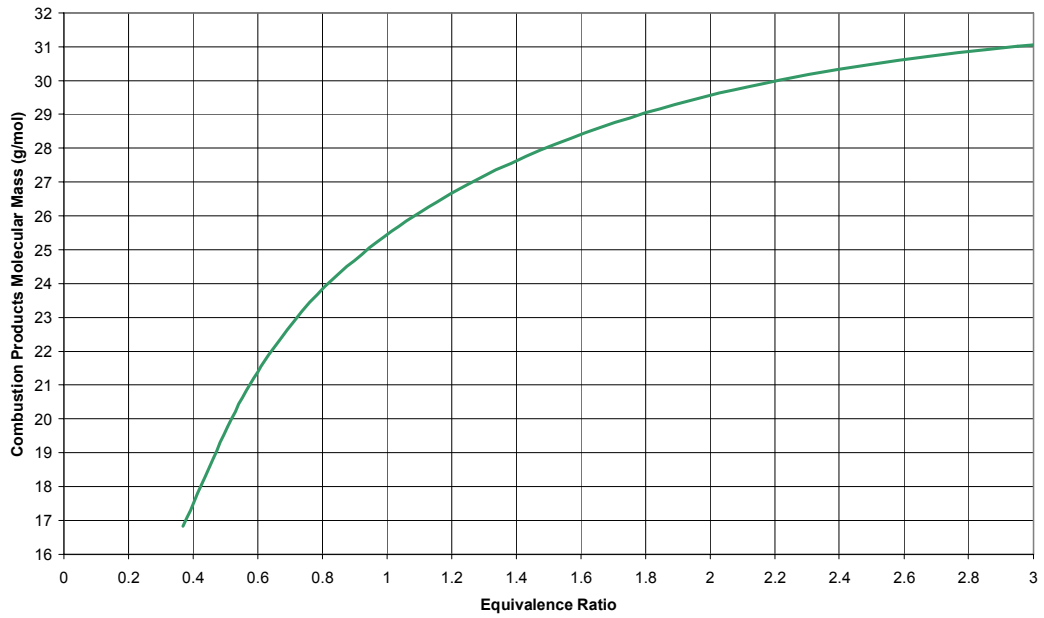**50% Lard/50% Paraffin and Oxygen (Pc = 500.38 psi)**

Figure 81: Molecular Mass vs. Equivalence Ratio, 50/50 LP/Oxygen, P_c = 500.38 psig
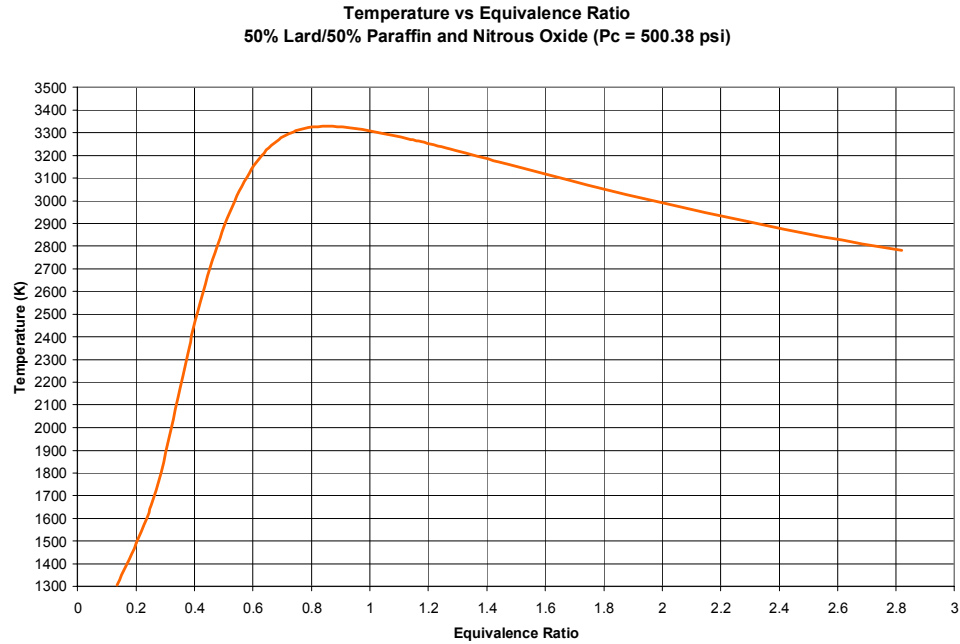
Temperature vs Equivalence Ratio
50% Lard/50% Paraffin and Nitrous Oxide (Pc = 500.38 psi)

Figure 82: Temperature vs. Equivalence Ratio, 50/50 LP/Nitrous Oxide, P_c = 500.38 psig

Specific Impulse vs Equivalence Ratio
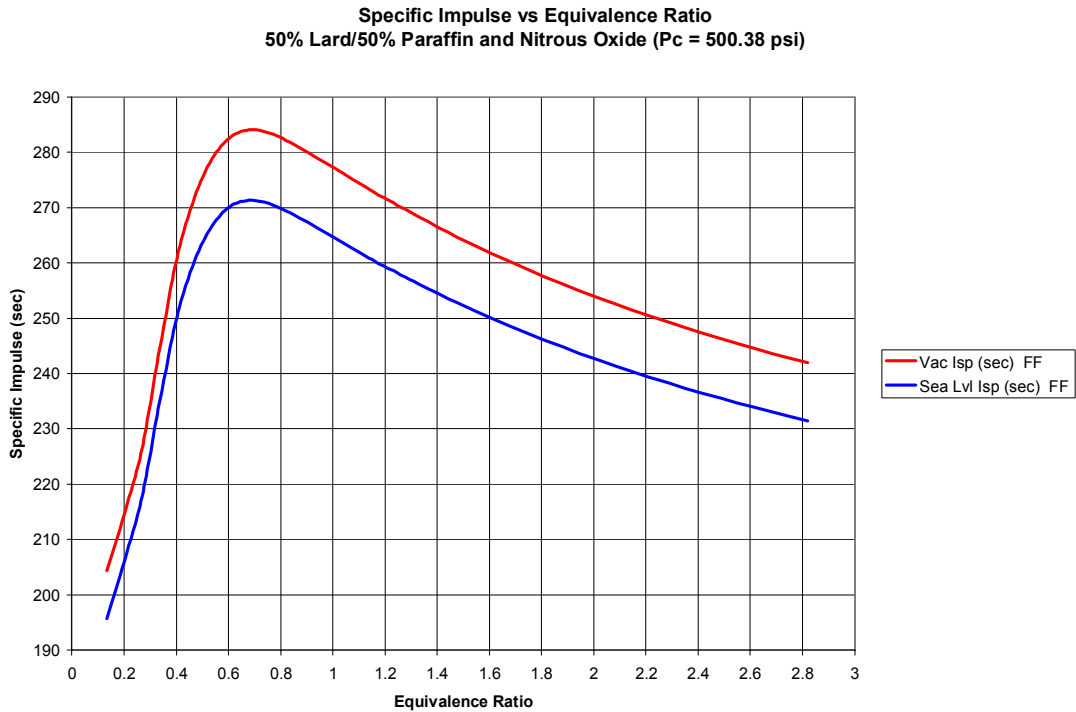**50% Lard/50% Paraffin and Nitrous Oxide (Pc = 500.38 psi)**

Figure 83: Specific Impulse vs. Equivalence Ratio, 50/50 LP/Nitrous Oxide, P_c = 500.38 psig

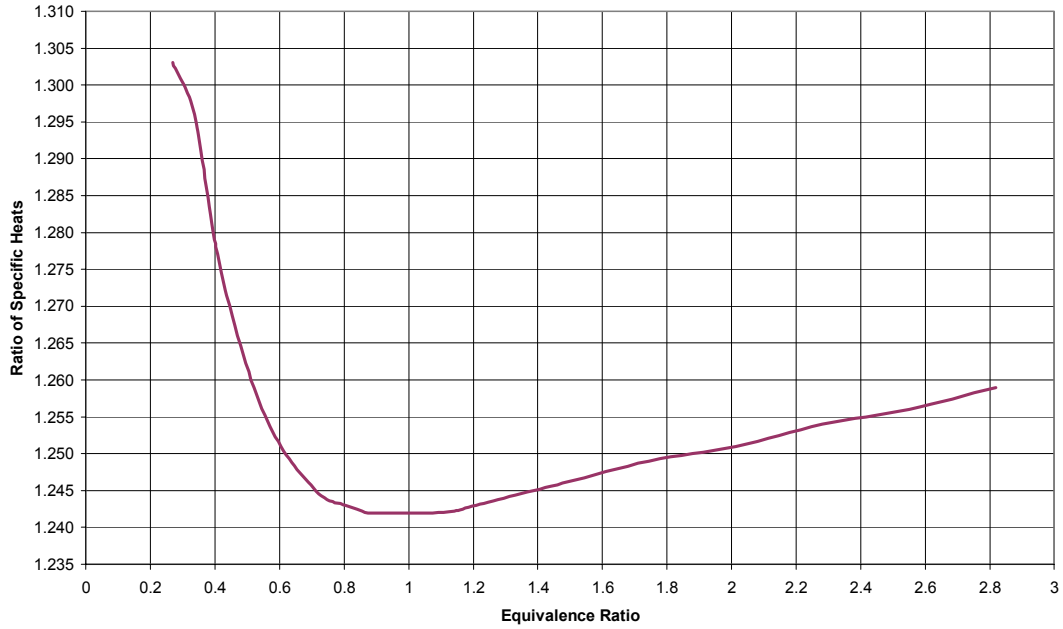Figure 84: Ratio of Specific Heats vs. Equivalence Ratio, 50/50 LP/Nitrous Oxide, P_c = 500.38 psig
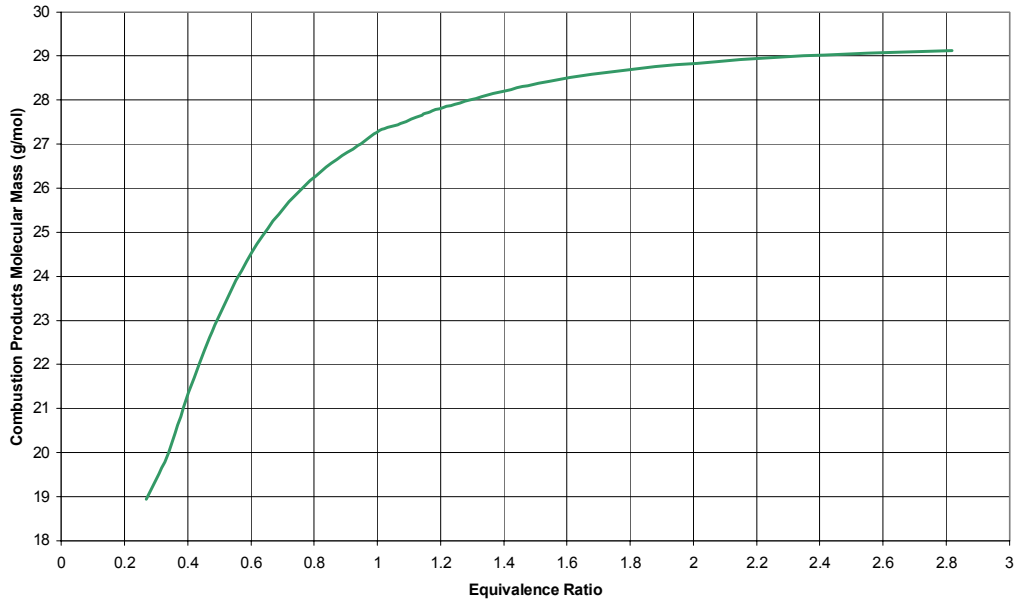

Figure 85: Molecular Mass vs. Equivalence Ratio, 50/50 LP/Nitrous Oxide, P_c = 500.38 psig

Figure 86: Temperature vs. Equivalence Ratio, Beeswax + 5% Al/Oxygen, P_c = 500.38 psig

Figure 87: Specific Impulse vs. Equivalence Ratio, Beeswax + 5% Al/Oxygen, P_c = 500.38 psig

114

Ratio of Specific Heats vs Equivalence Ratio
Beeswax + 5% Al and Oxygen, P_c = 500.38 psi

Figure 88: Ratio of Specific Heats vs. Equivalence Ratio, Beeswax + 5% Al/Oxygen, P_c = 500.38 psig

Combustion Products Molecular Mass vs Equivalence Ratio
Beeswax + 5% Al and Oxygen, P_c = 500.38 psi

Figure 89: Molecular Mass vs. Equivalence Ratio, Beeswax + 5% Al/Oxygen, P_c = 500.38 psig
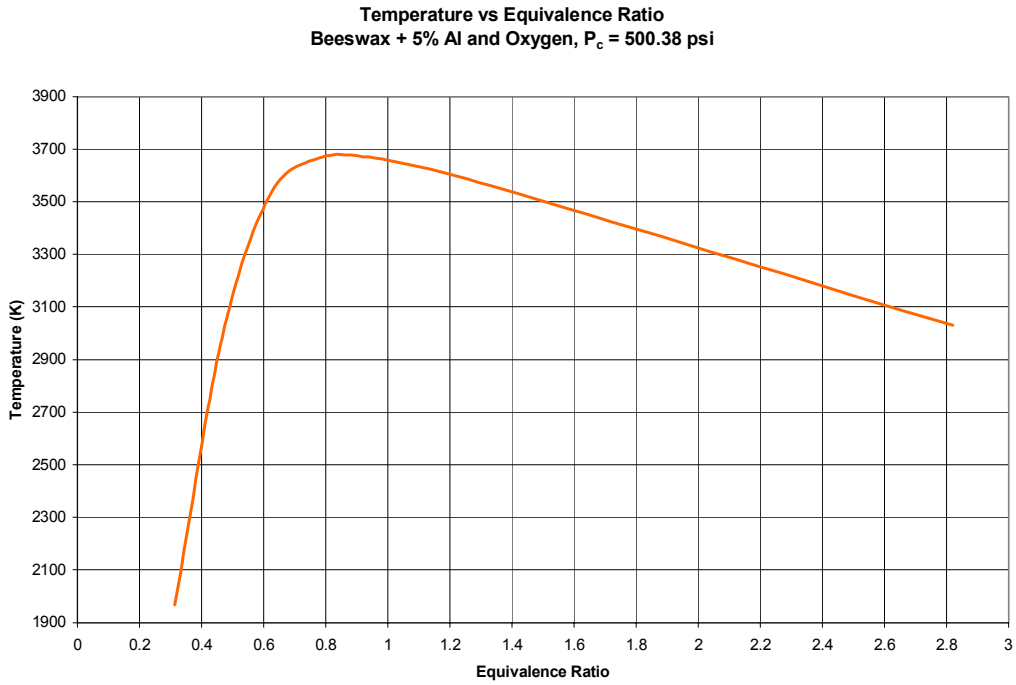
115

Figure 90: Temperature vs. Equivalence Ratio, Beeswax + 10% Al/Oxygen, P_c = 500.38 psig

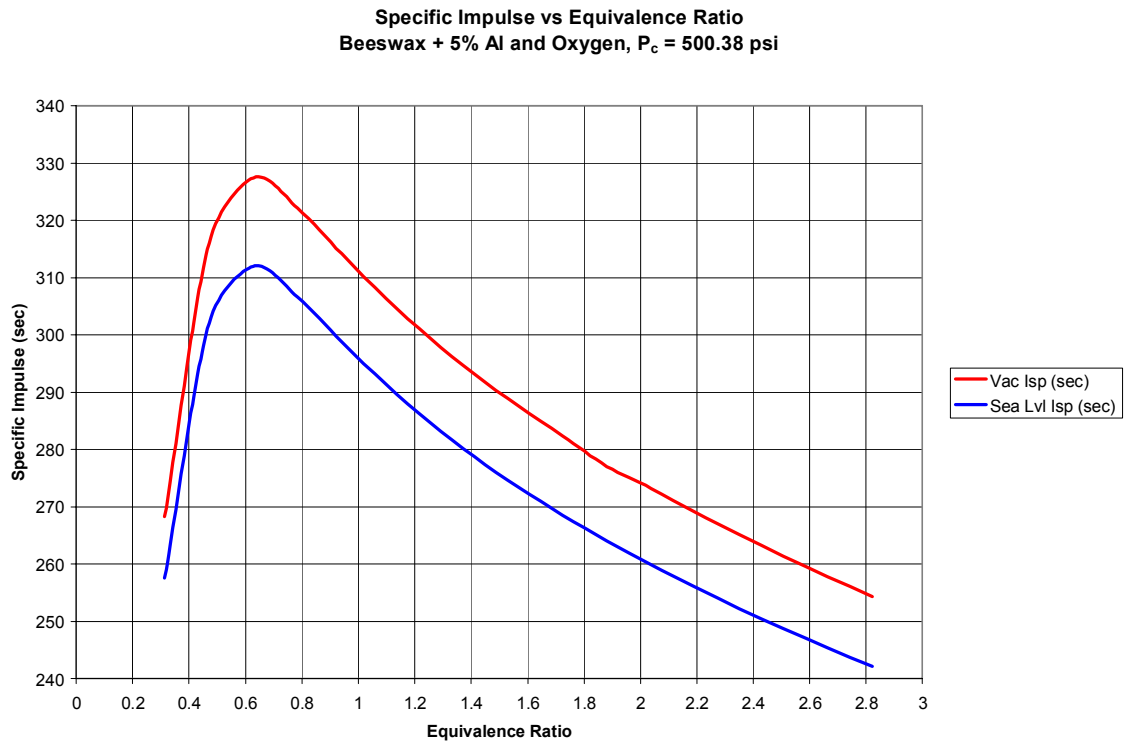Figure 91: Specific Impulse vs. Equivalence Ratio, Beeswax + 10% Al/Oxygen, P_c = 500.38 psig

Ratio of Specific Heats vs Equivalence Ratio
Beeswax + 10% Al and Oxygen, P_c = 500.38 psi

Figure 92: Ratio of Specific Heats vs. Equivalence Ratio, Beeswax + 10% Al/Oxygen, P_c = 500.38 psig

Combustion Products Molecular Mass vs Equivalence Ratio
Beeswax + 10% Al and Oxygen, P_c = 500.38 psi

Figure 93: Molecular Mass vs. Equivalence Ratio, Beeswax + 10% Al/Oxygen, P_c = 500.38 psig
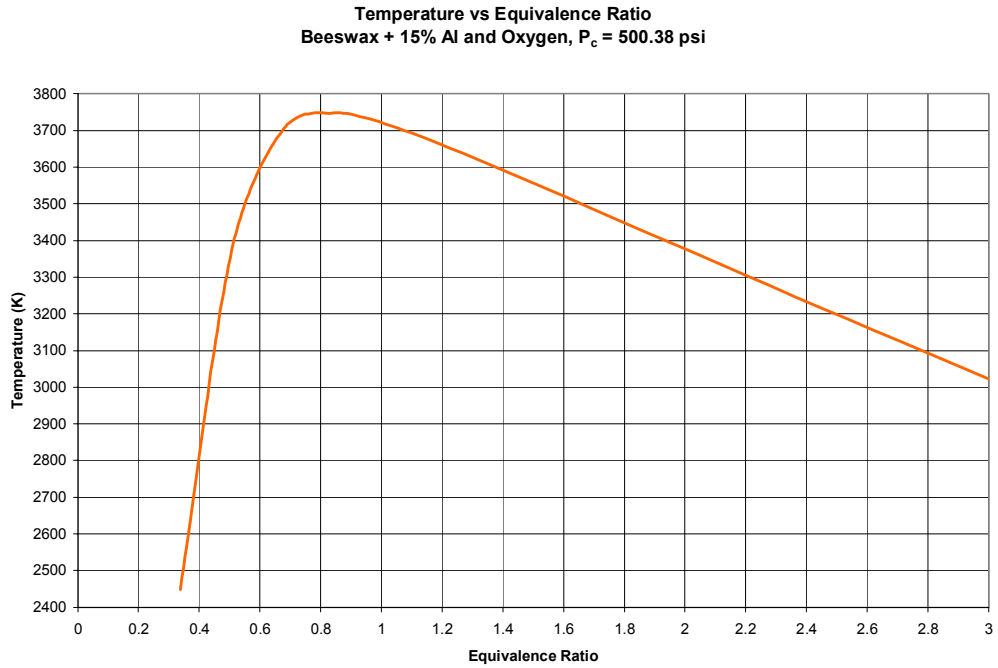
Figure 94: Temperature vs. Equivalence Ratio, Beeswax + 15% Al/Oxygen, P_c = 500.38 psig
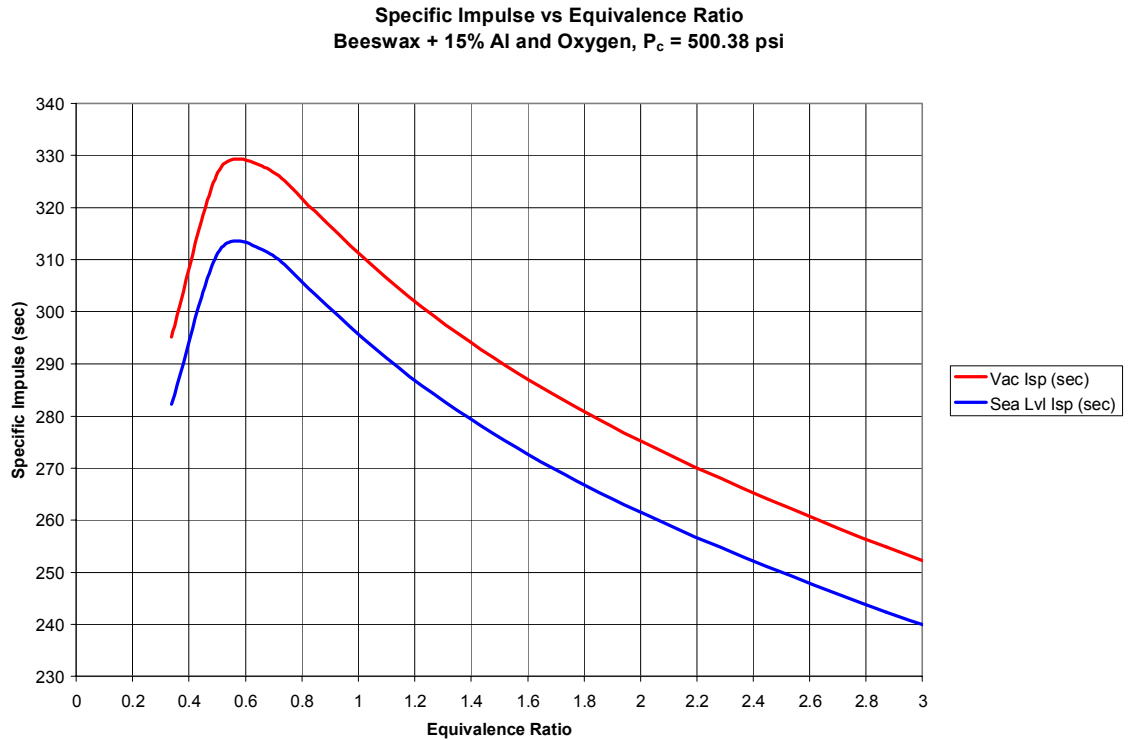
Figure 95: Specific Impulse vs. Equivalence Ratio, Beeswax + 15% Al/Oxygen, P_c = 500.38 psig

Ratio of Specific Heats vs Equivalence Ratio
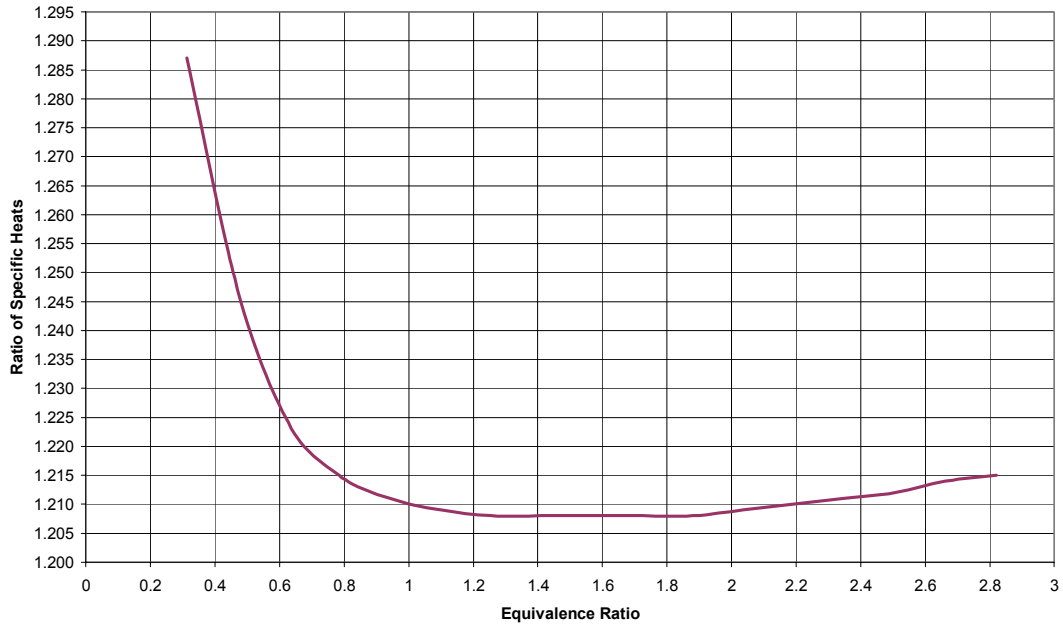**Beeswax + 15% Al and Oxygen, P_c = 500.38 psi**

Figure 96: Ratio of Specific Heats vs. Equivalence Ratio, Beeswax + 15% Al/Oxygen, P_c = 500.38 psig

Combustion Products Molecular Mass vs Equivalence Ratio
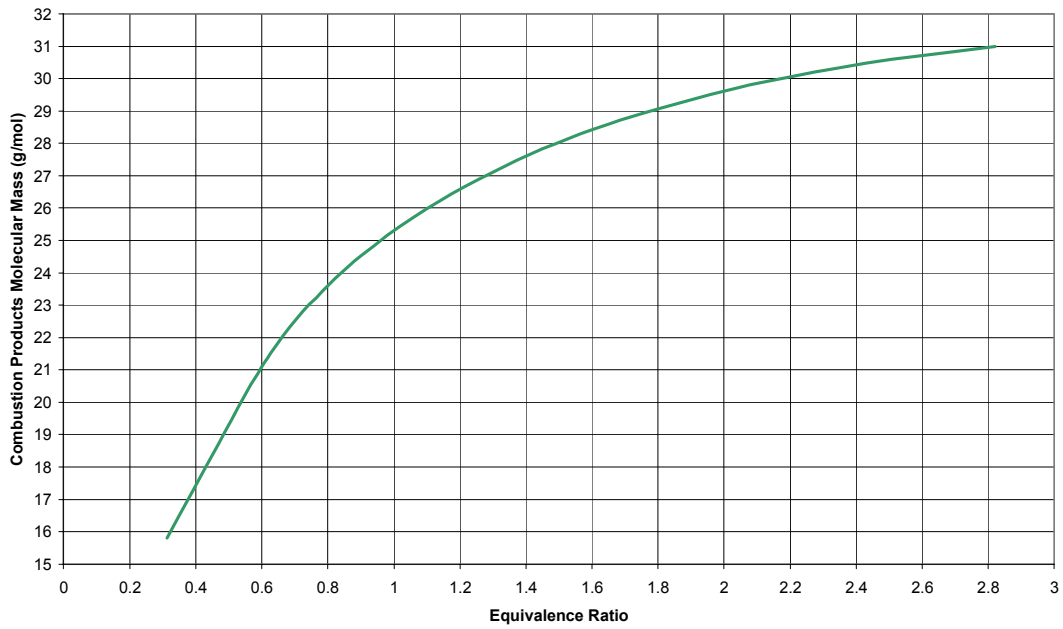**Beeswax + 15% Al and Oxygen, P_c = 500.38 psi**

Figure 97: Molecular Mass vs. Equivalence Ratio, Beeswax + 15% Al/Oxygen, P_c = 500.38 psig
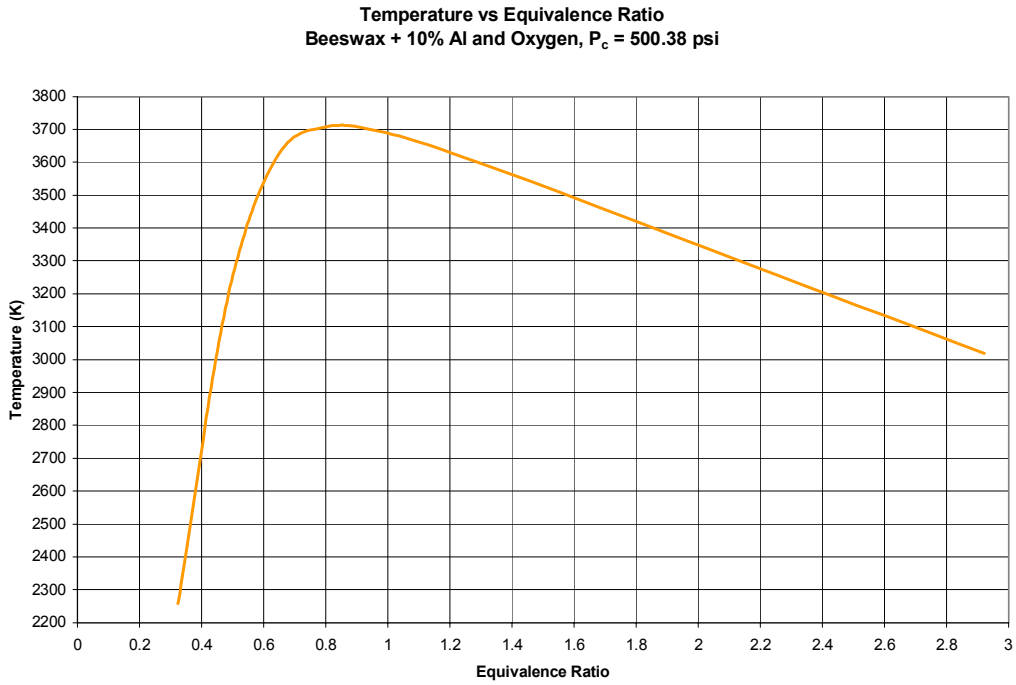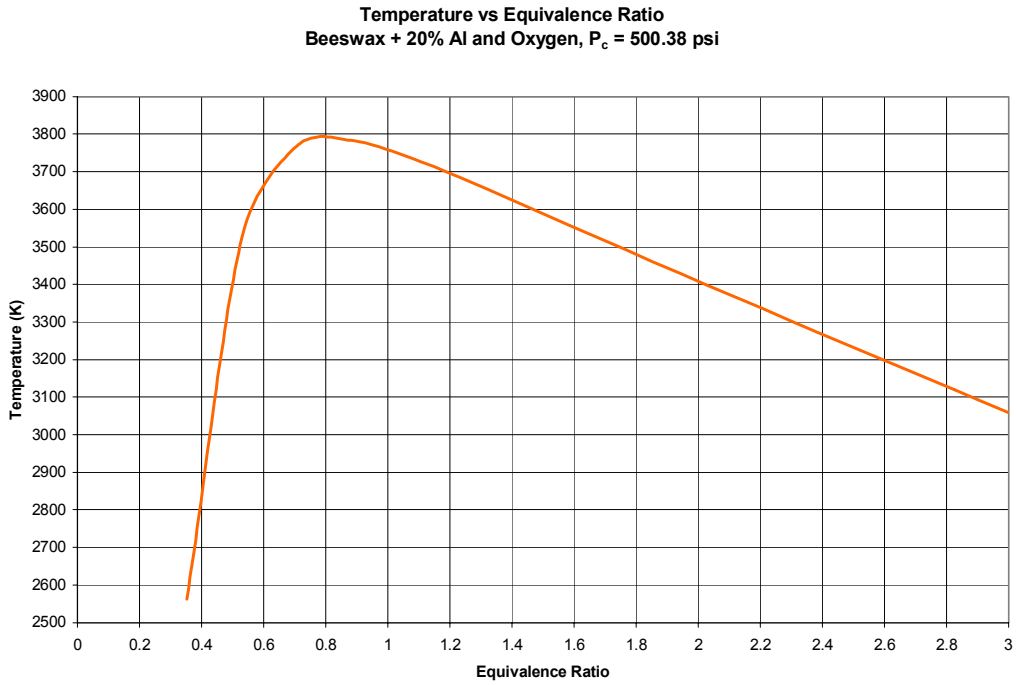
Figure 98: Temperature vs. Equivalence Ratio, Beeswax + 20% Al/Oxygen, P_c = 500.38 psig
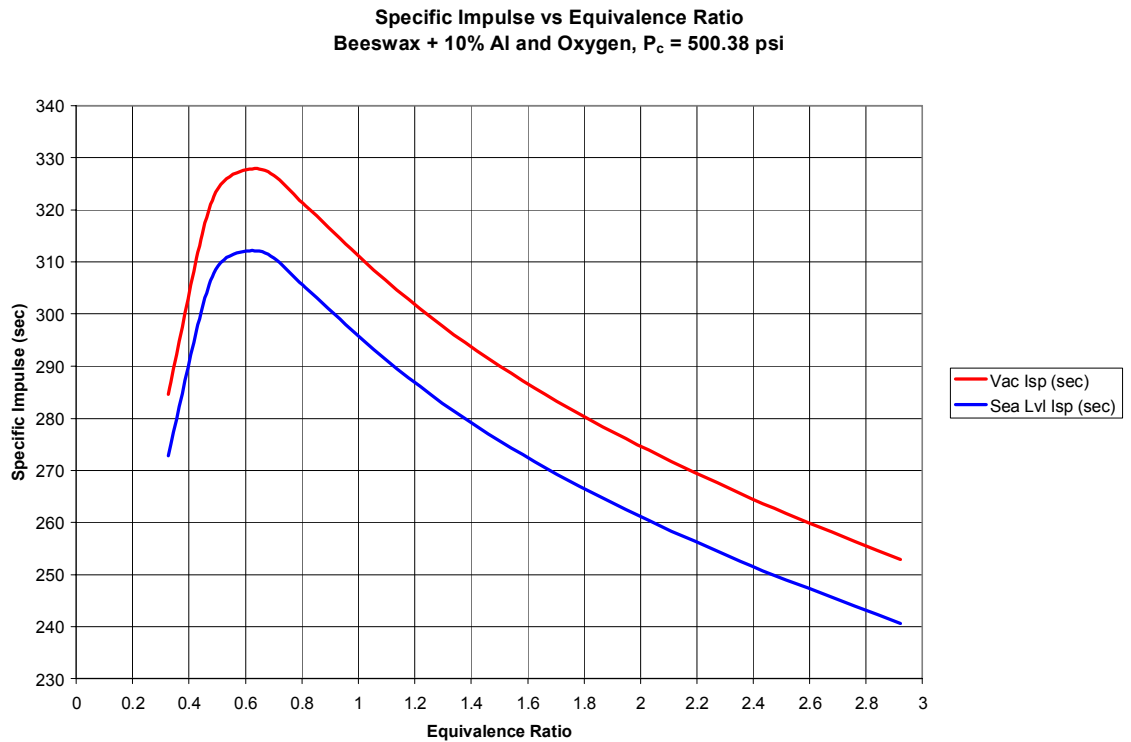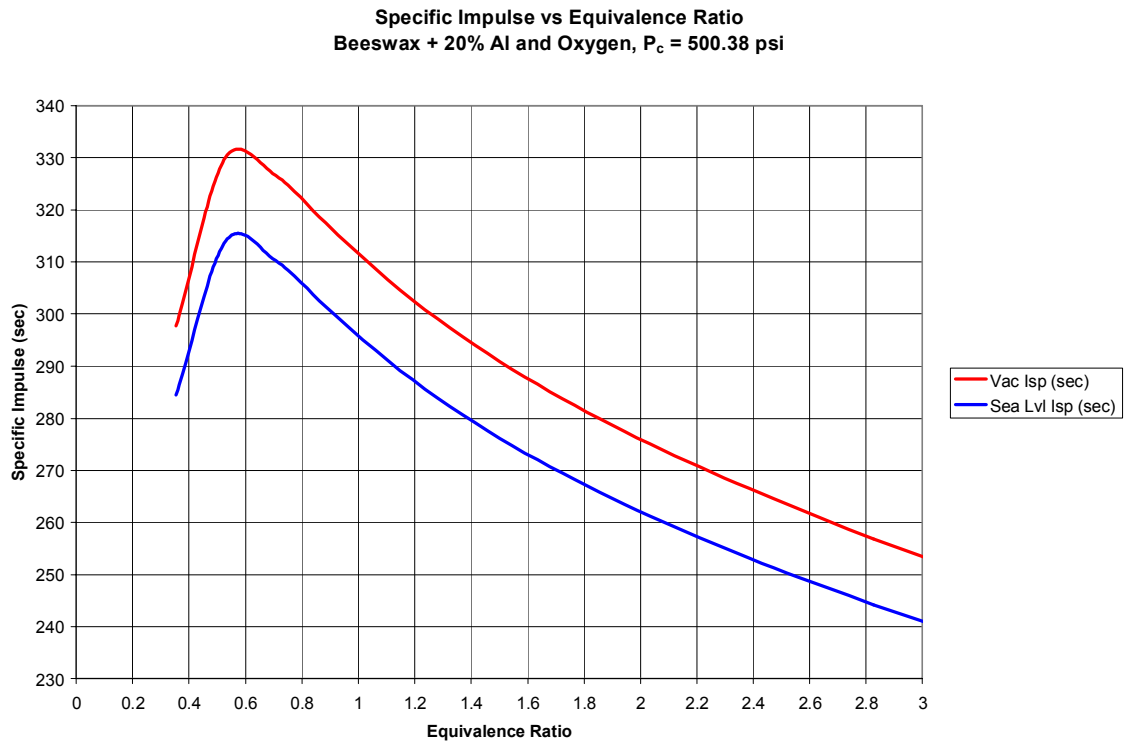

Figure 99: Specific Impulse vs. Equivalence Ratio, Beeswax + 20% Al/Oxygen, P_c = 500.38 psig

Ratio of Specific Heats vs Equivalence Ratio
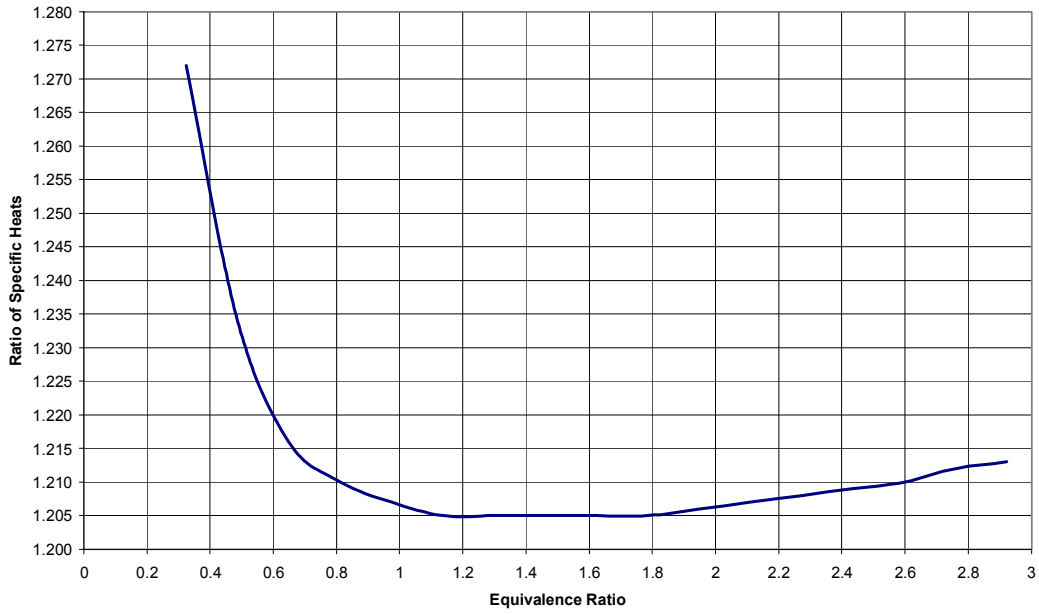**Beeswax + 20% Al and Oxygen, P$_c$ = 500.38 psi**
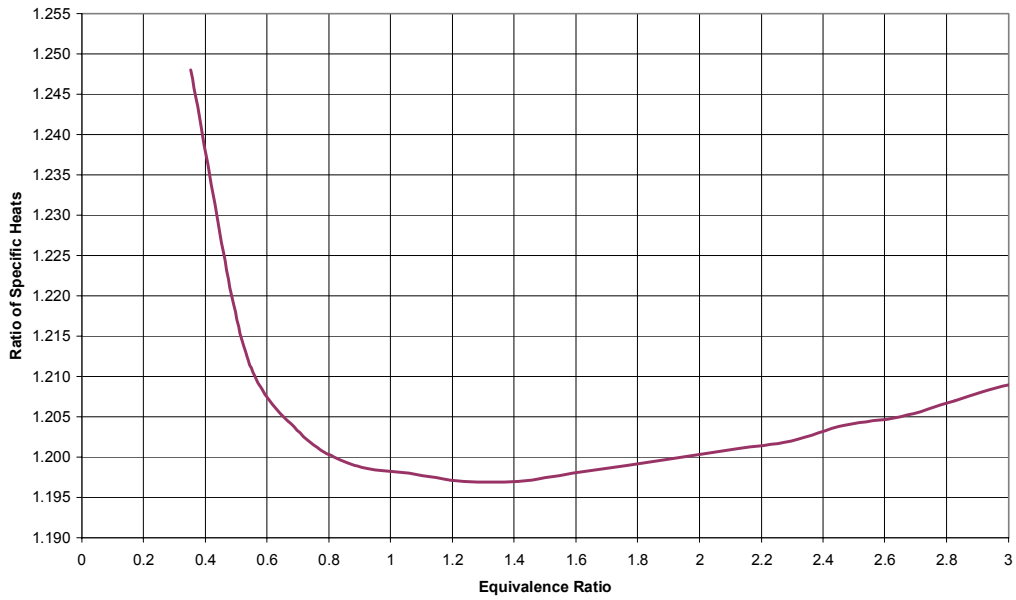
Figure 100: Ratio of Specific Heats vs. Equivalence Ratio, Beeswax + 20% Al/Oxygen, P$_c$ = 500.38 psig

Combustion Products Molecular Mass vs Equivalence Ratio
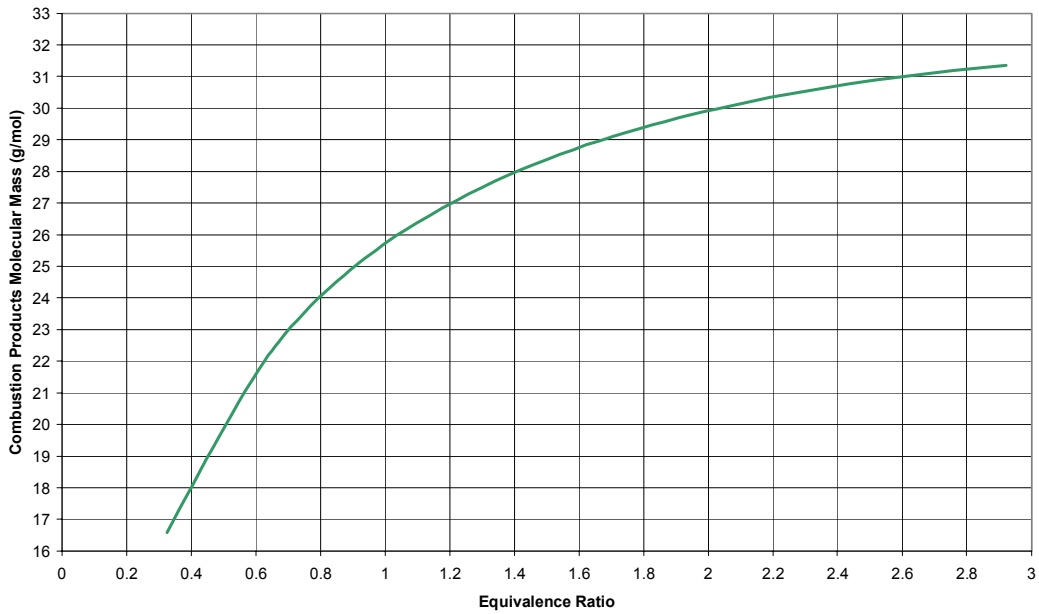**Beeswax + 20% Al and Oxygen, P$_c$ = 500.38 psi**

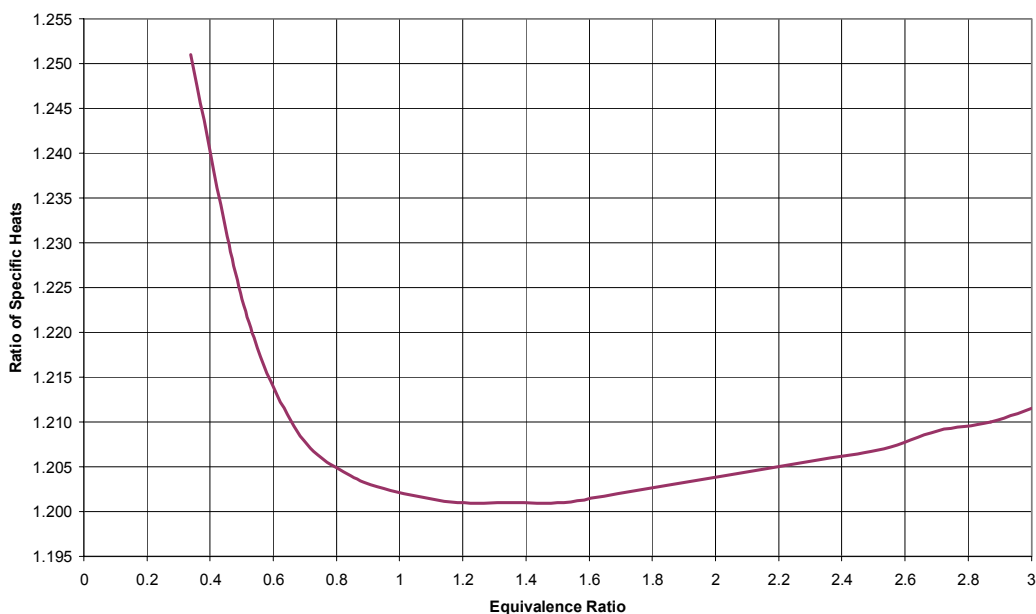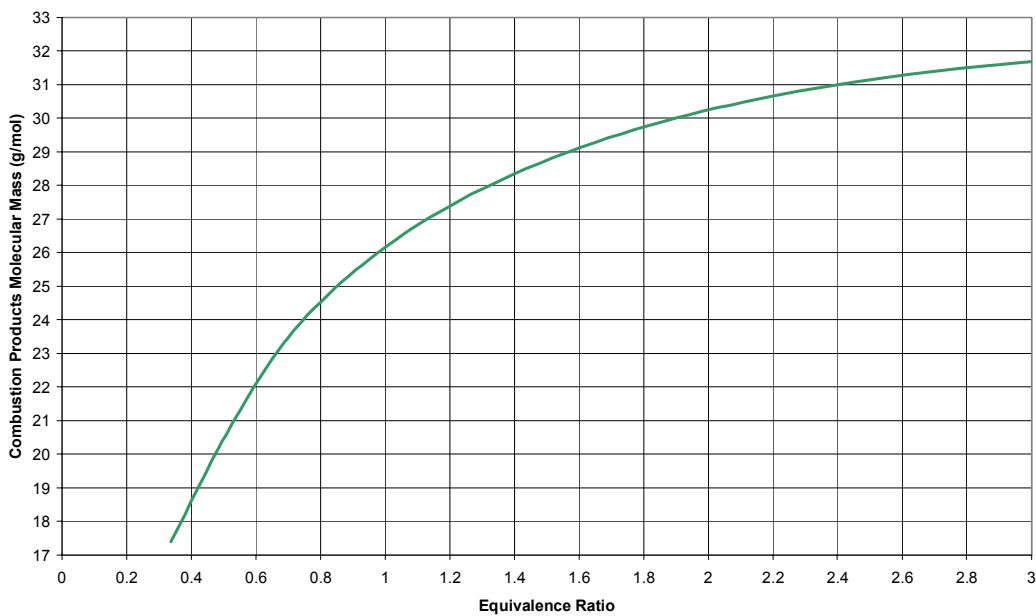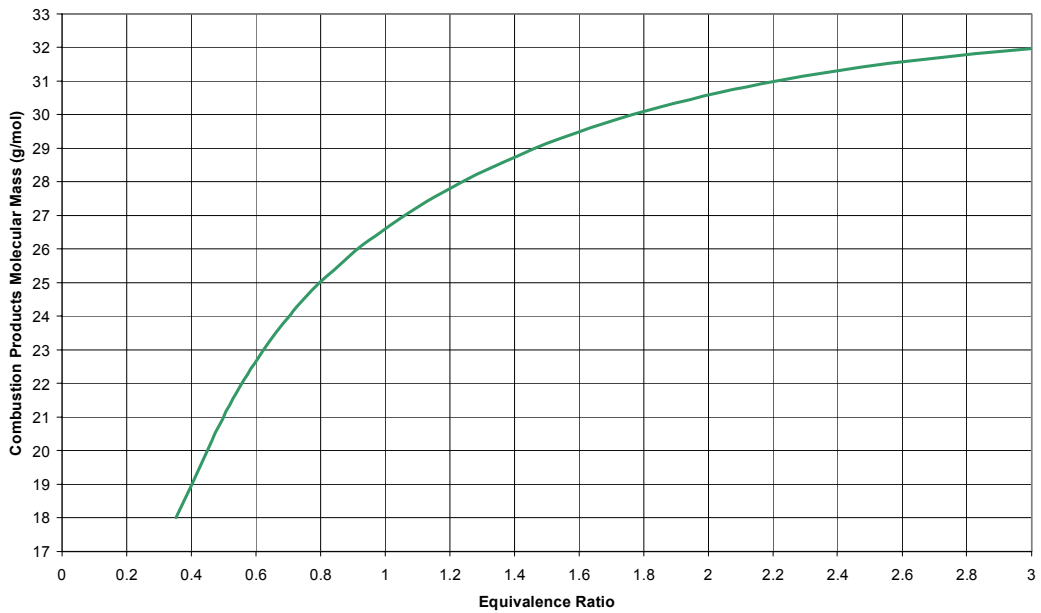Figure 101: Molecular Mass vs. Equivalence Ratio, Beeswax + 20% Al/Oxygen, P$_c$ = 500.38 psig

121

APPENDIX C: MASS FLOW RATE CALCULATIONS

Equations used in oxidizer mass flow rate chart calculation:

The mass flow rate is calculated as:

$$\dot{m}_{ox} = \frac{e * C * A_t * \sqrt{(2 * \rho * \Delta P)}}{\sqrt{(1 - \beta^4)}} \tag{32}$$

Beta ratio is the ratio of orifice plate hole diameter to pipe diameter:

$$\beta = \frac{d}{D} \tag{33}$$

The density is calculated using the ideal gas law (temperature is assumed constant):

$$\rho = \frac{P_{up}}{\dfrac{R_u}{\mu_{ox}} * T_{ox}} \tag{34}$$

The gas expansibility is determined as:

$$e = 1 - (0.41 + 0.35 * \beta^4) * \frac{\Delta P}{K * P_{up}} \tag{35}$$

The discharge coefficient for flange taps is calculated as:

$$C = \left[0.598 + 0.468 * \left(\beta^4 + 10 * \beta^{12} \right) \right] * \sqrt{(1 - \beta^4)} + (0.87 + 0.81 * \beta^4) * \sqrt{\frac{(1 - \beta^4)}{\mathrm{Re}_D}} \tag{36}$$

The last term in the discharge coefficient calculation is small compared to the other term and is neglected in the code.

%Matlab code used to create oxygen flow rate chart

```
%Clear memory
clear all;
clc;

%Orifice plate hole diameter (m)
d=0.00568706;
%Pipe diameter (m)
D=0.0157988;
%Beta ratio
b=d/D;
%Orifice and pipe diameters (m^2)
At=pi/4*d^2;
Ap=pi/4*D^2;
%Coefficients
k=1.29;
C=(0.598 +0.468*(b^4+10*b^12))*sqrt(1-b^4);
```

```
%Average upstream pressure (psig)
P=210;
%Convert to Pa
p1=P*6894.75729317;
%Temperature (K)---assumed value
T=297;
%Gas constant for oxygen (J/kg-K)
r=260;
%Standard pressure (Pa) and temperature (K)
pst=101325;
Tst=289;
%Density (kg/m^3)
rho=p1/r/T;

i=1;
dp(i)=0;
for i=1:1:101
%Expansion coefficient
e(i)=1-(0.41+0.35*b^4)*dp(i)/k/p1;
%Flow rate (kg/sec)
qm(i)=e(i)*C*At*sqrt(2*rho*dp(i))/sqrt(1-b^4);
%Other flow rates
qa(i)=qm(i)/rho;
qs(i)=qa(i)*p1*Tst/pst/T;
%Pressure differential (Pa)
dp(i+1)=dp(i)+6894.75729317;
end
%Print chart
fprintf('\n\t\t\t\t\t\tDifferential Pressure vs. Flow Rate\n')
fprintf('\t  0\t  1\t  2\t  3\t  4\t  5\t  6\t  7\t  8\t  9\t\n')
for i=1:10:100
fprintf('%2.0f\t%5.4f\t%5.4f\t%5.4f\t%5.4f\t%5.4f\t%5.4f\t%5.4f\t%5.4f\t%5.4f\t%5.4f\n
',i-1,qm(i),...
   qm(i+1),qm(i+2),qm(i+3),qm(i+4),qm(i+5),qm(i+6),qm(i+7),qm(i+8),qm(i+9))
end
fprintf('100\t%5.4f\n',qm(101))
```

APPENDIX D: UNCERTAINTY CALCULATIONS

Regression Rate

The regression rate equation was reduced to Eq. 37:

$$\dot{r} = \frac{r_i}{t_b}\left[1 - \sqrt{\frac{m_f}{m_i}}\right] \tag{37}$$

where $\dot{r}$ is the regression rate, r_i is the initial combustion port radius, t_b is the burn time, m_i is the initial fuel grain mass, and m_f is the final fuel grain mass. The uncertainty in the regression rate is given by Eq. 38:

$$\omega_{\dot{r}} = \sqrt{\left[\left(\frac{\partial \dot{r}}{\partial r_i}\omega_{r_i}\right)^2 + \left(\frac{\partial \dot{r}}{\partial t_b}\omega_{t_b}\right)^2 + \left(\frac{\partial \dot{r}}{\partial m_i}\omega_{m_i}\right)^2 + \left(\frac{\partial \dot{r}}{\partial m_f}\omega_{m_f}\right)^2\right]} \tag{38}$$

where $\omega_{\dot{r}}$ is the uncertainty in the regression rate, ω_{r_i} is the uncertainty in the initial combustion port radius, ω_{t_b} is the uncertainty in the burn time, ω_{m_i} is the uncertainty in the initial fuel grain mass, and ω_{m_f} is the uncertainty in the final fuel grain mass. The uncertainties are given as: $\omega_{r_i} = \pm 0.001\,\text{m}$, $\omega_{t_b} = \pm 0.05$ s, $\omega_{m_i} = \pm 0.001$ kg, and $\omega_{m_f} = \pm 0.05 m_f$. Due to spallation of unburned mass from the motor, the uncertainty of the final unburned fuel mass was conservatively estimated as 5% of the final mass. The other uncertainties come from the limitations of the instrumentation.

Specific Impulse

For ease in performing the uncertainty analysis, the specific impulse can be simplified to Eq. 39:

$$I_{sp} = \frac{Ft_b}{g_o(m_f + \dot{m}_{ox}t_b)} \tag{39}$$

where I_{sp} is the specific impulse, g_0 is acceleration due to gravity at sea level (9.81 m/s^2), F is the thrust, and $\dot{m}_{ox}$ is the oxidizer mass flow rate. The uncertainty in the specific impulse is calculated by Eq. 40:

$$\omega_{Isp} = \sqrt{\left[\left(\frac{\partial Isp}{\partial F}\omega_F\right)^2 + \left(\frac{\partial Isp}{\partial m_f}\omega_{mf}\right)^2 + \left(\frac{\partial Isp}{\partial \dot{m}_{ox}}\omega_{\dot{m}_{ox}}\right)^2 + \left(\frac{\partial Isp}{\partial t_b}\omega_{tb}\right)^2\right]} \tag{40}$$

where ω_F is the uncertainty in the thrust and $\omega_{\dot{m}_{ox}}$ is the uncertainty in the oxidizer mass flow rate. The uncertainties are given as: $\omega_F = \pm 0.01F$ and $\omega_{\dot{m}_{ox}} = \pm 0.25\dot{m}_{ox}$. The thrust uncertainty comes from the instrumentation and the oxidizer mass flow rate uncertainty is the average from the uncertainty due to the pressure transducers.

APPENDIX E: INSTRUMENTATION RECOMMENDATIONS

Differential Pressure Transducer for Oxidizer Mass Flow Rate Measurement

An Omega PX750-100-HDI-SS differential pressure transducer is recommended. At the

time of this writing, this transducer costs $1755. This transducer will also require a

oxygen cleaning service to allow it to operate with oxygen.

Thermocouple for Exit Temperature Measurement

To successfully measure the nozzle exit plane temperature, a thermocouple is needed that

can survive in a high speed, high temperature (at least 1800 K), and oxidizing

environment. A R or S type thermocouple and a platinum-rhodium sheath are

recommended. For an exact price, a custom quote will have to be requested from Omega.

Also, the response time of the thermocouple will have to be addressed to make sure the

burn time of the rocket motor is sufficiently long enough for the thermocouple to reach

saturation.

APPENDIX F: SUMMARY OF TEST RESULTS

Test #	P$_c$ (psig)	Thrust (N)	$\dot{m}_{ox}$ (kg/s)	$\dot{r}$ (mm/s)	Isp (sec)	α	O/F Ratio	Initial Mass (kg)	Final Mass (kg)
1	32.3	23.5	x	1.33	x	x	x	x	x
2	38.1	25.0	x	1.32	x	x	x	x	x
3	50.7	48.7	x	1.61	x	x	x	x	x
4	39.3	29.7	x	1.30	x	x	x	x	x
14	141.0	108.4	x	2.81	x	x	x	x	x
20	178.0	135.0	x	2.76	x	x	x	x	x
29	165.1	130.0	0.0397	2.85	141.6	0.23	0.76	3.535	3.194
30	149.3	115.8	0.0397	2.28	149.5	0.32	1.06	5.534	3.291
31	174.5	134.0	0.0395	3.26	130.0	0.19	0.63	3.466	3.065
32	155.5	113.0	0.0397	2.71	145.0	0.26	0.86	3.492	3.192
33	133.0	113.0	0.0380	1.94	160.0	0.41	1.36	3.505	3.324
34	154.5	113.0	0.0400	2.68	140.3	0.27	0.90	3.500	3.206
35	146.0	115.5	0.0256	2.41	173.0	0.20	0.66	3.498	3.247
36	178.0	113.0	0.0300	2.76	142.0	0.19	0.63	3.505	3.197
39	115.0	86.0	0.0240	2.40	132.0	0.19	0.63	3.497	3.248
40	104.0	79.0	0.0220	1.89	156.5	0.25	0.83	3.490	3.315
41	110.0	73.0	0.0220	2.35	118.7	0.18	0.60	3.501	3.260
47	109.0	80.6	0.0225	1.93	138.0	0.25	0.83	3.505	3.325
48	106.0	77.6	0.0218	1.92	151.0	0.24	0.80	3.462	3.283
49	233.0	129.0	0.0480	2.42	139.7	0.37	1.23	3.489	3.232
50	216.0	142.4	0.0525	2.14	167.0	0.45	1.49	3.527	3.345
123	100.2	37.2	0.0157	1.42	109.1	0.27	0.90	3.391	3.303
126	110.5	61.9	0.0160	1.76	157.5	0.20	0.66	3.390	3.272
129	84.2	50.6	0.0178	1.24	157.9	0.37	1.23	3.381	3.308
132	103.5	55.9	0.0170	1.70	140.5	0.23	0.76	3.413	3.301
133	102.1	63.8	0.0171	1.40	187.0	0.30	1.00	3.392	3.306
152	123.8	66.8	0.0195	1.40	133.0	0.34	1.13	3.405	3.291
153	112.6	81.4	0.0201	1.47	214.5	0.33	1.10	3.409	3.317

Test #	P_c (psig)	Thrust (N)	$\dot{m}_{ox}$ (kg/s)	$\dot{r}$ (mm/s)	Isp (sec)	α	O/F Ratio	Initial Mass (kg)	Final Mass (kg)
154	131.4	100.2	0.0220	1.56	230.6	0.33	1.10	3.401	3.301
155	135.2	92.5	0.0222	2.15	172.1	0.21	0.70	3.388	3.231
156	146.4	103.2	0.0243	1.69	222.9	0.33	1.10	3.354	3.245
159	153.6	108.6	0.0227	2.34	192.6	0.20	0.66	3.415	3.263
161	145.2	117.3	0.0229	1.72	257.9	0.30	1.00	3.370	3.256
162	138.1	111.0	0.0214	1.73	251.3	0.28	0.93	3.378	3.263
163	109.5	66.0	0.0170	1.53	138.3	0.26	0.86	3.380	3.283
168	220.8	170.4	0.0348	2.53	217.1	0.26	0.86	3.350	3.150
169	175.6	114.2	0.0261	1.90	210.0	0.30	1.00	3.403	3.272
170	213.8	160.2	0.0324	2.41	222.7	0.26	0.86	3.382	3.196
171	213.4	148.3	0.0334	2.22	216.5	0.30	1.00	3.380	3.215
172	137.6	86.8	0.0212	2.07	163.7	0.21	0.70	3.401	3.252
173	153.9	109.0	0.0238	2.15	190.0	0.23	0.76	3.395	3.283
176	206.9	115.1	0.0331	2.20	170.8	0.31	1.03	3.385	3.223
177	216.7	108.7	0.0335	2.51	144.2	0.26	0.86	3.402	3.205
178	190.1	132.0	0.0313	2.20	200.6	0.29	0.96	3.412	3.250
179	206.4	136.6	0.0322	2.12	210.3	0.31	1.03	3.393	3.239
180	196.8	109.9	0.0317	2.12	170.5	0.31	1.03	3.415	3.261

VITA

Scott Grayson Putnam was born on September 17, 1972 in Charleston, SC and graduated from Goose Creek High School in 1990. He earned a Bachelor's of Science degree in aerospace engineering at the University of Tennessee, Knoxville in May 1995. He then earned a Master's of Science degree in aerospace engineering from the University of Alabama in May 1997. On June 23, 1995, he entered the United States Air Force and was commissioned a Second Lieutenant upon the completion of Officer Training School on September 30, 1997. He was promoted to First Lieutenant on September 30, 1999 and to Captain on September 30, 2001. In December 2005, he was selected for promotion to the rank of Major, and will pin on that rank in 2007.